Discrete-Time Quantum Walk - Dynamics and Applications

by

Chandrashekar Madaiah

A thesis
presented to the University of Waterloo
in fulfillment of the
thesis requirement for the degree of
Doctor of Philosophy
in
Physics

Waterloo, Ontario, Canada, 2010

© Chandrashekar Madaiah 2010

Author's Declaration

I hereby declare that I am the sole author of this thesis. This is a true copy of the thesis, including any required final revisions, as accepted by my examiners.

I understand that my thesis may be made electronically available to the public.

Chandrashekar Madaiah

Abstract

This dissertation presents investigations on dynamics of discrete-time quantum walk and some of its applications. Quantum walks has been exploited as an useful tool for quantum algorithms in quantum computing. Beyond quantum computational purposes, it has been used to explain and control the dynamics in various physical systems. In order to use the quantum walk to its fullest potential, it is important to know and optimize the properties purely due to quantum dynamics and in presence of noise. Various studies of its dynamics in the absence and presence of noise have been reported. We propose new approaches to optimize the dynamics, discuss symmetries and effect of noise on the quantum walk. Making use of its properties, we propose the use of quantum walk as an efficient new tool for various applications in physical systems and quantum information processing.

In the first and second part of this dissertation, we discuss evolution process of the quantum walks, propose and demonstrate the optimization of discrete-time quantum walk using quantum coin operation from SU(2) group and discuss some of its properties. We investigate symmetry operations and environmental effects on dynamics of the walk on a line and an $n-$cycle highlighting the interplay between noise and topology.

Using the properties and behavior of quantum walk discussed in part two, in part three we propose the application of quantum walk to realize quantum phase transition in optical lattice, that is to efficiently control and redistribute ultracold atoms in optical lattice. We also discuss the implementation scheme. Another application we consider is creation of spatial entanglement using quantum walk on a quantum many body system.

Acknowledgements

I have been fortunate in having the benefit of interactions and collaboration with numerous people to whom I feel grateful and would like to thank at this occasion. I would particularly like to thank Prof. Raymond Laflamme for giving me support, guidance and many opportunities at Waterloo. It has been a great opportunity to be around so many talented people at Waterloo, the experience will have a lasting impact on my academic career. I am grateful to the Mike and Ophelia Lazaridis fellowship and University of Waterloo for their financial support.

I had number of great teachers back in India, during my stay at Oxford and Waterloo. I take this opportunity to thank them all for the insights they have shared. Particularly at Waterloo, I thank Frank Wilhelm, Joseph Emerson, Andrew Childs, Andris Ambainis and Ashwin Nayak for helping me when required.

Working with my collaborators has greatly benefited me. I thank R. Srikanth, Subhashish Banerjee, Sandeep Goyal for all that I have gained from our discussions and some of the work we did together.

I thank all my colleagues at the Institute for Quantum Computing including Jonathan Baugh, Jeremy Chamilliard, Mike Ditty, Osama Moussa, Gina Passante, Colm Ryan, Marcus da Silva, Urbasi Sinha and Jingfu Zhang for making my stay simulating and enjoyable. I also thank Wendy Reibel, Judy McDonnell and all other staff members at Institute for Quantum Computing, University of Waterloo and Perimeter Institute for Theoretical Physics for their support during my stay at Waterloo.

I thank my parents, brother, sister, relatives and friends for understanding and supporting me all these years. I also thank Indu for her love.

Finally, I thank R. Srikanth, Srinath Reddy, Sarvagya Upadhyay, and Sandeep Goyal for their comments on the draft.

To my parents…

Contents

Author's Declaration **iii**

Abstract **v**

Acknowledgements **vii**

Dedication **ix**

Contents **xi**

List of Figures **xv**

Preface **xxv**

Glossary of Notations **xxvii**

I Introduction **1**

1 Introduction **3**
1.1 Introduction 3
1.2 Dynamics of quantum walk 8
1.3 Applications 11

II Quantum Walks and Its Dynamics **13**

2 Quantum walks **15**

2.1 Introduction 15
2.2 Continuous-time quantum walk 16
2.3 Discrete-time quantum walk 18
    2.3.1 Hadamard walk 22
    2.3.2 Optimization using SU(2) coin 24
        2.3.2.1 Entropy of measurement 33
        2.3.2.2 Mixing time on an n-cycle 34
    2.3.3 Randomizing coin operations from SU(2) group 36
2.4 Recurrence of quantum walk 37
    2.4.1 Quantum recurrence theorem 39
    2.4.2 Fractional recurrence of quantum walk 41
        2.4.2.1 On a line 41
        2.4.2.2 On an $n-$cycle 45
2.5 Summary 51

3 Symmetries and noise on quantum walk **53**
3.1 Introduction 53
3.2 Symmetry and noise operations on a line 54
    3.2.1 Bit flip and phase flip symmetries 54
    3.2.2 Environmental effects 59
        3.2.2.1 Phase damping and bit flip channels 61
        3.2.2.2 Generalized amplitude damping channel 70
3.3 Symmetry and noise operations on an $n-$cycle 75
    3.3.1 Breakdown in symmetry 76
    3.3.2 Breakdown using a generalized phase gate 78
    3.3.3 Effect of noise and symmetry restoration 81
3.4 Experimental implications 86
    3.4.1 NMR quantum-information processor 87
    3.4.2 Ultracold atoms 87
    3.4.3 Other condensed matter systems 88
3.5 Summary 90

III Applications **91**

4 Quantum phase transition using quantum walks **93**
4.1 Introduction 93
4.2 Quantum phase transition in optical lattice 95
    4.2.1 Bose-Hubbard model 95
4.3 Quantum walk on atoms in 1D Mott insulator and superfluid regime 100
4.4 Quantum walk with a noisy channel as a toolbox 106
4.5 Implementation 110

4.5.1 Quantum walk using Bose-Einstein condensate 112
    4.5.1.1 Macroscopic cat state of Bose-Einstein condensate 114
    4.5.1.2 Unitary operator - Stimulated Raman kicks 116
    4.5.1.3 Physical setup for the implementation 119
4.6 Summary 123

5 Spatial entanglement using quantum walk on many body system 125
5.1 Introduction 125
5.2 Entanglement 126
    5.2.1 Position-particle entanglement 126
    5.2.2 Spatial Entanglement 129
        5.2.2.1 Using single particle quantum walk 129
        5.2.2.2 Using many particle quantum walk 130
5.3 Calculating spatial entanglement in a multipartite system 133
5.4 Summary 140

IV Conclusion 141

6 Conclusion and future perspective 143
6.1 Conclusion 143
6.2 Future perspective 145

Appendix 147

A Quantum walk and Dirac equation : derivation 147

B Variation of the variance as a function of θ 149

C Dipole trap for ^{87}Rb atoms using light of different wavelengths 153
C.1 Frequency-detuning and potential depth for different wavelength . . 154

Bibliography 157

List of Figures

1.1 Probability distribution of classical random walk and its quantum counterpart, quantum walk. Difference in the variance can been seen in the distribution. The distribution is after 100 steps of walk. 5

2.1 Spread of probability distribution of the Hadamard walk with the initial state $|0\rangle$ (dashed line) and initial state $|1\rangle$ (solid line) on the position space along with distribution of the classical random walk (dashed-circle). The distribution is for 100 steps. 23

2.2 Spread of probability distribution for different values of ξ, θ, ζ using quantum coin operator $B_{\xi,\theta,\zeta}$. Parameter ξ shifts the distribution to the left: (a) $= (\frac{\pi}{6}, \frac{\pi}{6}, 0)$ and (c) $= (\frac{5\pi}{12}, \frac{\pi}{3}, 0)$. Parameter ζ shifts it to the right: (b) $= (0, \frac{\pi}{6}, \frac{\pi}{6})$ and (d) $= (0, \frac{\pi}{3}, \frac{5\pi}{12})$. The initial state of the particle $|\Psi_{ins}\rangle = \frac{1}{\sqrt{2}}(|0\rangle + i|1\rangle) \otimes |\psi_0\rangle$ and the distribution is for 100 steps. 25

2.3 Spread of probability distribution for different values of θ using the quantum coin operator $B_{0,\theta,0}$. The distribution is wider for (a) $= (0, \frac{\pi}{12}, 0)$ than for (b) $= (0, \frac{\pi}{4}, 0)$ and (c) $= (0, \frac{5\pi}{12}, 0)$, showing the decrease in spread with increase in θ. The initial state of the particle $|\Psi_{ins}\rangle = \frac{1}{\sqrt{2}}(|0\rangle + i|1\rangle) \otimes |\psi_0\rangle$ and the distribution is for 100 steps. . 28

2.4 A comparison of variation of σ with θ for different number of steps of walk using operator $B_{0,\theta,0}$ using numerical integration. 29

2.5 Value of C for a given θ with increase in number of steps. C remains constant with increase in number of steps and decreases with increase in θ. 29

2.6 Plot of the variation of C_θ when $\eta = |\xi - \zeta| = 0°$ from numerical data and the function $(1 - \sin(\theta))$ to which it fits. The effect of maximum biasing, $\eta = 90°$ on C_θ is also shown and it is very small. 31

2.7 The probability distribution obtained using (2.41) for different value of θ. The distribution is for 100 steps. 32

2.8 Variation of entropy of measurement $H(j)$ with θ for different number of steps. The decrease in $H(j)$ is not drastic till θ is close to 0 or $\frac{\pi}{2}$. 33

2.9 A comparison of mixing time M of the time-averaged probability distribution of a quantum walk on an n-cycle for different value of θ using coin operation $B_{0,\theta,0}$, where n, the number of position, is 101. Mixing is faster for lower value of θ. The distribution is for 200 cycles. 35

2.10 Quantum walk using randomly picked coin operation for each step of walk from SU(2) group with randomly picked $\xi, \theta, \zeta \in \{0, \pi/2\}$ for $B_{\xi,\theta,\zeta}$ and $B_{0,\theta,0}$ respectively. We see that the variance of the distribution is very much close to the variance of the classical random walk (CRW) distribution. 36

2.11 Quantum walk using two different set of random picked parameters $\xi, \zeta \in \{0, \pi/2\}, \theta_1 \in \{0, \pi/4\}$ and $\theta_2 \in \{\pi/4, \pi/2\}$ for $B_{\xi,\theta_2,\zeta}$ and $B_{\xi,\theta_2,\zeta}$ respectively. The distribution is for 200 steps, walk using $\theta_1 \in \{0, \pi/4\}$ spreads wider in position space, whereas the walk using $\theta_2 \in \{\pi/4, \pi/2\}$ localizes the distribution. 37

2.12 The plot of $[1 - p_0(t)]$, where $P_0(t)$ is the probability of particle at the origin with t being the number of steps in the discrete-time quantum walk evolution. The plot for quantum walk on a line using different coin operation parameter $\theta = 15°, 45°$, and 75° is shown. With an increase in θ, the quantum Pólya number, which characterizes the fractional recurrence nature of the quantum walk, also increases. The plot with $\theta = 0°$ is for a walk on an $n-$cycle with a completely suppressed interference effect, where $n = 51$. For a walk to be completely recurrent there should exist a $t = T$ where $[1 - P_0(T)] = 0$. Any non-zero value can be used to characterize the fractional recurrence nature of the quantum walk and an absolute 1 for all t would show that the quantum walk is completely transient. (b) Close up of the plot. 42

2.13 Probability at the initial position after different number of steps of quantum walk on $15-$ and $24-$ cycle. This clearly shows that even for steps as large as 5000, their is no signature of complete recurrence. The distribution is obtained using Hadamard operation, $B_{0,\pi/4,0}$ as quantum coin operation. 46

2.14 Probability at the initial position on $8-$cycle. (a) The distribution is obtained using Hadamard operation $B_{0,\pi/4,0}$, due to return of amplitudes to initial position (constructive interference at the origin) before interference of amplitude dominates uniformly over the entire vertices, recurrence is seen. (b) The use of quantum coin, $B_{0,\pi/6,0}$ during the evolution does not lead to complete constructive interference at origin and hence complete recurrence is not seen. . . 47

2.15 Probability at the initial position on 10−cycle. The distribution is obtained using Hadamard operation $B_{0,\pi/4,0}$. A small deviation from complete recurrence can be seen. (a) and (b) are probability at initial position for quantum walk up to 250 steps and 5000 steps respectively and (c) is the close up of the probability and we note that the probability is not exact 1 at any time within 5000 steps. . 48

2.16 Probability at the initial position after different number of steps of quantum walk on 5−cycle, (a) is the complete plot whereas (b) is a close up of probability values between 0.9 and 1. At no step in the plot, probability is a unit value. This numerically shows that the quantum walk on an $n-$ cycle does not recur for n=5. 49

3.1 The effect of environmental decoherence on the position probability distribution of a quantum walk subjected to a noisy channel. Coin bias is of the form (2.37) with $\theta = 60°, \xi = \zeta = 0$. The noise is modeled as a phase flip (solid line) or bit flip (dashed line) channel, characterized by (3.24) and (3.30), respectively, at various noise levels p : (a) $p = 0.005$; (b) $p = 0.05$; (c) $p = 0.1$; (d) $p = 0.5$, which corresponds to a fully classical random walk. Comparing Figure (d) with Figure 3.2(d), we note that the distribution in the case of maximal bit flip noise is the same. The distribution is for 100 steps. 60

3.2 The effect of environmental decoherence on the position probability distribution of a quantum walk subjected to a noisy channel. Coin bias is of the form (2.37) with $\theta = 30°, \xi = \zeta = 0$. The noise is modeled as a phase flip (solid line) or bit flip (dashed line) channel, characterized by (3.24) and (3.30), respectively, at various noise levels p: (a) $p = 0.005$ (b) $p = 0.05$; (c) $p = 0.1$; (d) $p = 0.5$, which corresponds to a fully classical random walk. The distribution is for 100 steps. 61

3.3 Variation of standard deviation with noise level, for both phase noise and bit flip noise. (a) and (b) is for $\theta = 30°$; (c) is for Hadamard walk ($\theta = 45°$); (d) and (e) is for $\theta = 60°$ in the quantum coin operation $B_{0,\theta,0}$. In the classical limit of $p = 0.5$, the standard deviation converges to a fixed value for bit flip noise, irrespective of θ, but different for phase flip noise. The convergence happens because, at maximum bit flip noise ($p = 0.5$), the measurement outcome in the computational basis is completely randomized. On the other hand, the non-convergence in the case of phase flip noise is due to the fact that the asymptotic mixed state obtained via a phase damping channel depends on the value of the θ. The standard deviation was calculated for 100 steps of quantum walk. 62

3.4 Variation of the ratio of standard deviation without any symmetry operation to the bit flip symmetry operation with increasing bit flip noise level. The standard deviation was calculated for 100 steps of walk. 67

3.5 Variation of the ratio of standard deviation without any symmetry operation to the phase flip symmetry operation with increasing bit flip (phase flip) noise level. The standard deviation was calculated for 100 steps of walk. 67

3.6 Variation of the ratio of standard deviation without any symmetry operation to the bit flip symmetry operation with increasing phase flip noise level. The standard deviation was calculated for 100 steps of walk. 68

3.7 Amplitude damping channel acting on a Hadamard walk at temperature $T = 0$. The distribution corresponding to intermediate values of p clearly show the breakdown of the **RX** symmetry. However, the extended symmetry, **PRX** (where **P** stands for parity operation (spatial inversion)) holds good. This is observed at all temperatures. (a) Probability distribution of finding the particle on which amplitude damping channel is acting. This shows that even at $T = 0$, for sufficiently high coupling, the distribution turns classical. (b) Amplitude damping channel with a bit flip symmetry. 71

3.8 **PRX** symmetry seen to hold in quantum walk (with $\theta = 60°$ and $\theta = 30°$) subjected to amplitude damping ($T = 0$). The two cases are spatial inversions of each other. This holds for a generalized amplitude damping at any temperature. (a) walk with $\theta = 60°$; (b) $\theta = 30°$ and bit flip. 72

3.9 Onset of classicality is seen to be accentuated in a Hadamard walk subjected to generalized amplitude damping followed by bit flip with increasing temperatures (without bit flip the damping would have been to the right). Figure 3.7(a) depicts the $T = 0$ case ($\chi = 1$ in (3.43)). (a) Finite temperature corresponding to $\chi = 0.75$ (b) $T = \infty$, corresponding to $\chi = 0.5$. It may be noted that even at $T = \infty$, for sufficiently small coupling the distribution remains non-classical. 72

3.10 Variation of standard deviation with amplitude damping noise level for various value of θ, 15°, 30°, 45°, 60° and 75°. Note that the standard deviation for complementary angles converge to the same value. 73

3.11 An instance of breakdown of phase flip symmetry in a unitary quantum walk on a cycle, where the two extreme points (located at positions ± 50) on the plot are spatially adjacent. The number of sites is 101 and $t = 5000$ (in units of discrete time-steps), with coin parameter $\theta = 30°$. (a) The solid curve represents the positional probability distribution without any symmetry operation applied, while the dashed curve represents that with a phase flip operation applied at each walk step. (b) The same as the above, but with time-averaging applied over every 50 steps, in order to more clearly bring out the breakdown in symmetry. 78

3.12 Position probability distribution for a Hadamard walk, $B(0°, 45°, 0°)$ on (a) a line, and (b) an n-cycle, with $(n = 51)$ and initial state $(1/\sqrt{2})(|0\rangle + i|1\rangle)$, for the unitary case $(\gamma_0 = 0)$ and $\tau_u = 50$. Each figure presents the distribution with and without being subjected to the phase operation $G(40°)$. In (a), there is perfect symmetry, since both distributions coincide. In (b) the two plots do not overlap, indicating the breakdown of the symmetry. 80

3.13 Restoration of phase flip symmetry in a noisy quantum walk on a cycle, where the two extreme points on the plot are spatially adjacent. The number of sites is 101 and $t = 5000$ (in units of discrete time-steps), with coin parameter $\theta = 30°$. The figure depicts the position probability distribution with or without phase flip symmetry operation applied at each step, with phase damping noise level $p = 0.02$ (3.24). After sufficiently long time, the quantum walk reaches the uniform distribution, typical of classical random walk. . 80

3.14 Kolmogorov distance $d(\tau_u)$ against the number of turns (τ_u) of the cyclic quantum walk in the noiseless and noisy case with $n = 51$. For the unitary case ($\lambda = 0$, γ_0 ; bold line) the walk becomes increasingly asymmetric as the number of turns is increased, until about 7–10 turns, after which it fluctuates around $d \approx 0.15$. The plots represent generalized amplitude damping noise at different noise levels at temperature $T = 3.5$ (in units where $\hbar \equiv k_B \equiv 1$). The walk is evolved with the initial state of the particle parameters $\delta = 30°$, $\eta = 40°$ in (2.11), with $B(20°, 10°, 30°)$ and $G(10°)$. 82

3.15 Position probability distribution for a Hadamard walk $B(0, 45°, 0)$ on an n-cycle $(n = 51)$ with initial state $(1/\sqrt{2})(|0\rangle + i|1\rangle)$ when subjected to generalized amplitude damping noise with $\Delta = 0.1$ and finite T $(= 6.0)$ for $\tau_u = 11$. For (a) and (b) $\gamma_0 = 0.025$. (b) is the distribution for the quantum walk augmented by operation $G(20°)$ and (a) is without any augmented operation; note the overlap of (b) on (a), walk remains quantum yet with symmetry completely restored ; 83

3.16 Normalized coherence function $c(M)$ (bold) and the normalized Kolmogorov distance $D(\tau_u)$ (dashed) for an $n-$ cyclic quantum walk as a function of turns τ_u. An overall reduction of both $c(M)$ and $D(\tau_u)$ with time is seen for the generalized amplitude damping noise characterized by temperature $T = 3.5$ and $\Delta = 0.1$. The Hadamard walk is evolved with the initial state parameters (in degrees) $\delta = 45°$, $\eta = 0°$ (2.11), and $G(\beta)$. The line-with-circle plot represents $D(\tau_u)$ with $G(20°)$ and dashed line represents for $G(40°)$. The $c(M)$ (solid line) remains roughly the same for both β. For a clear depiction of the notion of symmetry restoration in the walk even in the quantum regime, Figure (3.15). 85

4.1 Mean-field phase diagram of the ground state of the boson Hubbard model $\mathbf{H}_B$. The notation MI n refers to a Mott insulator with $n_0(\mu/U) = n$. 98

4.2 Density profile of the evolution of 40 atoms starting from Mott insulator state in correlation with the position space when subjected to a quantum walk of different numbers of steps with the Hadamard operator $B_{0,45°,0}$ as the quantum coin. The distribution spreads with increase in the number of steps. 102

4.3 Density profile of the evolution of 40 atoms starting from superfluid state in correlation with the position space when subjected to a quantum walk of different numbers of steps with the Hadamard operator $B_{0,45°,0}$ as the quantum coin. The distribution spread with increase in the number of steps and is almost uniform between the lattice site ±20 when $t = 25$. At this stage the optical potential depth can be increased to cancel the correlation and obtain the Mott insulator state. 103

4.4 Distribution of atoms initially in Mott insulator state when subjected to quantum walk ($t = M = 40$) using different values for θ in the operator $B_{0,\theta,0}$. The spread is wider for $\theta = 30°$ and decreases with increasing θ. 104

4.5 Distribution of atoms initially in superfluid state when subjected to a quantum walk ($t = M = 40$) using different values for θ in the coin operator $B_{0,\theta,0}$. The distribution is almost uniform for $\theta = 60°$ between the lattice site ±20. At this value the optical potential depth can be increased to cancel the correlation and obtain the Mott insulator state. 105

4.6 Atoms in Mott insulator state after implementing the quantum walk ($t = M = 40, \theta = 45°$) with noise channel. With increased phase damping from $p_p = 0.02$ to $p_p = 0.1$ the distribution (n_j) at the central region gets closure to Gaussian. Amplitude damping of state $|1\rangle$ followed by a bit flip at each step introduces asymmetry to the distribution, $p_a = 0.2$ (without a bit flip the shift would have been to the left). 107
4.7 Atoms in superfluid state after implementing a quantum walk ($t = M = 40, \theta = 45°$). With noiseless quantum walk, the atoms spread, getting close to a uniform distribution. For phase damping $p_p = 0.02$ the distribution is uniform between ±20 and gets closer to Gaussian at $p_p = 0.1$. Amplitude damping of state $|1\rangle$ followed by a bit flip introduces asymmetry to the distribution, $p_a = 0.2$ (without a bit flip the shift would have been to the left). 108
4.8 Density profile of the evolution of atoms initially in MI state from other references. (a) Evolution of 100 atoms with time for atoms initially in MI state [1] . (b) Evolution of 20 atoms with time (the dynamics is driven by the potential depth and tunneling of atoms between the lattice) [2] . These profile have visibly similar distribution compared to Figure 4.2, Figure 4.4 and part of Figure 4.6 in this chapter. 109
4.9 Density profile of the evolution of 40 atoms initially in SF state from [3]. The initial SF profile in our plots and in [3] are different and hence the similarity are not as close as we have for atoms in MI state). The profile in Figure 4.3 after 25 steps of quantum walk is similar to the Profile at TG limit (Tonks-Girardeau limit - leading to MI state) in the above figure. 109
4.10 Light field configuration for a stimulated Raman transition process to give directional momentum kick. Δ is the detuning of the laser from its transition frequency. $|S\rangle$ signifies $(1/\sqrt{2})(|0\rangle \pm |1\rangle)$. 117
4.11 Physical setup to implement the quantum walk using the BEC. In the figure **a** is a BEC, **b** is a dipole trap with a long Rayleigh range, and **c** is the counterpropagating laser beam, ω_1 and ω_2 used to implement the stimulated Raman kick, unitary operator. A coin rotation and Raman pulse are applied throughout the trap region. The stimulated Raman pulse and the rf pulse are applied alternatively to realize the quantum walk. 120
4.12 Multiple microtraps which can be used to confine the atom observe the distribution of atoms after implementing a considerable number of steps of the quantum walk on the BEC. 120

5.1 Entanglement of single particle with position space when subjected to quantum walk. The initial state of the particle is $\frac{1}{\sqrt{2}}(|0\rangle + i|1\rangle)$ and is evolved in position space using different values for θ in the quantum coin operation $B_{0,\theta,0}$. The entanglement initially oscillates and approaches asymptotic value with increase in number of steps. For smaller values of θ the entanglement is higher and decreases with increase in θ. Initial oscillation is also larger for higher θ. . . . 127
5.2 Entanglement of single particle with position space when subjected to quantum walk. The initial state of the particle is given by form (2.11) with $\delta = 40^\circ$ and $\eta = 30^\circ$ and is evolved in position space using different values for θ in the quantum coin operation $B_{0,\theta,0}$. The entanglement initially oscillates and approaches asymptotic value with increase in number of steps. For smaller values of θ the entanglement is higher and decreases with increase in θ. Initial oscillation is also larger for higher θ. 128
5.3 Many particle state with one non-interacting particle at each position space. 131
5.4 Evolution of spatial entanglement with increase in the number of steps of the quantum walk for different number of particles in an open one dimensional lattice chain. The entanglement first increases and with the further increase in the the number of steps, the number of lattice positions exceeds the number of particles in the system resulting in the decrease of the spatial entanglement. The distribution is obtained by implementing quantum walk on particles in the initial state $\frac{1}{\sqrt{2}}(|0\rangle + i|1\rangle)$ and Hadamard operation $B_{0,\pi/4,0}$ as quantum coin operation. 134
5.5 Value of spatial entanglement for 20 particles on a one dimensional lattice after 20 steps of quantum walk using different values of θ in the quantum coin operation $B_{0,\theta,0}$. (a) and (b) are the distributions for particles initially in state $\frac{1}{\sqrt{2}}(|0\rangle + i|1\rangle)$ and state $|0\rangle$ $(|1\rangle)$ respectively. In (a), with increase in θ from 0 to $\pi/2$ the spread of the distribution in lattice position decreases first up to $\theta = \pi/4$ and again increase. Due to asymmetric distributions for particles in case of (b) the above effect is not very prominent. For both (a) and (b) when $\theta = \pi/2$, for every even number of steps of quantum walk, the system returns to the initial state where entanglement is 0. Entanglement is 0 for $\theta = 0$. 135

5.6 Evolution of spatial entanglement for a system with different number of particles in a closed chain. With increase in the number of steps, the entanglement value remains close to asymptotic value with some peaks in between. The peaks can be accounted for the cross over of the left and right propagating amplitudes of the internal state of the particle during quantum walk. The peaks are more for chain with smaller number of particles. Increase in the number of particles in the system results in the decrease in the entanglement value. The distribution is obtained by using $\frac{1}{\sqrt{2}}(|0\rangle + i|1\rangle)$ as the initial states of all the particles and Hadamard operation $B_{0,45^\circ,0}$ as quantum coin operation. 137

5.7 Value of spatial entanglement for 20 particles on a closed chain after 20 steps of quantum walk using different values of θ in the quantum coin operation $B_{0,\theta,0}$. (a) and (b) are the distributions for particles initially in state $\frac{1}{\sqrt{2}}(|0\rangle + i|1\rangle)$ and state $|0\rangle$ ($|1\rangle$) respectively. Since the system is in the closed chain, the quantum walk does not expand the position Hilbert space therefore for all values of θ from 0° to $\pi/2$ the entanglement value remains close to the asymptotic value except for a small peak at smaller values of θ. For $\theta = 0^\circ$ when number of steps equal to number of particles, the amplitudes goes round the chain and returns to its initial state making the entanglement 0 and for $\theta = \pi/2$, for every even number of steps of quantum walk, the system returns to the initial state where entanglement is again 0. . 138

Preface

This dissertation which is divided into four parts discusses *the dynamics of discrete-time quantum walk and some of its applications.* Part I, *Introduction* consists of Chapter 1 which introduces the reader to an overview of the subject followed by brief discussion of results presented in the latter chapters. Part II, *Quantum walks and its dynamics* consists of Chapters 2 and 3. In Chapter 2, we review the two standard forms of quantum walks (continuous- and discrete-time quantum walk) and study the dynamics of discrete-time quantum walk in detail. In Chapter 3, we study symmetries and effect of noise on the dynamics of the discrete-time quantum walk. Part III, *Applications* consists of Chapters 4 and 5. In Chapter 4, we demonstrate the use of discrete-time quantum walk to control the dynamics of ultracold in optical lattice and in Chapter 5, we create spatial entanglement using quantum walk on distinguishable multiparticle system. Part IV, *Conclusion* consists of Chapter 6 which concludes with summery and future perspective.

Information to the examiners

All the work presented in this dissertation was initiated by myself or was a follow up of the results from our earlier studies. Work presented in Chapter 2, *Quantum walks* and Chapter 4, *Quantum phase transition using quantum walks* published in *Phys. Rev. A* **77***, 032326 (2008)*, *Phys. Rev. A* **78***, 0052309 (2008)*, *arXiv : 0810.5592 (2008)*, *Phys. Rev. A* **74***, 032307 (2006)* and *Phys. Rev. A* **78***, 022314 (2008)* was mainly done my myself.

The work presented in Chapter 3, *Symmetries and noise in quantum walk* and published in *Phys. Rev. A* **76***, 022316 (2007)* and *Phys. Rev. A,* **78***, 052316 (2008)* was done in collaboration with R. Srikanth and Subhashish Banerjee. Writing codes to generates plots and structuring the results in the form of theorems was done in collaboration with R. Srikanth and Subhashish Banerjee helped us in understanding and implementing environmental effects on the quantum walk dynamics. The results presented in Chapter 5, *Spatial entanglement using quantum walk* was motivated from the earlier work presented in Chapter 4, *Quantum phase transition* in ultra cold atoms in optical lattice. To effectively measure the spatial entanglement using multipartite quantum walk on distinguishable particles, the codes were written in collaboration with Sandeep Goyal.

Glossary of Notations

NOTATIONS INTRODUCED IN CHAPTER 1

$\mathcal{H}$	Hilbert space
$\mathcal{H}_p$	*Position* Hilbert space
$\mathcal{H}_c$	*Coin* Hilbert space
$H = \frac{1}{\sqrt{2}}\begin{pmatrix} 1 & 1 \\ 1 & -1 \end{pmatrix}$	Hadamard operation
$B_\theta \equiv \begin{pmatrix} \cos(\theta) & \sin(\theta) \\ \sin(\theta) & -\cos(\theta) \end{pmatrix}$	U(2) operator with a single-variable parameter
$\vert 0\rangle = \begin{pmatrix} 1 \\ 0 \end{pmatrix}$	Single qubit notation
$\vert 1\rangle = \begin{pmatrix} 0 \\ 1 \end{pmatrix}$	Single qubit notation
$\frac{1}{\sqrt{2}}(\vert 0\rangle + i\vert 1\rangle)$	Symmetric superposition state of the particle
$\vert\psi_0\rangle$	State of the position
$\vert\Psi_{ins}\rangle \equiv \frac{1}{\sqrt{2}}(\vert 0\rangle + i\vert 1\rangle) \otimes \vert\psi_0\rangle$	Symmetric superposition state of particle in position space as initial state
$B_{\xi,\theta,\zeta} \equiv \begin{pmatrix} e^{i\xi}\cos(\theta) & e^{i\zeta}\sin(\theta) \\ -e^{-i\zeta}\sin(\theta) & e^{-i\xi}\cos(\theta) \end{pmatrix}$	SU(2) operator : generalized three parameter quantum coin operation

NOTATIONS INTRODUCED IN CHAPTER 2

In Section 2.2

$G = (V, E)$	Graph where V and E are vertex and edges set
(j, k)	The vertex set, form the edge when j and k are connected
$A_{j,k} = \begin{cases} 1 & (j,k) \in E \\ 0 & (j,k) \notin E \end{cases}$	Adjacency matrix
$\mathbf{H}$	Hamiltonian
$\mathbf{H}_{j,k} = \begin{cases} d_j\gamma & j = k \\ -\gamma & (j,k) \in E \\ 0 & \text{otherwise} \end{cases}$	Generator matrix

The Hamiltonian $\mathbf{H}$ of the walk process acts as the generator matrix $\mathbf{H}_{j,k}$ which will transform the probability amplitude at the rate of γ to the neighboring sites. Therefore we represent both Hamiltonian and generator matrix by $\mathbf{H}$. d_j is the degree of the vertex j.

$P_j(t)$	Probability of being at vertex j at time t

In Section 2.3

j	Position (vertex)
t	Time (t is also used for number of steps when unit time is required to implement each step of quantum walk)
$\vert\Psi_{in}\rangle = (\cos(\delta)\vert 0\rangle + e^{i\eta}\sin(\delta)\vert 1\rangle) \otimes \vert\psi_0\rangle$	General form of initial state : coin (particle) and position space

$\|\Psi_t\rangle = \|\Psi(t)\rangle$	Coin and position state after time t over entire position space
$\|\Psi_{j,t}\rangle = \|\Psi(j,t)\rangle$	Coin and position state after time t at position j
$\mathbb{1} = \begin{pmatrix} 1 & 0 \\ 0 & 1 \end{pmatrix}$	Identity operation
$\sigma_x = X = \begin{pmatrix} 0 & 1 \\ 1 & 0 \end{pmatrix}$	Pauli x operation
$\sigma_y = Y = \begin{pmatrix} 0 & -i \\ i & 0 \end{pmatrix}$	Pauli y operation
$\sigma_z = Z = \begin{pmatrix} 1 & 0 \\ 0 & -1 \end{pmatrix}$	Pauli z operation
$B_{\zeta,\alpha,\beta,\gamma} = e^{i\zeta} e^{i\alpha\sigma_x} e^{i\beta\sigma_y} e^{i\gamma\sigma_z}$	Quantum coin operation $B \in U(2)$
$S = \|0\rangle\langle 0\| \otimes \sum_{j\in\mathbb{Z}} \|\psi_{j-1}\rangle\langle\psi_j\| + \|1\rangle\langle 1\| \otimes \sum_{j\in\mathbb{Z}} \|\psi_{j+1}\rangle\langle\psi_j\|$	Conditional unitary shift operator on a line
$W_{\zeta,\alpha,\beta,\gamma} = S(B_{\zeta,\alpha,\beta,\gamma} \otimes \mathbb{1})$	Single step quantum walk operation
$P(j,\tau)$	Probability at position j after time t

In Section 2.3.2

$\mathcal{A}_{m,t}$	Amplitudes of state $\|0\rangle$ at position m after t steps of quantum walk
$\mathcal{B}_{m,t}$	Amplitudes of state $\|1\rangle$ at position m after t steps of quantum walk

$B'_{\xi,\theta,\zeta} \equiv \begin{pmatrix} e^{i\xi}\cos(\theta) & e^{i\zeta}\sin(\theta) \\ e^{-i\zeta}\sin(\theta) & -e^{-i\xi}\cos(\theta) \end{pmatrix}$	Three parameter quantum coin operation which is not in SU(2) group
$P(j) = P_j$	probability at position j
$P(j,t)$	Probability at position j after time t
$f(\phi) = t\cos(\theta)\sin(\phi)$	For any given θ, the position j can be parametrized by function $f(\phi)$
$H(j) = -\sum_j P_j \log P_j$	Shannon entropy
$S^c = \vert 0\rangle\langle 0\vert \otimes \sum_{j=0}^{n-1} \vert\psi_{j-1 \bmod n}\rangle\langle\psi_j\vert + \vert 1\rangle\langle 1\vert \otimes \sum_{j=0}^{n-1} \vert\psi_{j+1 \bmod n}\rangle\langle\psi_j\vert$	Conditional unitary shift operator on an $n-$cycle

In Section 2.4

A_o	Observable
X_p	Position operator
$\mathcal{P}_{crw} \equiv 1 - \frac{1}{\sum_{t=0}^{\infty} P_0(t)}$	Classical Pólya number
$P_0(t) = P(0,t)$	The probability of periodicity of dynamics that the particle returns to origin during the t steps of walk (recurrence probability)
$\vert\Psi_{j,T_M+1}\rangle$	state at position j after evolving up to time $(T{+}1)$ with intermediate measurement at time T
$\mathcal{P}_{qw} = 1 - \prod_{t=1}^{\infty} [1 - P_0(t)]$	Quantum Pólya number

NOTATIONS INTRODUCED IN CHAPTER 3

In Section 3.2

$\hat{a}$ and $\hat{a}^\dagger$	Unitary operators that are notationally reminiscent of annihilation and creation operations
X	Bit flip
Z	Phase flip
G	operation represent interchanging of coin operation which leave quantum walk symmetric
	P
Parity ($\hat{a} \leftrightarrow \hat{a}^\dagger$)	
R	Angular reflection ($\theta \rightarrow \pi/2 - \theta$, i.e., $\sin\theta \leftrightarrow \cos\theta$, and $\xi \leftrightarrow -\zeta$)
X, **Z**, **G**, **P** and **R**	Refers to application of X, Z, G, P and R operations at each step of quantum walk.
$\Phi(\phi) \equiv \|0\rangle\langle 0\| + e^{i\phi}\|1\rangle\langle 1\|$	Phase shift operation
$\mathcal{E}(\rho) = (1-p)\rho + pZ\rho Z$	Phase flip channel
$\mathcal{E}(\rho) = (1-p)\rho + pX\rho X$	Bit flip channel

$\mathbf{H} = \mathbf{H}_S + \mathbf{H}_R + \mathbf{H}_{SR}$	Interaction Hamiltonian
$\mathbf{H}_S$	Hamiltonian of the system (S)
$\mathbf{H}_R$	Hamiltonian of the reservoir (R)
$\mathbf{H}_{SR}$	Hamiltonian of the system-reservoir (SR) interaction
$\hat{b}$ and $\hat{b}^\dagger$	Annihilation and creation operators
$\sigma_+ = \|1\rangle\langle 0\| = \frac{1}{2}(\sigma_x + i\sigma_y)$	Raising operator
$\sigma_- = \|0\rangle\langle 1\| = \frac{1}{2}(\sigma_x - i\sigma_y)$	Lowering operator

In Section 3.3

$G(\beta) = \begin{pmatrix} 1 & 0 \\ 0 & e^{i\beta} \end{pmatrix}$	Generalized phase gate
$d(t) = (1/2)\sum_j \|P(j,t) - P'(j,t)\|$	Kolmogorov distance (trace distance), distance between the particle position distributions obtained without and with the symmetry operation, given by $P(j,t)$ and $P'(j,t)$
$D(t)$	Normalized Kolmogorov distance
$\boldsymbol{C}$	Coherence
$C(m)$	Coherence function
$c(m)$	Normalized coherence function

NOTATIONS INTRODUCED IN CHAPTER 4

In Section 4.2

$\mathbf{H}_B$	Bose-Hubbard Hamiltonian
$\hat{b}$ and $\hat{b}^\dagger$	Boson annihilation and creation operators
$\hat{b}_j$ and $\hat{b}_k^\dagger$	Boson annihilation and creation operators at position j and k respectively
$\hat{n}_j = \hat{b}_j^\dagger \hat{b}_j$	Boson number operator, counts the number of bosons at position j
μ	Chemical potential of the bosons
U	Repulsive interaction between atoms in single lattice site
J	Hopping element which allow hopping of bosons between the nearest neighbor sites
$\hat{N}_b$	Boson number operator, counts the total number of atoms in the entire system
$\mathbf{H}_{MF}$	Mean-field Hamiltonian
$E_{MF}(\Psi_B)$	Ground state energy of H_{MF}
M	Number of lattice site

In Section 4.3

$\vert j\rangle$	For notational convenience, position state $\vert\psi_j\rangle$ is written as $\vert j\rangle$
$\mathbf{H}_{BH_2}$	Bose-Hubbard Hamiltonian for two-state atoms
$\hat{b}_{j\uparrow}$ and $\hat{b}^{\dagger}_{k\downarrow}$	Boson annihilation and creation operators at position j and k respectively. $\uparrow$ and $\downarrow$ represent the terms for atoms in state $\vert 0\rangle$ and $\vert 1\rangle$ respectively

In Section 4.5

$\vert 0_{BEC}\rangle$ and $\vert 1_{BEC}\rangle$	Macroscopic state of N condensed atoms in state $\vert 0\rangle$ and $\vert 1\rangle$.
z_R	Rayleigh range : distance at which the diameter of the laser beam size increases by a factor of $\sqrt{2}$.
ω_R	Rabi frequency.
Δ	Laser detuning from radio frequency (rf) resonance.

NOTATIONS INTRODUCED IN CHAPTER 5

In Section 5.2.1

$E_c(t)$	Entropy of the reduced density matrix to quantify the position - particle entanglement
λ_j	Eigenvalues of the reduced density matrix of the coin

In Section 5.2.2.1

$\|1_j\rangle$	$j-$th position is occupied
$\|0_j\rangle$	$j-$th position is unoccupied
$\|\Psi_{lat}\rangle$	State of the lattice

In Section 5.2.2.2

$\|\Psi_0^M\rangle = \bigotimes_{j=-\frac{M-1}{2}}^{j=\frac{M-1}{2}} \left(\frac{\|0\rangle + i\|1\rangle}{\sqrt{2}}\right) \otimes \|\psi_j\rangle$	Initial state of M particle system
A, B and C	label for 3 particles

In Section 5.3

$\|\psi\rangle$, $\|\psi_1\rangle \cdots \|\psi_k\rangle$	General form of state
E and $E(\|\Psi_{lat}\rangle)$	Meyer-Wallach measure for entanglement
ρ_i	Reduced density matrix of each subsystem i
ρ_j	Reduced density matrix of the j lattice point

Part I

Introduction

Chapter 1

Introduction

1.1 Introduction

Theoretical studies and experimental evidences from the early and mid twentieth century led us to consider the physical world is governed by laws of quantum mechanics (see any standard text book on quantum mechanics. For example, Feynman (1970) [4] and R. Shenkar (1994) [5]). This, in early 1980's led Yuri Manin (1980) [6] and Feynman (1982) [7] to independently observe and suggest that the physical world can be ideally simulated using quantum computers. A decade later, theoretical studies and the experimental possibility to construct quantum computers based on the laws of quantum mechanics such as superposition and interference between quantum amplitudes became one of the active areas of research [8, 9]. Deutsch algorithm (1985) [10] and Deutsch-Jozsa algorithm (1992) [11] were among the first algorithms to show that quantum computers are capable of solving certain computational problems much more efficiently than classical deterministic computers. Simon's algorithm (1994) was one of the first example to show that a quantum algorithm can solve the problem of computing an unknown function with a polynomial number of queries, where a classical algorithm required an exponential number of queries [12, 13]. In 1994, Shor devised a quantum algorithm to factor arbitrary integers exponentially faster than the best known classical counterpart [14, 15]. In 1996, Grover devised an algorithm which can in principle search an unsorted database quadratically faster than any known classical algorithm [16]. Shor's algorithm unleashed active research in the area of quantum information and quantum computation across a broad range of disciplines: quantum physics, computers science, mathematics and engineering. This research has unveiled many new effects that are strikingly different from their classical counterparts. Design and analysis of quantum algorithms to solve various problems more efficiently than classical algorithms has become a vibrant research area (see Mosca (2008) [17] and Childs and van Dam (2008) [18] for recent reviews).

Among classical algorithms, many are based on classical random walk. Markov chain simulation, which has emerged as a powerful algorithmic tool [19] is one such example. Like classical random walk, the quantum version of it has also become an important constituent of quantum algorithms and computation.

The quantum walk as it is known today is a generalization of the classical random walk developed by using the aspects of quantum mechanics such as superposition and interference of quantum amplitudes. In the classical random walk the particle moves in the position space with a certain probability, whereas the quantum walk, which involves a superposition of states, moves by exploring multiple possible paths simultaneously with the amplitudes corresponding to different paths interfering. This makes the variance of the quantum walk on a line to grow quadratically with the number of steps (time), compared to the linear growth for the classical random walk [20, 21]. A probabilistic result is obtained in quantum walk upon measurement. Figure 1.1 shows the comparative difference in the probability distribution of classical random walk and quantum walk.

Like its classical counterpart, which has found applications in almost all branches of sciences [22, 23], quantum walk has also proven to be a useful tool for quantum algorithms, to study, control and explain the dynamics in various physical systems. Below, we will briefly summarize the history of quantum walk and the progress made in employing it for quantum algorithms and the study of the dynamics of physical systems.

Though quantum random walk[1] was first introduced by Aharonov *et al.* (1993) [24], the idea of exploring multiple paths simultaneously using path integrals dates

---

[1] Unlike its classical counterpart, the evolution of the quantum version is unitary, reversible and has no randomness associated with it during the evolution. Therefore, keeping away the term 'random', quantum walk has been the preferred usage.

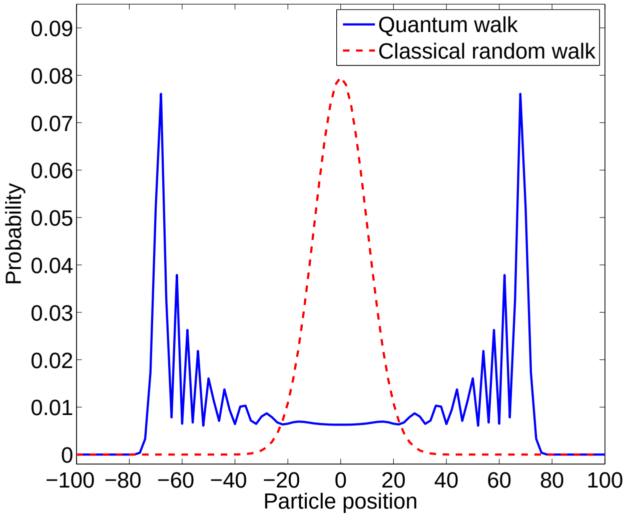

FIGURE 1.1: Probability distribution of classical random walk and its quantum counterpart, quantum walk. Difference in the variance can been seen in the distribution. The distribution is after 100 steps of walk.

back to works by Riazanov (1958) [25] and Feynman and Hibbs (1965) [26]. Meyer (1996) studied the dynamics of quantum particle in a quantum lattice gas formulation. The dynamics involved the interference of the left and the right moving components of the amplitude at given nodes [27, 28]. Building on these ideas, the concept of quantum walk was developed and now is studied in two standard forms: continuous-time quantum walk and discrete-time quantum walk. Continuous-time quantum walk was introduced by Farhi and Gutmann (1998) [29] and discrete-time quantum walk was introduced by Watrous (2001) [30]. A specific form of discrete-time quantum walk know as Hadamard walk was introduced by Ambainis *et al.* (2001) [20]. An early review by Kempe (2003) [31] discusses the two variants in detail with some algorithmic applications.

Both continuous- and discrete-time quantum walk have been widely used in algorithms for a variety of problems. Several quantum search algorithms have been proposed (see for example, Shenvi *et al.* (2003) [32]; Childs and Goldstone (2004) [33, 34]; Ambainis *et al.* (2005) [35]; Aaronson and Ambainis (2005) [36]; Magniez *et al.* (2007) [37]). The continuous-time quantum walk has been used by Childs *et al.* (2003) [38] to demonstrate the exponential speedup over classical computation for a hitting time problem on a glued tree. Ambainis (2004) [39] review discusses some of these algorithms in detail. Ambainis (2007) [40] applied quantum walk to give an optimal quantum algorithm for the element distinctness problem. It has been applied to various other problems in query model like triangle finding by Magniez *et al.* (2005) [41], checking matrix multiplication by Buhrman and Špalek (2006) [42], testing group commutativity by Maganiez and Nayak (2007) [43], for evaluating balanced binary game trees by Farhi *et al.* (2007)[44], Boolean formulas by Ambainis *et al.* (2007) [45] and Reichardt and Špalek [46] and to obtain general adversary bound to characterize the quantum query complexity by Reichardt [47].

Beyond applications in quantum algorithms, quantum walk is emerging as a potential tool to understand various phenomenon in physical systems and has been employed to demonstrate coherent control over quantum many body systems. Oka *et al.* (2005) [48] mapped the breakdown of electric-field driven system to quantum walk, Engel *et al.* (2007) [49] and Mohseni *et al.* (2008) [50] explained wavelike energy transfer within photosynthetic systems, Somma *et al.* (2008) [51] described quantum simulation of classical annealing processes, and Chandrashekar and Laflamme (2008) [52] demonstrated coherent quantum control over redistribution of atoms in optical lattice.

Some experimental progress on the implementation of quantum walk has been reported. Du *et al.* (2003) [53] and Ryan *et al.* (2005) [54] implemented continuous-time quantum walk on 2- qubit and discrete-time quantum walk on a 3- qubit Nuclear Magnetic Resonance (NMR) system respectively. Grossman *et al.* (2004) [55] with sodium Bose-Einstein condensates and recently, Perets *et al.* (2008) [56] using propagating photons in waveguide lattices have implemented the discrete-time quantum walk. Other implementation schemes have also been proposed: Travaglione and Milburn (2002) [57] in an ion trap, Dür *et al.* (2002) [58] and Eckert *et al.* (2005) [59] on neutral cold atoms in an optical traps, Chandrashekar (2006) [60] using Bose-Einstein condensates, Ma *et al.* (2006) [61] using quantum accelerator mode, Manouchehri and Wang (2008) [62] in an array of quantum dots and Sanders *et al.* (2003) [63] introduced quantum quincunx to physically demonstrate quantum walk in cavity quantum electrodynamics capabilities.

It is important to understand the dynamics and behavior of quantum walk, both in the presence and absence of environmental effects to effectively use it for developing algorithms, to simulate any natural physical process or to experimentally implement in any physical system. Considerable study has been done in this direction. Since this thesis involves results of some of these investigations, we will first list the main work that constitutes this thesis and briefly elaborate on them in the following sections.

The main constituents of this thesis are :

- Structure and dynamic properties of discrete-time quantum walk. Construction of a generalized model using quantum coin operation from SU(2) group to demonstrate control over the dynamics of the walk [64, 65].
- Using a coin-embedded shift operator, a generic quantum walk model which can be used to conveniently retrieve discrete- and continuous-time quantum walk under different conditions is proposed. The coin degree of freedom is retained while the standard variants are retrieved and the generic model simplifies the physical resources required to implement quantum walk compared to the resource required for the discrete-time quantum walk [66].
- Investigations on symmetries in discrete-time quantum walk on a line and its behavior in presence of environmental effects, breakdown of these symmetries for a walk on an $n-$cycle and restoration with noise. Relevance of these investigations in physical systems [67, 68].
- Demonstration of coherent control over the redistribution of atoms in optical lattice, use of noisy channels- bit flip, phase damping, and amplitude damping to act as an additional toolbox to control the dynamics of atoms and an experimental implementation scheme [52, 60].
- Spatial entanglement in many body system using quantum walk and its physical relevance [69].

1.2 Dynamics of quantum walk

In the continuous-time quantum walk, one can directly define the walk on the *position* Hilbert space $\mathcal{H}_p$ [29]. In the discrete-time quantum walk, in addition to $\mathcal{H}_p$ it is necessary to introduce a quantum coin operation, a *coin* Hilbert space $\mathcal{H}_c$ to define the direction in which the particle has to move [20]. Due to the coin degree of freedom, the discrete-time variant is shown to be more powerful than the other in some contexts (see Ambainis *et al.* (2005) [35]). To match the performance of a spatial search using the discrete-time quantum walk, the coin degree of freedom has been introduced in the continuous-time quantum walk model [34]. In this thesis, we mainly consider the discrete-time quantum walk for our study.

The dynamics of discrete-time quantum walk using the Hadamard operation

$$H \equiv \frac{1}{\sqrt{2}}\begin{pmatrix} 1 & 1 \\ 1 & -1 \end{pmatrix} \tag{1.1}$$

as quantum coin operation was analyzed and defined as Hadamard walk [20]. Most of the work thereafter on discrete-time quantum walk considered using Hadamard operation as quantum coin operation. Nayak and Vishwanath (2001) [21] analyzed using the single-variable parameter U(2) operator

$$B_\theta \equiv \begin{pmatrix} \cos(\theta) & \sin(\theta) \\ \sin(\theta) & -\cos(\theta) \end{pmatrix} \tag{1.2}$$

as a quantum coin[2]. The variance σ^2 was shown to be dependent on the parameter θ. The discrete-time quantum walk on a particle initially in a symmetric superposition state ($\frac{1}{\sqrt{2}}(|0\rangle + i|1\rangle)$) at position space ($|\psi_0\rangle$), $|\Psi_{ins}\rangle = \frac{1}{\sqrt{2}}(|0\rangle + i|1\rangle) \otimes |\psi_0\rangle$ using B_θ as the quantum coin was shown to return the symmetric probability distribution of the walk in the position space. Asymmetry in the initial state of the particle introduced an asymmetric probability distribution. This led to their conclusion that obtaining a symmetric distribution depends largely on the initial state of the particle [20, 21, 70].

---

[2] Meyer has used the U(2) operator as a scattering operator in lattice quantum gas automata model [27]

In Chapter 2, we will first define the continuous-time and discrete-time quantum walk, equivalence of their form to the Schrödinger and Dirac equations respectively. In Section 2.3.2, we present the discrete-time quantum walk using operation from the SU(2) group with three Caley-Klein parameters ξ, θ and ζ (Euler angles) as the quantum coin

$$B_{\xi,\theta,\zeta} \equiv \left(\begin{array}{cc} e^{i\xi}\cos(\theta) & e^{i\zeta}\sin(\theta) \\ -e^{-i\zeta}\sin(\theta) & e^{-i\xi}\cos(\theta) \end{array} \right). \tag{1.3}$$

We show that the variance is dependent on the parameter θ and takes the form $\sigma^2 \approx (1-\sin(\theta))t^2$, where t is number of steps of the quantum walk. For a particle with symmetric superposition as the initial state parameters ξ and ζ introduce asymmetry in the probability distribution and their effect on the variance is very small. For a particle with an asymmetric superposition as the initial state, the parameters ξ and ζ can be configured to obtain a symmetric probability distribution. We discuss the variation of measurement entropy in position space with the coin parameters and optimization of the quantum walk for the maximum variance, improving mixing time in an n-cycle and controlling the probability distribution using coin parameters [64].

Recurrence in the dynamics of physical systems is an important phenomenon. For a classical conservative system, whether discrete or continuous in time, the Poincaré recurrence theorem states that any phase-space configuration of a system enclosed in a finite volume will be repeated as accurately as one wishes after a finite interval of time (with no restriction on the interval) [71, 72]. A similar recurrence theorem is shown to hold in quantum theory as well [73, 74]. In a system with a discrete energy eigenvalue spectrum $\{E_n\}$; if $\Psi(t_0)$ is its state vector at the time t_0 and ϵ is any positive number, there exists a finite time T such that,

$$|\Psi(T) - \Psi(t_0)| < \epsilon. \tag{1.4}$$

Robinett's (2004) [75] review article discusses recurrence in quantum systems. In Section 2.4, we show the discrete-time quantum walk which evolves with interference of quantum amplitudes fails to recur completely in position space but fractional recurrence is seen [65].

Chapter 3 focuses on the symmetries and effects of noise on the dynamics of discrete-time quantum walk. The transition of walk from the quantum to the classical regime has been studied earlier by introducing decoherence to Hadamard walk [76–78](see review by Kendon (2006) [79]). In a scheme proposed by Chandrashekar [60] to implement the discrete-time quantum walk on Bose-Einstein condensates, stimulated Raman kick was used as shift operator. The stimulated Raman kick, in addition to shifting different states of atoms to different position space flips (bit-flip) the internal state of the atoms. However in spite of bit-flip on state of atoms along with shift in position space, the probability distribution remained invariant in position space. Motivated by this, the shift operator was augmented by other form of operations and the operation for which the distribution remains invariant have been studied and are called symmetries of quantum walk. These symmetries have been studied using generalized SU(2) coin operation $B_{0,\theta,0}$ as quantum coin. We further generalize the observations of these symmetries in the presence of environmental effects, modeled by various noise channels such as bit flip, phase-flip and generalized amplitude damping channels [67]. Interestingly, we find that the symmetry operations are sensitive to the walk topology. For example, a symmetry that holds for quantum walk on an one-dimensional line does not hold, in general, for a quantum walk on an $n-$cycle but leads to other interesting behavior. Noise on an $n-$cycle tends to restore these symmetry, both by “classicalizing” the walk and also desensitizing the symmetry operation as a topology probe for the quantum walk [68]. From Chapter 2, we can conclude that the symmetries and addition of small amount of experimentally engineered noise or environmental effect can be used as an additional tool to control the dynamics and hence the probability distribution of the quantum walk. These observations can have important implications for a better insight into quantum walk, and for simplifying certain implementations and are also of relevance in the study of dynamics in environment-assisted quantum systems.

1.3 Applications

By employing the properties of quantum walks due to purely quantum dynamics and small amount of engineered noise presented in Chapters 2 and 3, we demonstrate coherent quantum control over atoms in optical lattice in Chapter 4. Traditionally, theoretical studies of the dynamics of atoms in an optical lattice are done using mean field approaches [80] and quantum Monte Carlo methods [81–83]. Use of quantum walk can serve as an alternate method. In particular, we will consider the quantum phase transition from the Mott insulator (MI) to the superfluid (SF) state [84, 85] and vice versa. The simulation of the quantum phase transition using the quantum walk occurs quadratically faster in one dimension (1D) compared to varying the optical lattice depth and letting the atom-atom interaction follow the classical random walk behavior. In our study, we use the noise models discussed in Chapter 3 to act as an enhanced toolbox to control the redistribution of atoms in an optical lattice [52]. We will also discuss the experimental implementation of quantum walk on ultra cold atoms in an optical lattice [60].

Entanglement in many body system has not only been a computational resource, it has also been used as a signature of quantum phase transition [86–88]. With increase in dimension of the Hilbert space, the number of invariants and the measures of entanglement grows exponentially so that scaling becomes impractical. In 2002, Meyer and Wallach proposed a global entanglement measure - a polynomial measure of multiparticle entanglement to address the scalability problem [89]. In Chapter 5 we investigate the evolution of spatial entanglement, particle-number entanglement between regions of space in a many particle system subjected to quantum walk evolution using Meyer-Wallach measure. We use the coin degree of freedom to demonstrate the dependency of entanglement with the coin parameter, number of particles in the system and number of steps of quantum walk.

Part II

Quantum Walks and Its Dynamics

Chapter 2

Quantum walks

2.1 Introduction

Quantum walks are the quantum analog of the classical random walks [24–26] developed using the aspects of quantum mechanics such as interference and superposition. Like their classical counterpart, the quantum walks are also widely studied in two forms: continuous-time quantum walk and discrete-time quantum walk. In the continuous-time quantum walk, one can directly define the walk on the position space [29], whereas in the discrete-time quantum walk, it is necessary to introduce a quantum coin operation to define the direction in which the particle has to move [20]. The results from the continuous-time quantum walk and the discrete-time quantum walk are often similar, but due to the coin degree of freedom, the discrete-time variant has been shown to be more powerful than the other in some context [35]. To match the performance of the discrete-time quantum walk, the coin degree of freedom can be introduced in the continuous-time quantum walk [34]. We will only consider the discrete-time quantum walk for our study.

The main focus of this chapter is to present in detail the dynamics of the discrete-time quantum walk and demonstrate methods to control it. This chapter is organized as follows. For the completeness, we will first review the continuous-time quantum walk in Section 2.2. In Section 2.3, we will review the discrete-time quantum walk before demonstrating the optimization and randomization of the dynamics using quantum coin operations from the SU(2) group. In Section 2.4, we discuss the fractional recurrence nature of the quantum walk and conclude with a summary in Section 2.5.

2.2 Continuous-time quantum walk

To define the continuous-time quantum walk, it is easier to first define the continuous-time classical random walk and quantize it by introducing quantum amplitudes in place of classical probabilities.

The continuous-time classical random walk takes place entirely in the *position* space. To illustrate, let us define continuous-time classical random walk on the position space $\mathcal{H}_p$ spanned by a vertex set V of a graph G with edges set E, $G = (V, E)$. A step of the random walk can be described by a adjacency matrix A which transform the probability distribution over V, i.e.,

$$A_{j,k} = \begin{cases} 1 & (j,k) \in E \\ 0 & (j,k) \notin E \end{cases} \tag{2.1}$$

for every pair $j, k \in V$. The other important matrix associated with the graph G is the generator matrix $\mathbf{H}$ given by

$$\mathbf{H}_{j,k} = \begin{cases} d_j\gamma & j = k \\ -\gamma & (j,k) \in E \ , \\ 0 & \text{otherwise} \end{cases} \tag{2.2}$$

where d_j is the degree of the vertex j and γ is the probability of transition between neighboring nodes per unit time.

If $P_j(t)$ denotes the probability of being at vertex j at time t then the transition on graph G is defined as the solution of differential equation

$$\frac{d}{dt}P_j(t) = -\sum_{k\in V} \mathbf{H}_{j,k} P_k(t). \tag{2.3}$$

The solution of the differential equation is given by

$$P(t) = e^{-\mathbf{H}t}P(0). \tag{2.4}$$

By replacing the probabilities P_j by quantum amplitudes $a_j(t) = \langle j|\psi(t)\rangle$ where $|j\rangle$ is spanned by the orthogonal basis of the position Hilbert space $\mathcal{H}_p$ and introducing a factor of i we obtain

$$i\frac{d}{dt}a_j(t) = \sum_{k\in V}\mathbf{H}_{j,k}a_k(t). \tag{2.5}$$

We can see that (2.5) is the Schrödinger equation

$$i\frac{d}{dt}|\psi\rangle = \mathbf{H}|\psi\rangle. \tag{2.6}$$

Since generator matrix is an Hermitian operator, the normalization is preserved during the dynamics. The solution of the differential equation can be written in the form

$$|\psi(t)\rangle = e^{-i\mathbf{H}t}|\psi(0)\rangle. \tag{2.7}$$

Therefore, the continuous-time quantum walk is of the form of Schrödinger equation, a non-relativistic quantum evolution.

To implement the continuous-time quantum walk on a line, the position Hilbert space $\mathcal{H}_p$ can be written as a state spanned by the basis states $|\psi_j\rangle$, where $j \in \mathbb{Z}$. The Hamiltonian $\mathbf{H}$ is defined such that,

$$\mathbf{H}|\psi_j\rangle = -\gamma|\psi_{j-1}\rangle + 2\gamma|\psi_j\rangle - \gamma|\psi_{j+1}\rangle \tag{2.8}$$

and is made to evolve with time t by applying the transformation

$$U(t) = \exp(-i\mathbf{H}t). \tag{2.9}$$

The Hamiltonian $\mathbf{H}$ of the process acts as the generator matrix which will transform the probability amplitude at the rate of γ to the neighboring sites, where γ is time-independent constant.

2.3 Discrete-time quantum walk

We will first define the structure of the discrete-time classical random walk. The discrete-time classical random walk takes place on the position Hilbert space $\mathcal{H}_p$ with instruction from the coin operation. A coin flip defines the direction in which the particle moves and a subsequent position shift operation moves the particle in position space. For a walk on a line, a two sided coin with *head* and *tail* defines the movements to the *left* and *right* respectively.

The discrete-time quantum walk also has a very similar structure to that of its classical counterpart. The coin flip is replaced by the quantum coin operation which defines the superposition of direction in which the particle moves simultaneously. The quantum coin operation followed by the unitary shift operation is iterated without resorting to intermediate measurement to implement a large number of steps. During the walk on a line, interference between the left and the right propagating amplitude results in the quadratic growth of variance with the number of steps.

The discrete-time quantum walk on a line is defined on a Hilbert space

$$\mathcal{H} = \mathcal{H}_c \otimes \mathcal{H}_p, \tag{2.10}$$

where $\mathcal{H}_c$ is the *coin* Hilbert space and $\mathcal{H}_p$ is the *position* Hilbert space. For a discrete-time quantum walk in one dimension, $\mathcal{H}_c$ is spanned by the basis state (internal state) of the particle $|0\rangle$ and $|1\rangle$ and $\mathcal{H}_p$ is spanned by the basis state of the position $|\psi_j\rangle$, where $j \in \mathbb{Z}$. To implement the discrete-time quantum walk on a particle at origin in state

$$|\Psi_{in}\rangle = \big(\cos(\delta)|0\rangle + e^{i\eta}\sin(\delta)|1\rangle\big) \otimes |\psi_0\rangle, \tag{2.11}$$

the quantum coin toss operation $B \in U(2)$ which in general can be written as

$$B_{\zeta,\alpha,\beta,\gamma} = e^{i\zeta} e^{i\alpha\sigma_x} e^{i\beta\sigma_y} e^{i\gamma\sigma_z} \tag{2.12}$$

is applied. Where σ_x, σ_y and σ_z are the Pauli spin operators. Parameters of the coin operations $\zeta, \alpha, \beta, \gamma$ can be varied to get different superposition state of the particle. That is, quantum coin operation B is used to evolve the particle to superposition of its basis states such that it can serve as an instruction to shift to the *left* and *right* of its initial position in superposition. The quantum coin operation is followed by the conditional unitary shift operation S given by

$$S = e^{-i(|0\rangle\langle 0| - |1\rangle\langle 1|)\otimes Pl} = \left(|0\rangle\langle 0| \otimes e^{-iPl}\right) + \left(|1\rangle\langle 1| \otimes e^{iPl}\right) \tag{2.13}$$

where P is the momentum operator, l is the step length and $|0\rangle$ and $|1\rangle$ are the basis states of the particle. Therefore the operator S which delocalizes the wave packet in different basis states $|0\rangle$ and $|1\rangle$ over the position $(j-1)$ and $(j+1)$ when when step length $l = 1$ can also be written as

$$S = |0\rangle\langle 0| \otimes \sum_{j\in\mathbb{Z}} |\psi_{j-1}\rangle\langle\psi_j| + |1\rangle\langle 1| \otimes \sum_{j\in\mathbb{Z}} |\psi_{j+1}\rangle\langle\psi_j|. \tag{2.14}$$

The states in the new position is again evolved into the superposition of its basis state and the process of quantum coin toss operation $B_{\zeta,\alpha,\beta,\gamma}$ followed by the conditional unitary shift operation S,

$$W_{\zeta,\alpha,\beta,\gamma} = S(B_{\zeta,\alpha,\beta,\gamma} \otimes \mathbb{1}) \tag{2.15}$$

is iterated without resorting to intermediate measurement, to realize a large number of steps of the discrete-time quantum walk. The four variable parameters of the quantum coin, ζ, α, β and γ (2.12) can be varied to change and control the probability amplitude distribution in the position space.

Most widely studied form of the discrete-time quantum walk is the Hadamard walk, using Hadamard operation H as quantum coin operation and the role of coin operation and initial state to control the probability amplitude distribution has been discussed in earlier studies [20, 90]. We will discuss the Hadamard walk in detail in Section 2.3.1. In Section 2.3.2, we demonstrate that a three parameter SU(2) quantum coin operation is sufficient to describe the most general form of the discrete-time quantum walk. Before that, we will further analyze the structure of the discrete-time quantum walk.

Discrete-time quantum walk and Dirac equation :

The standard symmetric discrete-time classical random walk leads to

$$P(j, \tau + 1) = \frac{1}{2} \left[P(j-1, \tau) + P(j+1, \tau) \right], \tag{2.16}$$

where $P(j, \tau)$ denotes the probability of finding the particle at position j at discrete time τ. Subtracting $P(j, \tau)$ from both sides of (2.16) leads to the difference equation which corresponds to differential equation

$$\frac{\partial}{\partial \tau} P(j, \tau) = \frac{\partial^2}{\partial^2 j} P(j, \tau). \tag{2.17}$$

The above equation is irreversible because the coin is effectively thrown away after each toss. It is also non-relativistic in the sense that it is not symmetric in time and space, and leads to a dispersion relation that is essentially non-relativistic [91]. In the continuum limit, (2.17) leads to the standard classical diffusion. On the contrary, in the discrete-time quantum walk the information of the state of the quantum coin in the previous step is retained and carried over to the next step. This makes the quantum walk reversible.

To illustrate this, we consider the wavefunction describing the position of a particle and analyze how it evolves with time τ. Let τ be the time required to implement t steps of quantum walk. The two component vector of amplitudes of the particle, being at position j, at time τ, with right (R) and left (L) moving component is given by

$$\Psi(j, \tau) = \begin{pmatrix} \Psi_R(j, \tau) \\ \Psi_L(j, \tau) \end{pmatrix}. \tag{2.18}$$

The dynamics for Ψ driven by single parameter quantum coin operation is :

$$B = \begin{pmatrix} \cos(\theta) & -i \sin(\theta) \\ -i \sin(\theta) & \cos(\theta) \end{pmatrix} \tag{2.19}$$

and followed by the conditional shift operator S in terms of left moving and right moving component is given by

$$\begin{pmatrix} \Psi_R(j, \tau+1) \\ \Psi_L(j, \tau+1) \end{pmatrix} = S(B \otimes \mathbb{1}) \begin{pmatrix} \Psi_R(j, \tau) \\ \Psi_L(j, \tau) \end{pmatrix} \tag{2.20}$$

$$\begin{aligned} \Psi_R(j, \tau+1) &= \cos(\theta)\Psi_R(j-1, \tau) - i\sin(\theta)\Psi_L(j-1, \tau) \\ \Psi_L(j, \tau+1) &= \cos(\theta)\Psi_L(j+1, \tau) - i\sin(\theta)\Psi_R(j+1, \tau). \end{aligned} \tag{2.21}$$

We thus find that the coin degree of freedom is carried over during the dynamics of the quantum walk making it reversible.

Further, the components Ψ_L and Ψ_R are decoupled to obtain

$$\Psi_R(j, \tau+1) + \Psi_R(j, \tau-1) = \cos(\theta)[\Psi_R(j+1, \tau) + \Psi_R(j-1, \tau)]. \tag{2.22}$$

Subtracting $2\Psi_R(j, \tau)$ from both sides, we obtain a difference equation which corresponds to differential equation

$$\left[\cos(\theta)\frac{\partial^2}{\partial^2 j}(j, \tau) - \frac{\partial^2}{\partial^2 \tau}(j, \tau)\right] \Psi_R(j, \tau) = 2(1 - \cos(\theta))\Psi_R(j, \tau), \tag{2.23}$$

and similar expression can be obtained for $\Psi_L(j, \tau)$, see Appendix A for intermediate steps. This shows that each component follows a Klein-Gordon equation of the form

$$\left(\nabla^2 - \frac{1}{c^2}\frac{\partial^2}{\partial^2 \tau}\right)\phi - \mu^2\phi = 0 \tag{2.24}$$

showing the essentially relativistic character of the discrete-time quantum walk. Equation (2.21) can also be written as a compact first-order difference equation, which in the continuum limit would be analogous to the one-dimensional Dirac equation for a spinor (of spin 1/2).

Setting the time-step and spatial-step to 1, we obtain from (2.23), the equivalent of light speed c and mass m in the discrete-time quantum walk dynamics :

$$c \equiv \sqrt{\cos(\theta)}$$

$$\mu = \frac{mc}{\hbar} \quad \equiv \quad \sqrt{2(1 - \cos(\theta))}. \tag{2.25}$$

Thus, from Section 2.2 and the above analysis we conclude that a continuous-time quantum walk takes the form of Schrödinger equation and a discrete-time quantum walk takes the form of Dirac equation.

2.3.1 Hadamard walk

The simplest version of the discrete-time quantum walk is the walk using Hadamard operation as quantum coin operation and is known as the Hadamard walk [20]. A particle at origin in one of the basis state $|0\rangle$ or $|1\rangle$ of $\mathcal{H}_c$ (internal state of the particle) is evolved into the superposition of $\mathcal{H}_c$ with equal probability, by applying the Hadamard operation

$$H = \frac{1}{\sqrt{2}} \begin{pmatrix} 1 & 1 \\ 1 & -1 \end{pmatrix}, \tag{2.26}$$

such that

$$\begin{aligned} (H \otimes \mathbb{1})(|0\rangle \otimes |\psi_0\rangle) &= \frac{1}{\sqrt{2}}(|0\rangle + |1\rangle) \otimes |\psi_0\rangle \\ (H \otimes \mathbb{1})(|1\rangle \otimes |\psi_0\rangle) &= \frac{1}{\sqrt{2}}(|0\rangle - |1\rangle) \otimes |\psi_0\rangle. \end{aligned} \tag{2.27}$$

The operation H is then followed by the conditional shift operation S (2.14), $W = S(H \otimes \mathbb{1})$. The process is iterated without resorting to intermediate measurements to evolve the particle in superposition of position space and realize a large number of steps of the Hadamard walk. After the first two iterations of W, the left and right moving components of the amplitude begin to interfere, deviating from the classical evolution, resulting in a quadratic speedup in the growth of the variance. The probability amplitude distribution arising from the iterated application of W is significantly different from the probability distribution of the classical random walk, Figure 2.1. The particle initially in the state $|0\rangle$ drifts to the left and the particle with an initial state $|1\rangle$ drifts to the right. This asymmetry arises from the fact that the Hadamard operation treats the two states $|0\rangle$ and $|1\rangle$ differently, phase difference of -1 in case of state $|1\rangle$. This phase difference, depending on the initial state of the particle contributes to the constructive interference on one side and to the destructive interference on the other side of the position space.

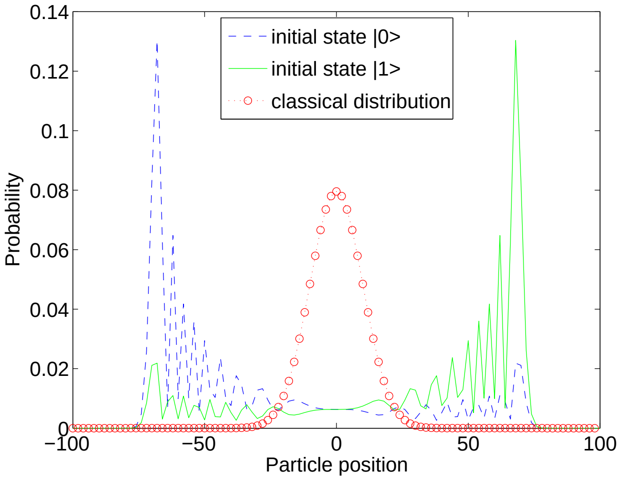

FIGURE 2.1: Spread of probability distribution of the Hadamard walk with the initial state $|0\rangle$ (dashed line) and initial state $|1\rangle$ (solid line) on the position space along with distribution of the classical random walk (dashed-circle). The distribution is for 100 steps.

To obtain left-right symmetry in the probability distribution, Figure 2.3(b), one needs to start the walk with the particle initially in a symmetric superposition state

$$|\Psi_{ins}\rangle \equiv \frac{1}{\sqrt{2}}\left(|0\rangle + i|1\rangle\right) \otimes |\psi_0\rangle. \tag{2.28}$$

For Hadamard walk on the line it is shown that after t steps, the probability distribution is spread over the interval $[\frac{-t}{\sqrt{2}}, \frac{t}{\sqrt{2}}]$ and reduce quickly outside this region [20]. The moments have been calculated for asymptotically large number of steps t and the variance is shown to vary as

$$\sigma^2(t) = \left(1 - \frac{1}{\sqrt{2}}\right) t^2. \tag{2.29}$$

Hadamard walk has been extensively studied and the symmetric distribution depends on the initial state of the particle (see [20, 21, 70, 92]).

In the following section we will present a quantum walk using an operation from SU(2) group as a generalized quantum coin. The parameters in the SU(2) group will give control over the dynamics and amplitude distribution of the quantum walk. This eliminates the role of initial state of the particle to obtain a symmetric amplitude distribution.

2.3.2 Optimization using SU(2) coin

In the introduction to this section we defined a discrete-time quantum walk using $B \in$U(2) (2.12) as quantum coin operation. To control and optimize the dynamics of the discrete-time quantum walk we consider the three parameter operator from the group SU(2) rather than the complete U(2) operator. Apart from the global phase which does not affect the amplitude distribution, the effect of U(2) operator on the quantum walk can be completely reproduced using SU(2) operator.

We consider the group SU(2) which has for its elements, matrices of the form

$$B = \begin{pmatrix} \alpha & \beta \\ -\beta^* & \alpha^* \end{pmatrix} = \begin{pmatrix} \alpha_1 + i\alpha_2 & \beta_1 + i\beta_2 \\ -\beta_1 + i\beta_2 & \alpha_1 - i\alpha_2 \end{pmatrix}, \qquad \alpha_1^2 + \alpha_2^2 + \beta_1^2 + \beta_2^2 = 1. \tag{2.30}$$

as the generalized quantum coin operation. α's and β's are real values. For our present purpose the parametrization of SU(2) in terms of Euler angles turns out to be the convenient one,

$$B_{\xi,\theta,\zeta} \equiv \begin{pmatrix} e^{i\xi}\cos(\theta) & e^{i\zeta}\sin(\theta) \\ -e^{-i\zeta}\sin(\theta) & e^{-i\xi}\cos(\theta) \end{pmatrix}. \tag{2.31}$$

We can get the Hadamard operator up to global phase by choosing $\zeta = \xi = \pi/2$, $\theta = \pi/4$ or by choosing $\zeta = \xi = 0$, $\theta = \pi/4$ and multiplying the operator by σ_z from left.

For the analysis of generalized discrete-time quantum walk we consider the initial state of a particle to be in the symmetric superposition of basis states $|\Psi_{ins}\rangle$ (2.28).

Implementing $W_{\xi,\theta,\zeta} = S(B_{\xi,\theta,\zeta} \otimes \mathbb{1})$ on $|\Psi_{ins}\rangle$ evolves the particle to,

$$\begin{aligned} W_{\xi,\theta,\zeta}|\Psi_{ins}\rangle = \frac{1}{\sqrt{2}} \Big[&\big(e^{i\xi}\cos(\theta) + ie^{i\zeta}\sin(\theta)\big)\,|0\rangle \otimes |\psi_{-1}\rangle \\ &+ \big(-e^{-i\zeta}\sin(\theta) + ie^{-i\xi}\cos(\theta)\big)\,|1\rangle \otimes |\psi_{+1}\rangle \Big]. \end{aligned} \tag{2.32}$$

The position probability distribution in (2.32) after first step corresponding to the left and right positions are $\frac{1}{2}[1 \pm \sin(2\theta)\sin(\xi - \zeta)]$. These probability distribution would be equal and lead to a left-right symmetry in position, if and only if $\xi = \zeta$. That is, the parameters $\xi \neq \zeta$ introduce asymmetry in the position space probability distribution from the first step itself. The effect of different values of coin parameters after 100 steps of walk is shown in Figure 2.2 plotted using numerically obtained values. We thus find that the generalized operator $B_{\xi,\theta,\zeta}$ as a quantum coin can bias the probability distribution of the quantum walk in spite of the symmetry of initial state of the particle. This is not true in case of the Hadamard walk, where obtaining symmetric distribution depends largely on the initial state of the particle [20, 21, 70, 92]. This can be verified by substituting $\xi = \zeta = 0, \theta = \pi/4$ and multiplying the components of state $|1\rangle$ in (2.32) by -1.

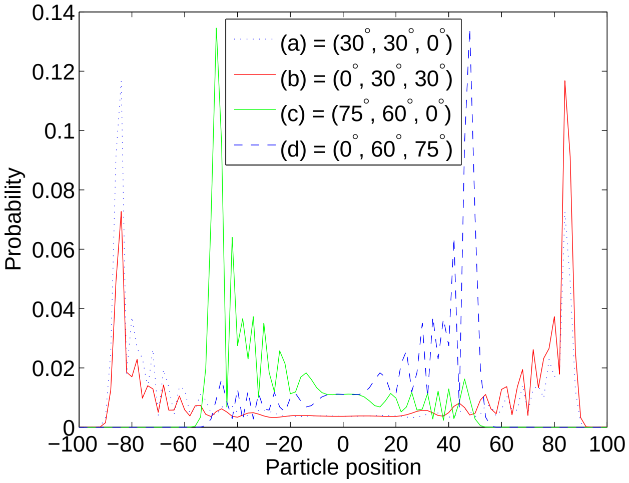

FIGURE 2.2: Spread of probability distribution for different values of ξ, θ, ζ using quantum coin operator $B_{\xi,\theta,\zeta}$. Parameter ξ shifts the distribution to the left: (a) $= (\frac{\pi}{6}, \frac{\pi}{6}, 0)$ and (c) $= (\frac{5\pi}{12}, \frac{\pi}{3}, 0)$. Parameter ζ shifts it to the right: (b) $= (0, \frac{\pi}{6}, \frac{\pi}{6})$ and (d) $= (0, \frac{\pi}{3}, \frac{5\pi}{12})$. The initial state of the particle $|\Psi_{ins}\rangle = \frac{1}{\sqrt{2}}(|0\rangle + i|1\rangle) \otimes |\psi_0\rangle$ and the distribution is for 100 steps.

The walk beyond the first step involves interference and hence, it is appropriate to analyze the evolution after t steps using $B_{\xi,\theta,\zeta}$ as coin operator. The analysis shows how non-vanishing ξ and ζ introduces bias. Therefore, the state after t steps can be written as

$$[W_{\xi,\theta,\zeta}]^t|\Psi_{ins}\rangle = |\Psi(t)\rangle = \sum_{m=-t}^{t} (\mathcal{A}_{m,t}|0\rangle|\psi_m\rangle + \mathcal{B}_{m,t}|1\rangle|\psi_m\rangle) \tag{2.33}$$

and proceeds according to the iterative relations,

$$\mathcal{A}_{m,t} = e^{i\xi}\cos(\theta)\mathcal{A}_{m+1,t-1} + e^{i\zeta}\sin(\theta)\mathcal{B}_{m+1,t-1} \tag{2.34a}$$

$$\mathcal{B}_{m,t} = e^{-i\xi}\cos(\theta)\mathcal{B}_{m-1,t-1} - e^{-i\zeta}\sin(\theta)\mathcal{A}_{m-1,t-1}. \tag{2.34b}$$

After $(t+1)^{\text{th}}$ step, $\mathcal{A}_{m,t}$ and $\mathcal{B}_{m,t}$ shifts to position $(m-1)$ and $(m+1)$ respectively. A little algebra reveals that the solutions to $\mathcal{A}_{m,n}$ and $\mathcal{B}_{m,n}$ (2.34) can be decoupled and shown to satisfy the following equations :

$$\mathcal{A}_{m,t} = \cos(\theta)\left(e^{i\xi}\mathcal{A}_{m+1,t-1} + e^{-i\xi}\mathcal{A}_{m-1,t-1}\right) - \mathcal{A}_{m,t-2} \tag{2.35a}$$

$$\mathcal{B}_{m,t} = \cos(\theta)\left(e^{i\xi}\mathcal{B}_{m+1,t-1} + e^{-i\xi}\mathcal{B}_{m-1,t-1}\right) - \mathcal{B}_{m,t-2}. \tag{2.35b}$$

The decoupled expression (2.35) shows dependence of amplitude on the values from previous two steps. By repeatedly substituting the dependence relation for amplitudes on the right hand side of (2.35) until amplitude term at $t = 0$ appears, reveals the dependency of $\mathcal{A}_{m,t}$ and $\mathcal{B}_{m,t}$ on amplitudes of the initial state and coin operation (2.32). We know that to obtain a spatial symmetry of the probability distribution from a particle initially in symmetric superposition state, the walk should be invariant under an exchange of $|0\rangle \leftrightarrow |1\rangle$, and hence should evolve $\mathcal{A}_{m,t}$ and $\mathcal{B}_{m,t}$ alike (as in the Hadamard walk [93]). From the above analysis we see that $\mathcal{A}_{m,t}$ and $\mathcal{B}_{m,t}$ are symmetric to each other and evolve alike for all value of θ only when $\xi = \zeta$. Positive ζ contributes to constructive interference towards right and destructive interference to the left, and vice versa in case of ξ, as shown in Figure 2.2. The inverse effect can be noticed when the ξ and ζ are negative.

One can show that the coin operator

$$B_{\xi,\theta,\zeta} = \begin{pmatrix} e^{i\zeta} & 0 \\ 0 & e^{-i\zeta} \end{pmatrix} B_{\xi-\zeta,\theta,0} = \begin{pmatrix} e^{i\xi} & 0 \\ 0 & e^{-i\xi} \end{pmatrix} B_{0,\theta,\zeta-\xi}. \tag{2.36}$$

Setting $\xi \neq \zeta$ introduce asymmetry, biasing the walk. Therefore, a quantum coin operation $B_{\xi,\theta,\zeta}$ when $\xi \neq \zeta$ can be called as a *biased quantum coin operation* on a particle initially in symmetric superposition state[1]. In Figure 2.2 we show the biasing effect for $(\xi, \theta, \zeta) = (0^\circ, 60^\circ, 75^\circ)$ and for $(75^\circ, 60^\circ, 0^\circ)$.

From (2.35) we know that only when $\xi = \zeta$ the quantum walk on a particle initially in symmetric superposition state evolve symmetrically in position space. From Section 2.3.1 we also know that the Hadamard walk on particle initially in basis state $|0\rangle$ biases the distribution to the left and in state $|1\rangle$ biases the distribution to the right. Therefore, for a particle initially in symmetric superposition state, by varying the parameter ξ and ζ the results obtained for walk starting with one of the basis $|0\rangle$ or $|1\rangle$ (or any other nonsymmetric superposition) state can be reproduced. Similarly, a particle initially in one of its basis states $|0\rangle$ or $|1\rangle$ can also be evolved to obtain symmetric probability distribution by making an appropriate choice of the parameter ξ and ζ. For example, quantum walk on a particle initially in state $|0\rangle$ with coin parameters θ being any value, $\xi = 0$ and $\zeta = \pi/2$ and for a particle initially in state $\rangle$, $\xi = \pi/2$ and $\zeta = 0$ return a symmetric probability distribution in the position space (symmetric distribution similar for Figure 2.3). Therefore quantum coin operation $B_{\xi,\theta,\zeta}$ and initial state of the particle complement each other. The variance can be varied using the parameter θ. Compared to the Hadamard walk or a walk using single variable parameter unitary coin [21], a walk using a SU(2) operator as a quantum coin gives better access to control the dynamics of discrete-time quantum walk irrespective of the initial state of particle.

We note that using of three parameter operator $\mathrm{U}(2) \neq \mathrm{SU}(2)$ of the form

$$B'_{\xi,\theta,\zeta} \equiv \begin{pmatrix} e^{i\xi}\cos(\theta) & e^{i\zeta}\sin(\theta) \\ e^{-i\zeta}\sin(\theta) & -e^{-i\xi}\cos(\theta) \end{pmatrix} \tag{2.37}$$

---

[1] It should be noted that for a particle initially in one of its basis state $|0\rangle$ or $|1\rangle$, the coin operation $B_{0,\theta,0}$ itself biases the walk, state $|0\rangle$ to the left and $|1\rangle$ to the right. When the initial state is a symmetric superposition of the basis state, the biasing on state $|0\rangle$ is compensated by biasing on state $|1\rangle$ leaving the effective walk distribution symmetric.

in place of $B_{\xi,\theta,\zeta}$ will also produce the same effect on amplitude distribution during the quantum walk evolution. That is,

$$S(B_{\xi,\theta,\zeta} \otimes \mathbb{1})|\Psi_{ins}\rangle \equiv S(B'_{\xi,\theta,\zeta} \otimes \mathbb{1})|\Psi_{ins}\rangle \tag{2.38}$$

when $|\Psi_{ins}\rangle$ is (2.28). The operator $B'_{\xi,\theta,\zeta}$ reproduces the Hadamard operation for $\xi = \zeta = 0$ and $\theta = \pi/4$ (whereas $B_{\xi,\theta,\zeta}$ needs an additional Pauli z operation, σ_z). For the convenience of reproducibility of properties of Hadamard walk, in this thesis we will switch between these two operators since it does not alter any of the results. We justify this claim as the existence of symmetries in quantum walk in Chapter 3.

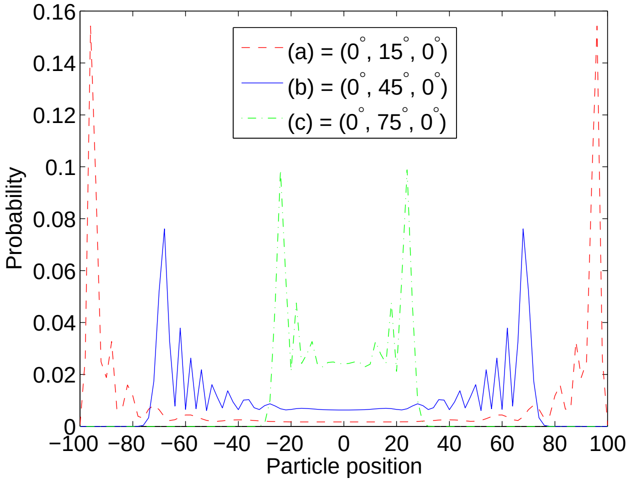

FIGURE 2.3: Spread of probability distribution for different values of θ using the quantum coin operator $B_{0,\theta,0}$. The distribution is wider for (a) $= (0, \frac{\pi}{12}, 0)$ than for (b) $= (0, \frac{\pi}{4}, 0)$ and (c) $= (0, \frac{5\pi}{12}, 0)$, showing the decrease in spread with increase in θ. The initial state of the particle $|\Psi_{ins}\rangle = \frac{1}{\sqrt{2}}(|0\rangle + i|1\rangle) \otimes |\psi_0\rangle$ and the distribution is for 100 steps.

Approximating the variance:

The effect of parameter θ in coin operation $B_{\xi,\theta,\zeta}$ on the distribution when $\xi = \zeta = 0$ is shown in Figure 2.3, obtained by numerically evolving the density matrix. The numerical results in Figure 2.4 shows decrease in variance with increase in the value of θ for different number of steps of quantum walk.

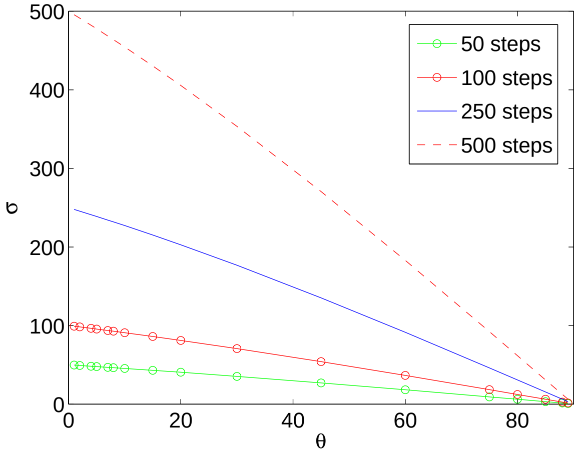

FIGURE 2.4: A comparison of variation of σ with θ for different number of steps of walk using operator $B_{0,\theta,0}$ using numerical integration.

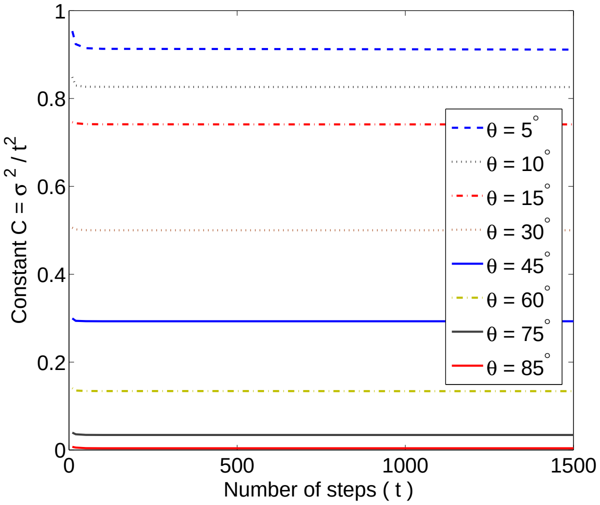

FIGURE 2.5: Value of C for a given θ with increase in number of steps. C remains constant with increase in number of steps and decreases with increase in θ.

The change in variance for different values of θ is attributed to change in the value of C_θ, a constant for a given θ, Figure 2.5. The dependence can be written in the form

$$\sigma^2 = C_\theta t^2. \tag{2.39}$$

Therefore, starting from Hadamard walk ($\theta = \frac{\pi}{4}; \xi = \zeta = 0$), the variance can be increased ($\theta < \frac{\pi}{4}$) or decreased ($\theta > \frac{\pi}{4}$) using $B_{\xi,\theta,\zeta}$. Figure 2.6 shows the dependence of C on θ. To analyze the effect of θ on variance further, it is instructive to first consider the extreme values of parameters in $B_{\xi,\theta,\zeta}$. If $\xi = \theta = \zeta = 0$, $B_{0,0,0} = \sigma_z$, the Pauli z operation, then $W_{\xi,\theta,\zeta} \equiv S$ and the two superposition states, $|0\rangle$ and $|1\rangle$, move away from each other without any diffusion and interference having high $\sigma^2 = t^2$. On the other hand, if $\theta = \frac{\pi}{2}$, then $B_{0,\frac{\pi}{2},0} = \sigma_x$, the Pauli x operation, and the two states $|0\rangle$ and $|1\rangle$ cross each other going back and forth, thereby remaining close to position $j = 0$ and hence giving very low $\sigma^2 \approx 0$. These two extreme cases are not dominated by interference effect, but they define the limits of the variance. Intermediate values of θ between these two extremes show intermediate drifts and quantum interference and after t steps, the probability distribution is spread over the interval $(-t\cos(\theta), t\cos(\theta))$ [21]. Probability distribution is almost 0 beyond $|t\cos(\theta)|$ and for all practical purpose it can be considered to be equal to 0. This is also verified by analyzing the distribution obtained using numerical integration technique.

Numerically obtained data of variance for different θ overlaps with $(1 - \sin(\theta))t^2$. That is, the best fit function of θ for the numerical data can be written in the form

$$\sigma^2 = C_\theta t^2 \approx [1 - \sin(\theta)]t^2. \tag{2.40}$$

To arrive at an expression for variance as a function of θ, a function of θ for the probability distribution of quantum walk can be used. A function of θ for probability distribution can be approximated by fitting a function that envelop the probability distribution obtained for different values of θ from the numerical integration technique, Figure 2.7 [2].

---

[2] Arriving at θ dependent function from first principles, that is from the analytics of the dynamics of quantum walk is an ideal method. For this thesis, I have not considered that method due to constrains from the complexity of the dynamics of quantum walk.

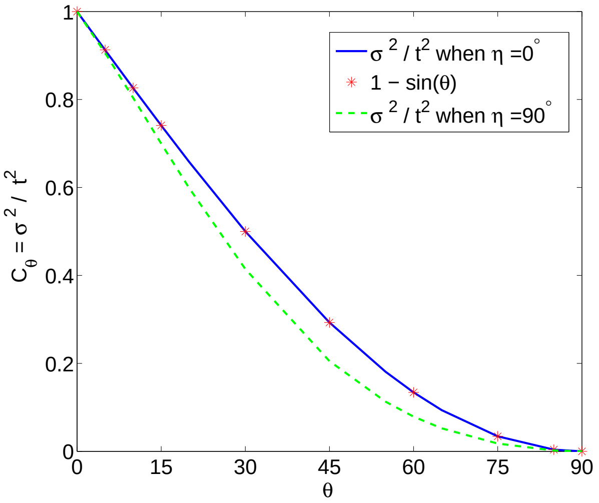

FIGURE 2.6: Plot of the variation of C_θ when $\eta = |\xi - \zeta| = 0^\circ$ from numerical data and the function $(1 - \sin(\theta))$ to which it fits. The effect of maximum biasing, $\eta = 90^\circ$ on C_θ is also shown and it is very small.

One of the θ dependent function that envelop the probability distribution is,

$$\int P(j)dj \approx \int_{-t\cos(\theta)}^{t\cos(\theta)} \frac{[1+\cos^2(2\theta)]e^{K(\theta)\left(\frac{j^2}{t^2\cos^2(\theta)}-1\right)}}{\sqrt{t}} dj \approx 1, \tag{2.41}$$

where, $K(\theta) = \frac{\sqrt{t}}{2}\cos(\theta)[1+\cos^2(2\theta)][1+\sin(\theta)]^3$. The above probability distribution $P(j)$ as a function of θ was obtained by trying out different function of θ until a reasonable fit for the numerically obtained distribution for quantum walk was obtained. Figure 2.7 shows the probability distribution obtained by using (2.41).

The probability distribution for any θ is spread over the position j in the interval $(-t\cos(\theta), t\cos(\theta))$. Therefore, for any θ the position j can be parametrized by introducing a function of ϕ, $f(\phi)$. That is,

$$j \approx f(\phi) = t\cos(\theta)\sin(\phi) \tag{2.42}$$

---

[3] Since $K(\theta)$ is an approximate function, other forms of $K(\theta)$ which closely fit the envelop can also be considered.

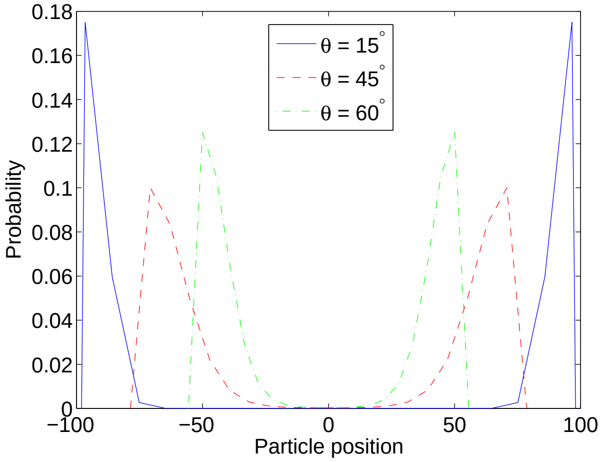

FIGURE 2.7: The probability distribution obtained using (2.41) for different value of θ. The distribution is for 100 steps.

where ϕ range from $-\frac{\pi}{2}$ to $\frac{\pi}{2}$. For a walk with coin $B_{0,\theta,0}$, the mean of the distribution is zero and hence variance can be analytically obtained by evaluating

$$\sigma^2 = \int P(j)j^2 dj \approx \int_{-t\cos(\theta)}^{t\cos(\theta)} P(j)j^2 dj = \int_{-\frac{\pi}{2}}^{\frac{\pi}{2}} P(f(\phi))(f(\phi))^2 f'(\phi)d\phi. \tag{2.43}$$

Substituting appropriate values and simplifying we get

$$\sigma^2 \approx \int_{-\frac{\pi}{2}}^{\frac{\pi}{2}} \frac{(1+\cos^2(2\theta))}{\sqrt{t}} e^{K(\theta)\left(\sin^2(\phi)-1\right)} \left(t\cos(\theta)\sin(\phi)\right)^2 \\ \times \left(t\cos(\theta)\cos(\phi)\right) d\phi = t^2(1-\sin(\theta)), \tag{2.44}$$

That is,

$$\sigma^2 = C_\theta t^2 \approx (1-\sin(\theta))t^2. \tag{2.45}$$

The function matches the result $C_\theta = (1-\sin(\theta))$ obtained from the numerical data, as shown in Figure 2.6. Intermediate steps are presented in the Appendix B.

We note that biasing the walk by setting $\xi \neq \zeta$ in $B_{\xi,\theta,\zeta}$ does not alter the width of the distribution in the position space but the probability decreases as a function of $\cos(\eta)$ on one side and increases as a function of $\sin(\eta)$ on the other side, where

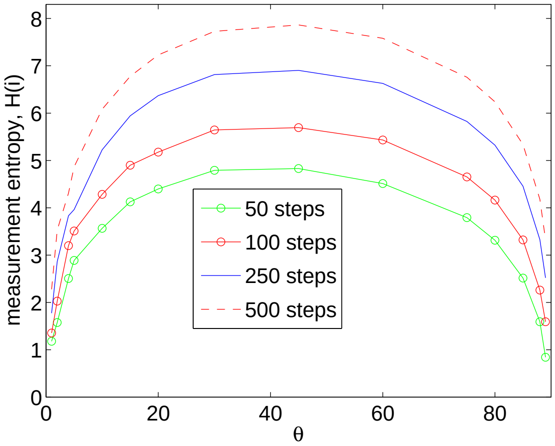

FIGURE 2.8: Variation of entropy of measurement $H(j)$ with θ for different number of steps. The decrease in $H(j)$ is not drastic till θ is close to 0 or $\frac{\pi}{2}$.

$\eta = |\xi - \zeta|$. The mean value $\bar{j}$ of the distribution, which is zero for $B_{0,\theta,0}$, attains finite value with non-vanishing η, that contributes for an additional term in (2.43),

$$\sigma^2 \approx \int_{-t\cos(\theta)}^{t\cos(\theta)} P(j)(j - \bar{j})^2 dj. \tag{2.46}$$

The contribution of η is a very small decrease in the variance of biased quantum walk, see Figure 2.6.

2.3.2.1 Entropy of measurement

As an alternative measure of fluctuation in position, we consider the Shannon entropy of the quantum walk. Shannon entropy of the walk is obtained using position probability distribution P_j obtained by tracing over the coin basis,

$$H(j) = -\sum_j P_j \log P_j. \tag{2.47}$$

The quantum walk with a Hadamard coin toss, $B_{0,\frac{\pi}{4},0}$, has maximum uncertainty associated with the probability distribution and hence measurement entropy is maximum. For $\xi = \zeta = 0$ and low θ, operator $B_{0,\theta,0}$ is almost a Pauli z operationσ_z, leading to localization of walker at $\pm t$. At θ close to $\frac{\pi}{2}$, with $\xi = \zeta = 0$, S

approaches the Pauli x operation σ_x, leading to localization close to the origin, and again, low entropy. However, as θ approaches $\frac{\pi}{4}$, the splitting of amplitude in the position space increases towards the maximum. The resulting enhanced diffusion is reflected in the relatively large entropy at $\frac{\pi}{4}$, as seen in Figure 2.8. Figure 2.8 is the measurement entropy with variation of θ in the coin $B_{0,\theta,0}$ for different number of steps of quantum walk. The decrease in entropy from the maximum by changing θ on either side of $\frac{\pi}{4}$ is not drastic until θ is close to 0 or $\frac{\pi}{2}$. Therefore for all practical purposes, small entropy can be compensated for by the relatively large C_θ, and hence σ^2. The effect of ξ and ζ on the measurement entropy is of very small magnitude. These parameters do not affect the spread of distribution and variation in height reduces the entropy by a very small fraction. In other cases, such as mixing of quantum walk on an $n-$cycle briefly discuss in Section 2.3.2.2, it is ideal to use a lower value of θ.

2.3.2.2 Mixing time on an n-cycle

The simplest finite Cayley graph is an n-cycle with n vertices in closed path [94]. Due to closed structure of the $n-$cycle graph, with n positions in $\mathcal{H}_p$, the conditional shift operation S (2.14) for a discrete-time quantum walk on a line takes the form

$$S^c = |0\rangle\langle 0| \otimes \sum_{j=0}^{n-1} |\psi_{j-1 \bmod n}\rangle\langle\psi_j| + |1\rangle\langle 1| \otimes \sum_{j=0}^{n-1} |\psi_{j+1 \bmod n}\rangle\langle\psi_j|. \tag{2.48}$$

The quantum state after t steps of discrete-time quantum walk on particle initially in state $|\Psi_{in}\rangle$ (2.11) is written as

$$|\Psi_t\rangle = W^t_{\xi,\theta,\zeta}|\Psi_{in}\rangle = \sum_{j=0}^{n-1} |\Psi_{j,t}\rangle, \tag{2.49}$$

where $|\Psi_{j,t}\rangle$ is the state at position j after t steps of quantum walk.

Mixing time: Mixing time is the time it takes for the probability distribution on a graph (position space) to converge to a stationary distribution. The classical random walk approaches a stationary distribution independent of its initial state

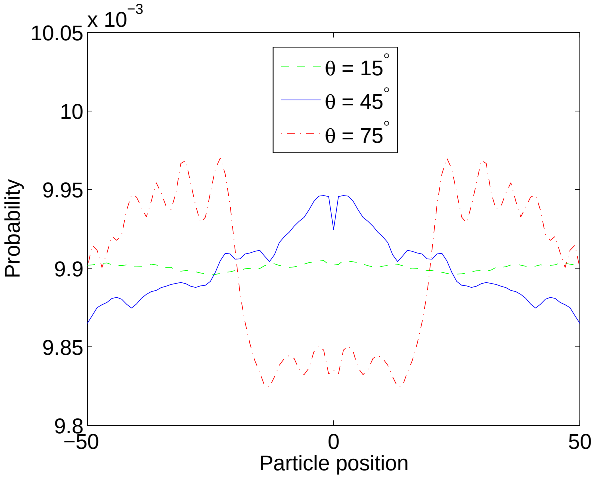

FIGURE 2.9: A comparison of mixing time M of the time-averaged probability distribution of a quantum walk on an n-cycle for different value of θ using coin operation $B_{0,\theta,0}$, where n, the number of position, is 101. Mixing is faster for lower value of θ. The distribution is for 200 cycles.

on a finite graph. Unitary (i.e., non-noisy) quantum walk, does not converge to any stationary distribution. But by defining a time-averaged probability distribution,

$$\overline{P(j,T)} = \frac{1}{T}\sum_{\tau=0}^{T-1} P(j,\tau), \tag{2.50}$$

obtained by uniformly picking a random time τ between 0 and $(T-1)$, evolving for t time steps and measure to find a particle at a given vertex (position j), a convergence in the probability distribution can be seen even in the quantum case. It has been shown that for the quantum walk on an n-cycle, the mixing time is bounded above by $M = O(n \log n)$, almost quadratically faster than the classical case which is $O(n^2)$ [94]. From previous section, we know that a quantum walk can be optimized for maximum variance and wide spread in position space, between $(-t\cos(\theta),\ t\cos(\theta))$ after t steps. For a walk on an n-cycle, choosing θ slightly above 0 would give the maximum spread over n vertices in the cycle for $n/2$ steps of the quantum walk. Maximum spread during each cycle distributes the probability over the cycle faster and this would optimize the mixing time. For optimal mixing time, it turns out to be ideal to fix $\xi = \zeta$ in $B_{\xi,\theta,\zeta}$, since biasing impairs a proper mixing. Figure 2.9 is the time averaged probability distribution of a quantum walk on an n-cycle graph after time $t = n \log n$, where n is 101. It can be seen that the variation of probability distribution over the position space is least for $\theta = 15°$ compared to $\theta = 45°$ and $\theta = 75°$.

2.3.3 Randomizing coin operations from SU(2) group

In Section 2.3.1 and 2.3.2 we discussed quantum walk using Hadamard operation and SU(2) operation as quantum coins. Though we used a generalized SU(2) coin $B_{\xi,\theta,\zeta}$ (2.31), identical coin parameters were used during each step of the walk and we also saw the dependence of variance on the coin parameter θ.

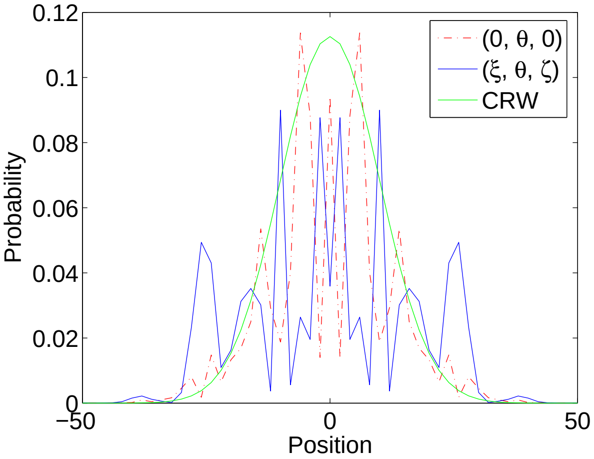

FIGURE 2.10: Quantum walk using randomly picked coin operation for each step of walk from SU(2) group with randomly picked $\xi, \theta, \zeta \in \{0, \pi/2\}$ for $B_{\xi,\theta,\zeta}$ and $B_{0,\theta,0}$ respectively. We see that the variance of the distribution is very much close to the variance of the classical random walk (CRW) distribution.

Evolution of quantum walk using randomized coin operation can be constructed by randomly chosen quantum coin operator for each step from a set of operators in SU(2) group. That is,

$$S(B_{\xi_t,\theta_t,\zeta_t} \otimes \mathbb{1}) \cdots S(B_{\xi_x,\theta_x,\zeta_x} \otimes \mathbb{1}) \cdots S(B_{\xi_0,\theta_0,\zeta_0} \otimes \mathbb{1})|\Psi_{in}\rangle \tag{2.51}$$

with randomly chosen parameters $\xi, \theta, \zeta \in \{0, \pi/2\}$ for each step. Though the coin parameters are randomly chosen for each step, the evolution is unitary and involves interference of amplitudes, and the effect is seen in probability distribution, see Figure 2.10. From the numerical evolution we also see that variance of the distribution is much closer to variance of the classical random walk distribution. However by restricting the range of the coin parameters that can be used for the walk, the probability distribution can be localized or made to spread wide in position space. One simple example we can consider is, by randomly picking different θ for each step from a subset of complete range of θ, subset with $\theta_1 \in \{0, \pi/4\}$ and $\theta_2 \in \{\pi/4, \pi/2\}$ for $B_{\xi,\theta_1,\zeta}$ and $B_{\xi,\theta_2,\zeta}$ respectively, where other parameters are still picked from the complete range, $\xi, \zeta \in \{0, \pi/2\}$. Probability distribution obtained is shown in Figure 2.11. Walk using $\theta_1 \in \{0, \pi/4\}$ spreads wider in position space, whereas the walk using $\theta_2 \in \{\pi/4, \pi/2\}$ localizes the distribution.

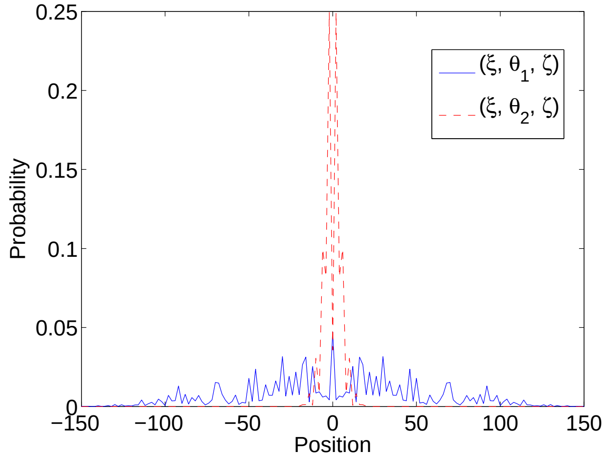

FIGURE 2.11: Quantum walk using two different set of random picked parameters $\xi, \zeta \in \{0, \pi/2\}, \theta_1 \in \{0, \pi/4\}$ and $\theta_2 \in \{\pi/4, \pi/2\}$ for $B_{\xi,\theta_2,\zeta}$ and $B_{\xi,\theta_2,\zeta}$ respectively. The distribution is for 200 steps, walk using $\theta_1 \in \{0, \pi/4\}$ spreads wider in position space, whereas the walk using $\theta_2 \in \{\pi/4, \pi/2\}$ localizes the distribution.

2.4 Recurrence of quantum walk

In the dynamics of physical system, from a single free particle to stellar dynamics, understanding of recurrence phenomenon have significantly contributed to a better understanding of the system dynamics [23]. For a classical conservative system, whether discrete or continuous in time, the Poincaré recurrence theorem states that any phase-space configuration of a system enclosed in a finite volume will be repeated as accurately as one wishes after a finite interval of time (with no restriction on the interval) [71, 72]. A similar recurrence theorem is shown to hold in quantum theory as well [73, 74]. In a system with a discrete energy eigenvalue spectrum $\{E_n\}$; if $\Psi(t_0)$ is its state vector at the time t_0 and ϵ is any positive number, there exists a finite time T such that,

$$|\Psi(T) - \Psi(t_0)| < \epsilon. \tag{2.52}$$

For classical random walk we can consider the recurrence probability $P_0(t)$, i.e., the probability of periodicity of dynamics that the particle returns to origin during the time evolution (t steps). It is characterized by the Pólya number

$$\mathcal{P}_{crw} \equiv 1 - \frac{1}{\sum_{t=0}^{\infty} P_0(t)}. \tag{2.53}$$

If the Pólya number equals one, the classical random walk is recurrent, otherwise the walk is transient, i.e., with nonzero probability the particle never returns to the origin. For a classical random walk to be transient the series $\sum_{t=0}^{\infty} P_0(t)$ must converge [95]. Pólya proved that the one- and two- dimensional classical random walk are recurrent [96], while in higher dimension for each dimension a unique Pólya number is associated and the classical random walk is transient.

In standard quantum mechanics, initially localized wave packet in state $|\Psi(t_0)\rangle$ which can spread significantly in a closed system can also reform later in the form of a quantum revival, i.e., the spreading reverses itself and the wave packet relocalizes [75]. The relocalized wave packet can again spread and the periodicity in the dynamics can be seen validating the quantum recurrence theorem. The time evolution of a state $|\Psi(t)\rangle$ over entire position j, or a wavefunction $\Psi(j,t)$ at a position j after time t is given by a deterministic unitary transformation associated with the Hamiltonian. During quantum evolution we deal with amplitudes and probability density $P(j,t) = |\Psi(j,t)|^2$ at position j after time t appears only when we collapse the wave packet to perform measurement.

Unlike standard wave packet spreading in free space and harmonic potential[4], the quantum walk spreads the wave packet in multiple possible paths with amplitudes corresponding to different paths interfering. In this section we show that due to particle-position entanglement and interference effect during the evolution of the quantum walk, the wave packet delocalizes over the position space as a small copies of the initial wave packet. These delocalized copies of fractional wave packet fails to satisfy the complete quantum recurrence theorem during quantum walk evolution. That is for quantum walk, the recurrence we considered is return of the unit probability amplitude at the origin during the dynamics. However, due to revival of fractional wave packets, a fractional recurrence can be seen in the quantum walk. The probabilistic characterization of the recurrence in quantum walk has been done in [20] and the characterization using quantum Pólya number defined in [97] can be used to show the fractional recurrence nature of quantum walk. In Section 2.4.2.2, we also show the exceptional cases of quantum walk that can be constructed by suppressing or minimizing the interference effect and get closer to complete recurrence.

2.4.1 Quantum recurrence theorem

Quantum recurrence theorem in the dynamics of a closed system states that there exist a time T when

$$|\Psi(T) - \Psi(t_0)| < \epsilon, \tag{2.54}$$

where $\Psi(T) = |\Psi_T\rangle$ is the state of the system after time T, $\Psi(t_0) = |\Psi_0\rangle$ is the initial state of the system and ϵ is any positive number [73].

The recurrence of the complete state of the system or exact revival happens when all the expectation values of observables A_o of the two states $|\Psi_T\rangle$ and $|\Psi_0\rangle$ are equal to one another, that is,

$$\langle\Psi_T|A_o|\Psi_T\rangle = \langle\Psi_0|A_o|\Psi_0\rangle. \tag{2.55}$$

---

[4] During standard wave packet spreading in free space and harmonic potential, a wave packet which is initially Gaussian, spreads retaining the Gaussian shape causing increase in the full-width at half maxima (FWHM).

In classical dynamics, the characterization of the nature of recurrence can be conveniently done using probabilistic measures. Measurements on a quantum system leaves the state in one of its basis states with certain probability. Therefore, recurrence in quantum systems can be analyzed using comparative evolution of the two identically prepared quantum system with the initial states $|\Psi_{0,0}\rangle$ at position $j = 0$ and time $t = 0$. We will consider two cases of comparative analysis.

Case 1: Consider two identically prepared particle wave packets which revive completely in the position space at time T. One of the two particle wave packets at position $j = 0$ and time $t = 0$ is first evolved to spread in position space and then reverse the spreading till it relocalizes completely at position $j = 0$ at time T. The measurement performed on this particle will collapse the wave packet at the relocalized position with an expectation value

$$\langle\Psi_{0,T}|X_p|\Psi_{0,T}\rangle = \langle\Psi_{0,0}|X_p|\Psi_{0,0}\rangle = 1, \tag{2.56}$$

where X_p is the position operator. After the measurement at time T, the system is further evolved for an additional unit time and the corresponding state can be given by $|\Psi_{j,T_M+1}\rangle$. The subscripts j and $(T_M + 1)$ stand for position and time $(T + 1)$ with intermediate measurement being performed at time T. The second particle wave packet at position $j = 0$ and time $t = 0$ is evolved up to time $(T+1)$ directly without any measurement being performed at time T and the state can be written as $|\Psi_{j,T+1}\rangle$. Since both the wave packets completely relocalize at position $j = 0$ after the evolution for time period T, irrespective of the measurement being performed, expectation value for both the particles after time $(T + 1)$ would be identical,

$$\langle\Psi_{j,T_M+1}|X_p|\Psi_{j,T_M+1}\rangle = \langle\Psi_{j,T+1}|X_p|\Psi_{j,T+1}\rangle, \tag{2.57}$$

with j spanning over all position space.

Case 2: Consider two identically prepared particle wave packets which does not relocalize completely at position $j = 0$ at time T, i.e., revive fractionally or does not revive at all. The measurement will collapse the wave packet and return the expectation value

$$\langle\Psi_{0,T}|X_p|\Psi_{0,T}\rangle = \delta \;\; ; \quad 0 < \delta < 1. \tag{2.58}$$

In this case the two identically prepared particle evolved to time $(T+1)$, one with a measurement being performed at time T and an other without any measurement being performed. With very high probability the measurement will not return the same expectation value, that is

$$\langle \Psi_{j,T_M+1}|X_p|\Psi_{j,T_M+1}\rangle \neq \langle \Psi_{j,T+1}|X_p|\Psi_{j,T+1},\rangle \tag{2.59}$$

with j spanning over all position space. Non-zero values in both expectation values in the inequality can act as a signature of fractional recurrence of the quantum state at time T and a zero expectation value on the left hand side shows transient dynamics.

From the analysis of the above two cases we can conclude that, if a system is completely recurrent at time T the two states $|\Psi_{j,T_M+1}\rangle$ and $|\Psi_{j,T+1}\rangle$, one with intermediate measurement at time T and other without any measurement at time T will be equal to one another. This will be helpful for us in understanding the fractional recurrence nature of the quantum walk.

2.4.2 Fractional recurrence of quantum walk

2.4.2.1 On a line

The state of the particle wave packet after implementing the discrete-time quantum walk of t steps on a line with unit time required to implement each step can be written as

$$|\Psi_t\rangle = W^t_{\xi,\theta,\zeta}|\Psi_{0,0}\rangle = \sum_j |\Psi_{j,t}\rangle. \tag{2.60}$$

Where $|\Psi_t\rangle$ is the state after time t over entire position space, $|\Psi_{j,t}\rangle$ is the state of the delocalized wave packet at each position j in $\mathcal{H}_p$ and $|\Psi_{0,0}\rangle$ is the coin and position state of the wave packet before implementing the quantum walk. In the quantum walk process that involves a deterministic unitary evolution, the particle wave packet delocalize and spread over the position space forming a mini wave packet. During this delocalization process the mini wave packets interfere and entangle the position and coin Hilbert space, $\mathcal{H}_p$ and $\mathcal{H}_c$. The interference

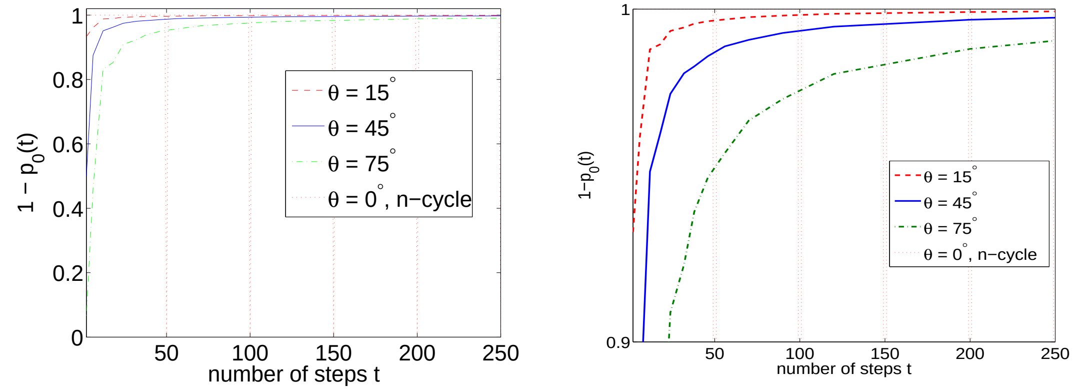

(a) (b)

Figure 2.12: The plot of $[1 - p_0(t)]$, where $P_0(t)$ is the probability of particle at the origin with t being the number of steps in the discrete-time quantum walk evolution. The plot for quantum walk on a line using different coin operation parameter $\theta = 15^\circ, 45^\circ$, and 75° is shown. With an increase in θ, the quantum Pólya number, which characterizes the fractional recurrence nature of the quantum walk, also increases. The plot with $\theta = 0^\circ$ is for a walk on an $n-$cycle with a completely suppressed interference effect, where $n = 51$. For a walk to be completely recurrent there should exist a $t = T$ where $[1 - P_0(T)] = 0$. Any non-zero value can be used to characterize the fractional recurrence nature of the quantum walk and an absolute 1 for all t would show that the quantum walk is completely transient. (b) Close up of the plot.

and the entanglement between the $\mathcal{H}_p$ and $\mathcal{H}_c$ during the standard quantum walk evolution does not permit complete relocalization of the wave packet at initial position after any given number of steps t. Therefore the argument leading to (2.58) and (2.59) holds to show that the complete recurrence of the quantum state does not occur during the evolution of the quantum walk process on a line. That is,

In a discrete-time quantum walk evolution on a line and on an $n-$cycle dominated by the interference of quantum amplitude [5]*, there exists no time T when the quantum state of the system revive completely and repeat the delocalization and revival at regular interval of time.*

---

[5] By choosing extreme value of θ (0 or $\pi/2$) in the quantum coin operation, quantum walk on a line can be evolved without constructive or destructive interference taking place.

The above statement can also be quantified in the following way: After implementing a quantum walk, the wavefunction describing the particle at position j and time t can be written as a two component vector of amplitudes of particle being at position j at time t with left and right propagating component

$$|\Psi_{j,t}\rangle = \begin{pmatrix} \Psi_L(j,t) \\ \Psi_R(j,t) \end{pmatrix}. \tag{2.61}$$

Lets analyze the dynamics of discrete-time quantum walk on wave packet $\Psi(j,t)$ driven by single parameter quantum coin

$$B_\theta = \begin{pmatrix} \cos(\theta) & \sin(\theta) \\ \sin(\theta) & -\cos(\theta) \end{pmatrix} \tag{2.62}$$

and shift operator S ($W = S(B_\theta \otimes \mathbb{1})$). In terms of left and right propagating component it is given by

$$\begin{aligned} \Psi_R(j,t+1) &= \cos(\theta)\Psi_R(j-1,t) + \sin(\theta)\Psi_L(j-1,t) \\ \Psi_L(j,t+1) &= \sin(\theta)\Psi_R(j+1,t) - \cos(\theta)\Psi_L(j+1,t). \end{aligned} \tag{2.63}$$

Then the probability of being at position j and t is

$$P(j,t) = |\Psi_L(j,t)|^2 + |\Psi_R(j,t)|^2. \tag{2.64}$$

and sum of probability over the entire position space is

$$\sum_j P(j,t) = 1. \tag{2.65}$$

After time t with unit time required to implement each step of the quantum walk on a line, the wavefunction will be spread between $j = -t$ to $+t$ and can be written over position space as

$$\sum_{j=-t}^{t} \Psi(j,t) = \sum_{j=-t}^{t} \left[\Psi_R(j,t) + \Psi_L(j,t)\right]. \tag{2.66}$$

It should be noted that for even number of steps the amplitude at odd labeled positions is 0 and for odd number of steps amplitude at even labeled position is 0.

For classical random walk, each step of walk is associated with the *randomness* and the *probability* of the entire particle therefore, however small the probability is at the origin, it is attributed to the recurrence of the entire particle. That is, $0 < P_{crw}(0,T) < 1$ at some time T shows the recurrence of complete particle at the origin with some finite probability. For the discrete-time quantum walk evolution described by (2.63) we found that the information of the coin degree of freedom is carried over to the later steps during the dynamics of the walk making it reversible (2.35). The *randomness* and the *probability* in quantum walk comes into consideration only when the wave packet is collapsed to discard the signature of the quantum coin degree of freedom from earlier steps. Therefore, for a discrete-time quantum walk to be completely recurrent, the condition

$$P(0,T) = |\Psi_L(0,T)|^2 + |\Psi_R(0,T)|^2 = 1 \tag{2.67}$$

has to be satisfied for some time T. Any $P(0,t) < 1$ shows that the particle is present in superposition of position space (origin and other positions), which we will call as the fractional recurrence nature of the quantum walk. From (2.63) and (2.64), we can conclude that (2.67) is satisfied only when $\theta = \pi/2$ and t is even, that is when there is no interference of the quantum amplitudes. For $\theta = 0$ the two left and right component move in opposite directions without returning and for any $0 < \theta < \pi/2$ we get $P(0,t) < 1$ showing the fractional recurrence of the quantum walk.

Alternatively, using quantum Fourier analysis to study the evolution of the discrete-time quantum walk on a line, it is shown that the amplitude at the origin and to a very good approximation for any position j between two dominating peaks (for example see Figure 2.3) decreases by $O(1/\sqrt{t})$[20]. Therefore,

$$\langle \Psi_{j,t} | \Psi_{j,t} \rangle = O\left(\frac{1}{t}\right) < 1. \tag{2.68}$$

and their exists no time $T = t$ where the walk is completely recurrent showing the fractional recurrence nature of the quantum walk.

A probability based characterization of the recurrence nature of the quantum walk, quantum Pólya number was defined for an ensemble of identically prepared quantum walk systems by the expression

$$\mathcal{P}_{qw} = 1 - \prod_{t=1}^{\infty} [1 - P_0(t)], \tag{2.69}$$

where $P_0(t)$ is the recurrence probability of the particle. Each identically prepared particle is subjected to different number of steps of quantum walk from 1 to ∞ and the probability of the particle at the origin is measured and discarded [97]. The probability that the particle is found at the origin in a single series of such measurement records is the quantum Pólya number. The quantum Pólya number was calculated for various coined quantum walks and it is shown that in the higher dimension it depends both on the initial state and the parameters of the coin operator whereas, for the classical random walk the Pólya number is uniquely determined by its dimensionality [98].

To show the quantum walk to be completely recurrent adopting a probability based characterization given by (2.69) needs to have at least one of the many particles, each evolved to different steps t from 1 to ∞, to return $P_0(t) = 1$. If $0 < P_0(t) < 1$ for any t, then only with certain probability $P_0(t)$ the wave packet collapses at $j = 0$, that is, prior to measurement the particle existed in superposition of position space. If $0 < P_0(t) < 1$ for all the particles evolved to different steps from 1 to ∞ then the fractional recurrence of the quantum walk is characterized by the $\mathcal{P}_{qw}$.

In Figure 2.12 the plot of $[1 - P_0(t)]$ is shown for a discrete-time quantum walk on a line where the different coin operation parameter $\theta = 15^\circ, 45^\circ, 75^\circ$. With increase in θ the quantum Pólya number, which can also be called as the *fractional recurrence number* $\mathcal{P}_{qw}$, also increases.

2.4.2.2 On an $n-$cycle

We have discussed the dynamics of discrete-time quantum walk on an $n-$cycle and the mixing time using coin degree of freedom in Section 2.3.2.2. In this section we

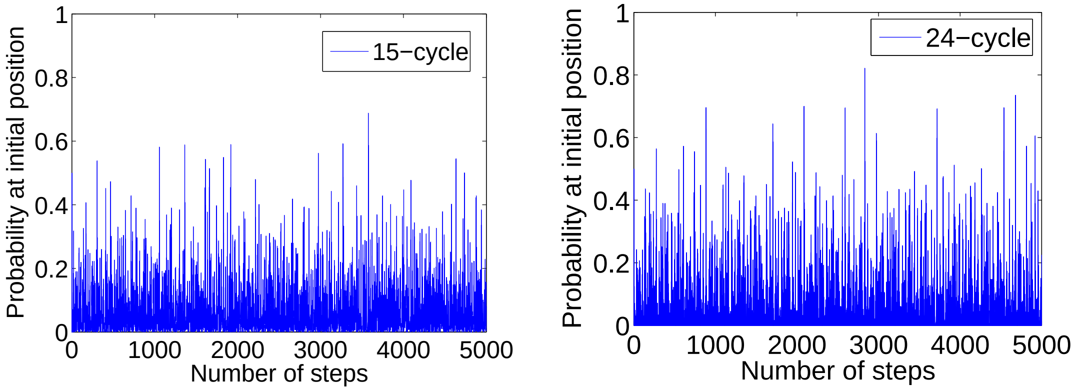

(a) (b)

FIGURE 2.13: Probability at the initial position after different number of steps of quantum walk on 15− and 24− cycle. This clearly shows that even for steps as large as 5000, their is no signature of complete recurrence. The distribution is obtained using Hadamard operation, $B_{0,\pi/4,0}$ as quantum coin operation.

will discuss the recurrence nature of quantum walk on an $n-$cycle.

As discussed earlier, in the case of classical random walk walk on a line a non-zero probability is sufficient to show the recurrence of the entire particle and a uniform distribution returns a non-zero probability at the origin. Whereas uniform distribution in the quantum case does not reveal the complete recurrence nature of the particle as it does in the classical case.

In Figure 2.13 we show numerically that the probability of finding the particle at the initial position j_0 after different number of steps of quantum walk on 15− and 24− cycle. The distribution is obtained for up to as large as 5000 steps. At no time $t =$ number of steps, a unit probability value is returned at the initial position showing that the wave packet evolved using quantum walk on an $n-$cycle fails to revive completely at the initial position.

The failure of the wave packet to completely revive and recur at initial position can be attributed to the interference effect caused by the mixing of the left and right propagating components of the amplitude. By suppressing the interference effect during the evolution in a closed path one can get closer to the complete relocalization, revival at initial position j_0. For example, the wave packet can be completely relocalized at $j = 0$ on an $n-$cycle at $t = n$ and make the quantum walk

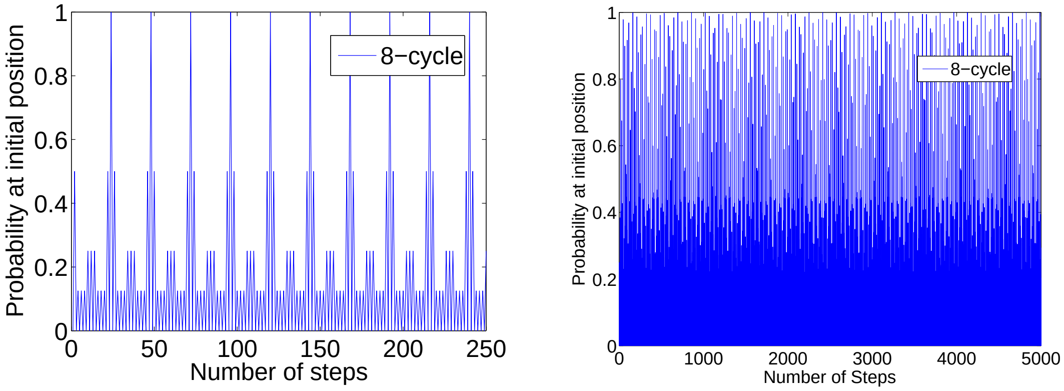

(a) (b)

FIGURE 2.14: Probability at the initial position on 8−cycle. (a) The distribution is obtained using Hadamard operation $B_{0,\pi/4,0}$, due to return of amplitudes to initial position (constructive interference at the origin) before interference of amplitude dominates uniformly over the entire vertices, recurrence is seen. (b) The use of quantum coin, $B_{0,\pi/6,0}$ during the evolution does not lead to complete constructive interference at origin and hence complete recurrence is not seen.

recurrent by choosing an extreme value of coin parameters $(\xi, \theta, \zeta) = (0^\circ, 0^\circ, 0^\circ)$. By choosing $\theta = \delta$, δ being very small and close to 0° during the evolution, the interference effect is minimized and will return a near complete recurrence on an $n-$cycle. In Figure 2.12, the plot of $[1 - P_0(t)]$ is shown for $\theta = 0^\circ$ and $n = 50$. The interference effect is completely suppressed and the quantum walk recurs after every 50 steps.

From the numerically data for upto 5000 steps of quantum walk we note that for small $n-$, especially when n is even, the left and right propagating amplitude return back completely to the initial position (origin) before the mixing and repeated interference of the amplitudes takes over at non-initial position in the evolution process. Therefore, for a quantum walk on an $n-$cycle with n being even up to 8 a complete revival and recurrence of wave packet at initial position $j = 0$ is seen, Figure 2.14 [70]. For a quantum walk on particle initially in symmetric superposition state $|\Psi_{ins}\rangle$ with coin operation $B_{0,\theta,0}$ and $n > 8$, due to larger position Hilbert space the interference effect at the non-initial position dominates reducing the recurrence nature of the dynamics. In Figure 2.15, for quantum walk on 10−cycle, a small deviation from complete recurrence is shown.

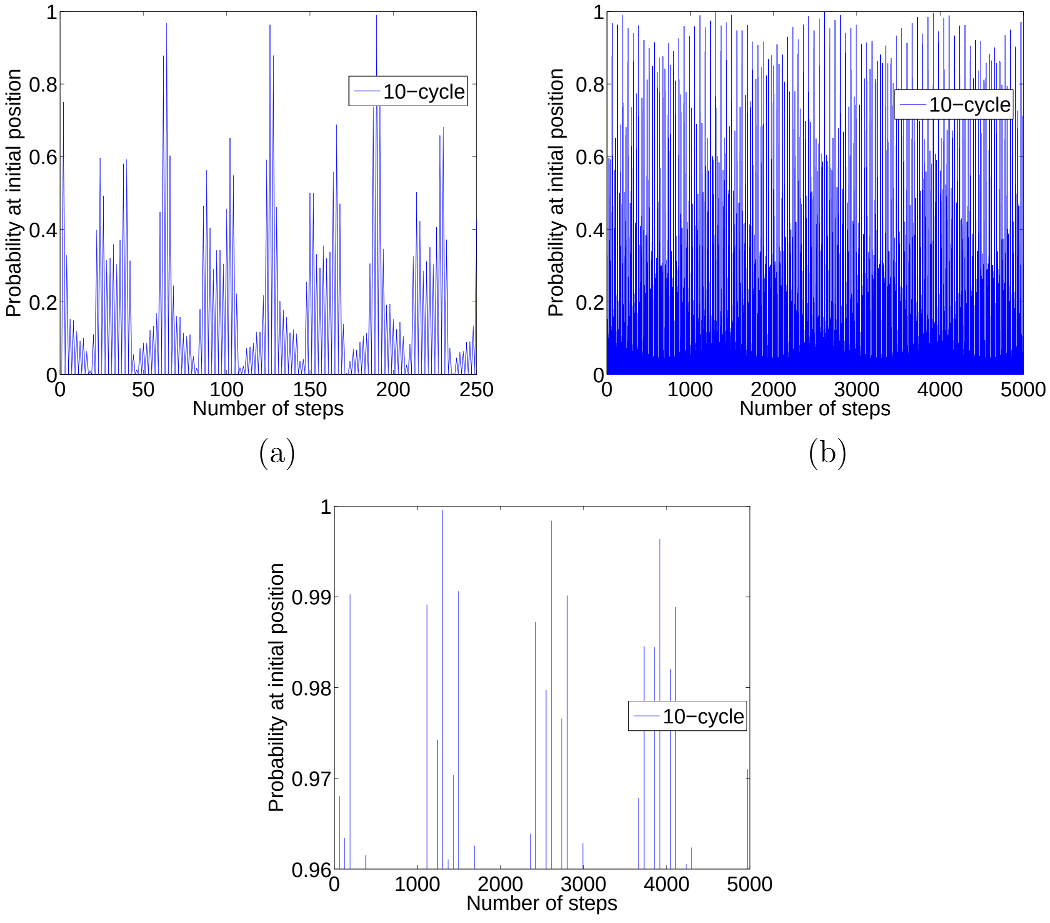

(a) (b)

(c)

FIGURE 2.15: Probability at the initial position on 10−cycle. The distribution is obtained using Hadamard operation $B_{0,\pi/4,0}$. A small deviation from complete recurrence can be seen. (a) and (b) are probability at initial position for quantum walk up to 250 steps and 5000 steps respectively and (c) is the close up of the probability and we note that the probability is not exact 1 at any time within 5000 steps.

For example, we will consider a small, odd $n = 5$. If the positions on a cycle are marked as $j = 0, 1, 2, 3, 4$ after the third step of the quantum walk, the left propagating amplitude move from position 2 to 3 and the right propagating amplitude move from 3 to 2. That is, after the second and third step of quantum walk using shift operator of the form S^c for a walk on an $n-$cycle (3.1) and Hadamard operation H as coin operation on a particle initially in superposition state $|\Psi_{ins}\rangle$

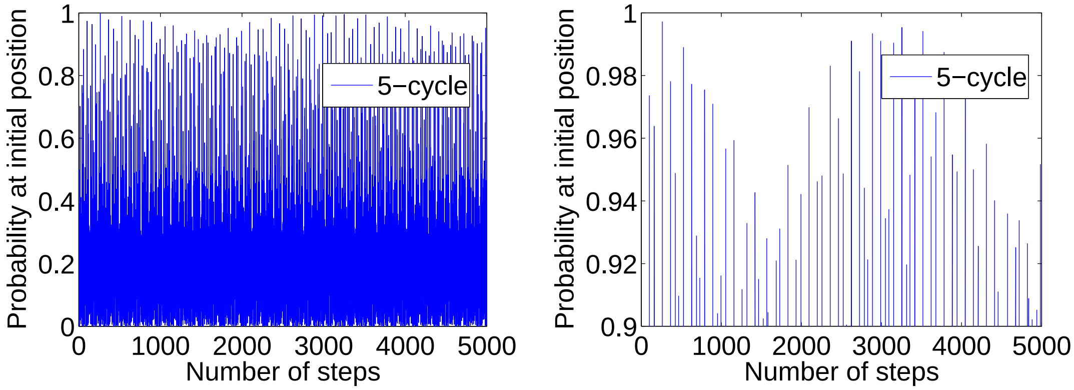

(a) (b)

FIGURE 2.16: Probability at the initial position after different number of steps of quantum walk on 5−cycle, (a) is the complete plot whereas (b) is a close up of probability values between 0.9 and 1. At no step in the plot, probability is a unit value. This numerically shows that the quantum walk on an $n-$ cycle does not recur for n=5.

(2.28) takes the form,

$$S^c(H \otimes \mathbb{1})S^c|\Psi_{ins}\rangle = \frac{1}{2}\{|0\rangle \otimes |\psi_3\rangle + (\,|1\rangle + i|0\rangle\,) \otimes |\psi_0\rangle - i|1\rangle \otimes |\psi_2\rangle\} \qquad (2.70)$$

$$S^c(H \otimes \mathbb{1})S^c(H \otimes \mathbb{1})S^c|\Psi_{ins}\rangle = \frac{1}{2\sqrt{2}}\{|0\rangle \otimes |\psi_2\rangle + (|0\rangle + |1\rangle + i|0\rangle) \otimes |\psi_4\rangle - (|1\rangle - i|0\rangle + i|1\rangle) \otimes |\psi_1\rangle + i|1\rangle \otimes |\psi_3\rangle\}. \qquad (2.71)$$

The left and right propagating amplitude crossover without suppressing the mixing, therefore the constructive interference effect continues to exist even at positions other than the origin during the evolution. In Figure 2.16 the probability of finding the particle at the initial position is shown. Due to the small size of the Hilbert space, the probability is seen to be close to unity but the closer look reveals that its only a fractional revival.

We also note that localization effect found in 2D [99], in quantum walk using multi quantum coins to diminish the interference effect [100] or in walk using selective randomization of coin operations (Section 2.3.3) can result in increasing the fractional recurrence number $\mathcal{P}_{qw}$ on a line and higher dimension. If the particle wave packet is evolved in a *position* Hilbert space $\mathcal{H}_p$ with the edges that permits the wave packet to escape, the fractional recurrence nature of the quantum walk does not allow the quantum walk to be completely transient. Therefore, the fractional transient nature of the quantum walk is seen to complement the fractional recurrence nature.

From this section we conclude that as long as the wave packet spread in position space interfering, forming mini wave packets during the evolution of the quantum walk process, it fails to satisfy the complete recurrence theorem. However, fractional recurrence can be seen.

2.5 Summary

- Expression used to understand the continuous- and discrete-time quantum walk which are mathematically identical to Schrödinger and Dirac equations respectively are reviewed. Our simple decoupling analysis of the evolution shows the similarity between the discrete-time quantum walk evolution expression and the Dirac equation.

- Our construction of discrete-time quantum walk model using three parameter quantum coin operation $B_{\xi,\theta,\zeta}$ from SU(2) group optimizes the control over the quantum walk evolution. For example, parameter θ to control the variance and maximize the variance for a walk on a line, control the mixing time on an $n-$cycle, and parameters ξ and ζ to bias and control biasing in the walk.

- We have shown that the quantum walk evolution dominated by the interference of quantum amplitudes fails to satisfy complete recurrence theorem. However, fractional recurrence characterized by the quantum Pólya number can be seen.

Chapter 3

Symmetries and noise on quantum walk

3.1 Introduction

The probability distribution of discrete-time quantum walk on a line remains invariant in position space when the operations to implement each step of the walk is augmented by certain operations. We refer to these discrete operations as symmetries of the quantum walk. In this chapter we will study some of these symmetry operations. We further generalize the observations of these symmetries in the presence of environmental effects, modeled by various noise channels such as, bit flip, phase-flip (decoherence without net dissipation), generalized amplitude damping (decoherence with dissipation) and squeezed generalized amplitude damping channels [8, 67, 101, 102] on the coin space. We have found it convenient to explain the symmetries and effect of noise using quantum trajectories, and the numerical results are obtained by numerical integration by evolving the density operator of the system.

We extend these studies to quantum walk on an $n-$cycle. Interestingly, we find that the symmetry operations is sensitive to the walk topology, in the sense that the symmetry which holds for quantum walk on an one-dimensional line does not hold, in general, for a quantum walk on an $n-$cycle but leads to other interesting behavior. The difference between the walk on the line and an $n-$cycle can be attributed to the different ways the interference occurs between the propagating wavefunction. Quantum walk on the line involves interference between the forward and backward propagating wavefunctions whereas, the walk on an $n-$cycle involves interference between forward (backward) propagating waves from both the sides of the loop along with the interference between the forward and backward propagating wavefunctions. Noise on an $n-$cycle tends to restore these symmetry both by classicalizing the walk and also desensitizing the symmetry operation as a topology probe for the quantum walk.

These observations can have important implications for a better insight into, and for simplifying certain implementations of, quantum walks and are also of relevance to studies in quantum optics and condensed matter systems. Later in this chapter and in Chapter 4 we show that the application of these ideas can help simplify certain experimental implementations of quantum walk and can be used as an additional degree of freedom in applications of quantum walk in physical systems.

This chapter is organized as follows. In Section 3.2, we discuss symmetries and noise on quantum walk on a line with Section 3.2.1 focusing on bit flip and phase flip symmetries and Section 3.2.2 focuses on the environmental effects. In Section 3.3 we extend the studies to walk on an $n-$cycle and discuss the breakdown in symmetry. In Section 3.4 we discuss the experimental implications and conclude with summary in Section 3.5.

3.2 Symmetry and noise operations on a line

3.2.1 Bit flip and phase flip symmetries

As defined in Section 2.3 each step of the discrete-time quantum walk consists of the quantum coin operation $B_{\xi,\theta,\zeta}$ (2.31) followed by the shift operation

$$\begin{aligned} S &= |0\rangle\langle 0| \otimes \sum_{j\in\mathbb{Z}} |\psi_{j-1}\rangle\langle\psi_j| + |1\rangle\langle 1| \otimes \sum_{j\in\mathbb{Z}} |\psi_{j+1}\rangle\langle\psi_j| \\ &\equiv |0\rangle\langle 0| \otimes \hat{a} + |1\rangle\langle 1| \otimes \hat{a}^{\dagger}. \end{aligned} \tag{3.1}$$

Here $\hat{a}$ and $\hat{a}^\dagger$ are unitary operators that are notationally reminiscent of annihilation and creation operations, respectively. Lets consider the application of the modified conditional shift operator of the form

$$S' = (X \otimes \mathbb{I}) \exp(-i(|0\rangle\langle 0| - |1\rangle\langle 1|) \otimes Pl), \tag{3.2}$$

$$\begin{aligned} S' &= |1\rangle\langle 0| \otimes \sum_{j \in \mathbb{Z}} |\psi_{j-1}\rangle\langle\psi_j| + |0\rangle\langle 1| \otimes \sum_{j \in \mathbb{Z}} |\psi_{j+1}\rangle\langle\psi_j| \\ &\equiv |1\rangle\langle 0| \otimes \hat{a} + |0\rangle\langle 1| \otimes \hat{a}^\dagger \end{aligned} \tag{3.3}$$

instead of S (3.1). Where $X = \sigma_x$ is the Pauli x operator. Since $S' = (X \otimes \mathbb{I})S$, i.e., it is equivalent to an application of bit flip following S, conditioned on the internal state being $|0\rangle$ ($|1\rangle$). That is, at any given position j, the particle will move to the left (right) and changes its internal state to $|1\rangle$ ($|0\rangle$). Thus,

$$S'(|0\rangle \otimes |\psi_j\rangle) = |1\rangle \otimes |\psi_{j-1}\rangle \quad \text{and} \quad S'(|1\rangle \otimes |\psi_j\rangle) = |0\rangle \otimes |\psi_{j+1}\rangle. \tag{3.4}$$

A relevant observation in this context is that there are physical systems where the implementation of S' is easier than that of S. We will discuss one such system in Section 4.5.1 [60]. In that case, applying a compensatory bit flip on the internal state, after each application of S', reduces the modified quantum walk to the usual scheme. In all, this would require $(t-1)$ compensatory bit flip operation in addition for a t step quantum walk, which adds to the complexity of the experimental realization. However, this additional complexity can be eliminated. For a quantum walk using $B_{\xi,\theta,\zeta}$ (2.31) as coin operation, applying a bit flip in each step can be shown to be equivalent to a spatial inversion of the position probability distribution. A quick way to see why bit flips are harmless is to note that they are also equivalent to relabeling the edges of the graph on which the quantum walk takes place, so that each end of each edge has the same label [103][1]. We may in this sense call a bit flip together with spatial inversion a *symmetry* of the quantum walk on a line. To be specific, when any unitary operation augmented during each step of quantum walk which may leave the position probability distribution unaffected, then it is called a quantum walk symmetry.

---

[1] It is worth noting that in [58], bit flips are employed to improve the practical implementation of a quantum walk on atoms in an optical lattice

Experimentally, the symmetries are useful in identifying variants of a given quantum walk protocol that are equivalent to it. This motivates us to look for other (discrete) symmetries of the quantum walk, which we study below. We begin with Theorem 1, where we note four discrete symmetries, associated with the matrices $B^{(\mathrm{f})}$ ($\mathrm{f} = 1, 2, 3, 4$) (3.5), of the quantum walk. Thereafter two of these symmetries, $B^{(1)}$ and $B^{(2)}$, are identified with operations that are relevant from the perspective of physical implementation. It is an interesting open question with relevance to practical implementation of quantum walks, whether other such symmetries of the quantum walk exist.

Theorem 1. If $B = B_{\xi,\theta,\zeta}$[2] in (2.37) is replaced by any of $B^{(1)}$, $B^{(2)}$, $B^{(3)}$, or $B^{(4)}$, given by,

$$\begin{aligned}
B^{(1)} &\equiv \begin{pmatrix} e^{i\xi}\cos(\theta) & e^{i\zeta}\sin(\theta) \\ e^{i(\phi-\zeta)}\sin(\theta) & -e^{i(\phi-\xi)}\cos(\theta) \end{pmatrix}, \\
B^{(2)} &\equiv \begin{pmatrix} e^{i\xi}\cos(\theta) & e^{i(\phi+\zeta)}\sin(\theta) \\ e^{-i\zeta}\sin(\theta) & -e^{i(\phi-\xi)}\cos(\theta) \end{pmatrix}, \\
B^{(3)} &\equiv \begin{pmatrix} e^{i(\phi+\xi)}\cos(\theta) & e^{i(\phi+\zeta)}\sin(\theta) \\ e^{-i\zeta}\sin(\theta) & -e^{-i\xi}\cos(\theta) \end{pmatrix}, \\
B^{(4)} &\equiv \begin{pmatrix} e^{i(\phi+\xi)}\cos(\theta) & e^{i\zeta}\sin(\theta) \\ e^{i(\phi-\zeta)}\sin(\theta) & -e^{-i\xi}\cos(\theta) \end{pmatrix},
\end{aligned} \tag{3.5}$$

the resulting position probability distribution of the quantum walk remains invariant.

Proof. With the notation $B \equiv \{b_{q,r}\}$ and $B^{(\mathrm{f})} \equiv \{b^{(\mathrm{f})}_{q,r}\}$, we find

$$b^{(1)}_{q,r} = b_{q,r}e^{iq\phi} \;\; ; \;\; b^{(2)}_{q,r} = b_{q,r}e^{ir\phi} \;\; ; \;\; b^{(3)}_{q,r} = b_{q,r}e^{i\bar{q}\phi} \;\; ; \;\; b^{(4)}_{q,r} = b_{q,r}e^{i\bar{r}\phi}, \tag{3.6}$$

where the matrix indices q, r take values 0 and 1, $i \equiv +\sqrt{-1}$, and the overbar denotes a NOT operation ($0 \leftrightarrow 1$). The state vector obtained, after t steps, using

---

[2] Three parameter quantum coin operation (2.37) is used instead of SU(2) operation so that B reduces to Hadamard operation operation for $\xi = \zeta = 0, \theta = \pi/4$

B and $B^{(1)}$ as the coin rotation operations, are, respectively, given by

$$\begin{aligned}
|\Psi_1\rangle &= (SB)^t|\alpha,\beta\rangle = \sum_{q_1,q_2,\cdots,q_t} b_{q_t,q_{t-1}}\cdots b_{q_2,q_1}b_{q_1,\alpha}|q_t,\beta+2Q-t\rangle, \\
|\Psi_2\rangle &= (SB^{(1)})^t|\alpha,\beta\rangle \\
&= \sum_{q_1,q_2,\cdots,q_t} b_{q_t,q_{t-1}}\cdots b_{q_2,q_1}b_{q_1,\alpha}(e^{i\phi})^{q_{t-1}+\cdots+q_1+\alpha}|q_t,\beta+2Q-t\rangle, \quad (3.7)
\end{aligned}$$

where $Q = q_1 + \cdots + q_t$. Consider one of the element $|a,b\rangle$ in the computational-and-position basis. Now,

$$\langle a,b|\Psi_1\rangle = e^{i\eta\phi}\langle a,b|\Psi_2\rangle, \tag{3.8}$$

where $\eta = q_{t-1} + \cdots + q_1 + \alpha$, which is fixed for given α and b, and determined by $b = \beta + 2Q - t$ and $q_t = a$. As a result,

$$|\langle a,b|\Psi_1\rangle|^2 + |\langle \bar{a},b|\Psi_1\rangle|^2 = |\langle a,b|\Psi_2\rangle|^2 + |\langle \bar{a},b|\Psi_2\rangle|^2. \tag{3.9}$$

A similar proof of invariance of the position distribution can be demonstrated to hold when B is replaced by one of the other $B^{(\mathrm{f})}$'s (f $= 2,3,4$). On account of the linearity of quantum mechanics, the invariance of the walk statistics under exchange of the $B^{(\mathrm{f})}$'s and B holds even when the initial state $|\alpha,\beta\rangle$ is replaced by a general superposition or a mixed state. ■

Interchanging B and the $B^{(\mathrm{f})}$'s may be considered as a discrete symmetry operation $G : B \to B^\star$ (where $B^\star$ denotes any of the $B^{(\mathrm{f})}$'s in (3.5)), that leaves the positional probability distribution invariant. We express this by the statement that

$$\widehat{W} \simeq \mathbf{G}\widehat{W}, \tag{3.10}$$

where $\mathbf{G}$ refers to the application of G at each step of the walk, and $\widehat{W}$ refers to the walk operation of evolving the initial state through t steps and then measuring in the position basis. Knowledge of this symmetry can help simplify practical quantum walks. Below we identify two of these quantum walk symmetry operations $B \leftrightarrow B^{(1)}$ and $B \leftrightarrow B^{(2)}$, associated with physical operations of interest.

We first consider the phase shift operation

$$\Phi(\phi) \equiv |0\rangle\langle 0| + e^{i\phi}|1\rangle\langle 1| \tag{3.11}$$

as a *symmetry operation* of a quantum walk. In our model, the quantum operation for each step is augmented by the insertion of $\Phi(\phi)$ just after the operation $S(B\otimes \mathbb{1})$. At each step, the walk evolves according to

$$\begin{aligned} W_\Phi \ &\equiv \ \begin{pmatrix} 1 & 0 \\ 0 & e^{i\phi} \end{pmatrix} \left[\begin{pmatrix} 1 & 0 \\ 0 & 0 \end{pmatrix} \otimes \hat{a} + \begin{pmatrix} 0 & 0 \\ 0 & 1 \end{pmatrix} \otimes \hat{a}^\dagger \right] \begin{pmatrix} e^{i\xi}\cos(\theta) & e^{i\zeta}\sin(\theta) \\ e^{-i\zeta}\sin(\theta) & -e^{-i\xi}\cos(\theta) \end{pmatrix} \\ &= \ \left[\begin{pmatrix} 1 & 0 \\ 0 & 0 \end{pmatrix} \otimes \hat{a} + \begin{pmatrix} 0 & 0 \\ 0 & 1 \end{pmatrix} \otimes \hat{a}^\dagger \right] \begin{pmatrix} e^{i\xi}\cos(\theta) & e^{i\zeta}\sin(\theta) \\ e^{i(\phi-\zeta)}\sin(\theta) & -e^{i(\phi-\xi)}\cos(\theta) \end{pmatrix}. \end{aligned} \tag{3.12}$$

This is equivalent to replacing B by $B^{(1)}$, which, according to Theorem 1, leaves the walk distribution invariant. Thus the operation $\Phi(\phi)$, applied at each step, is a symmetry of the quantum walk.

As a special case, the phase flip operation $Z = \sigma_z$, a Pauli z operation applied at each step, obtained by setting $\phi = \pi$, is a symmetry of the quantum walk. Representing the inclusion of operations Φ or Z at each step of the walk by $\mathbf{\Phi}$ or $\mathbf{Z}$, respectively, we express this symmetry by the statements :

$$\widehat{W} \simeq \mathbf{\Phi}\widehat{W}, \tag{3.13a}$$

$$\widehat{W} \simeq \mathbf{Z}\widehat{W}. \tag{3.13b}$$

Unlike the phase flip operation, bit flip is not a symmetry of the quantum walk on a line. However, the combined application of bit flip along with angular reflection R ($\theta \to \pi/2 - \theta$, i.e., $\sin\theta \leftrightarrow \cos\theta$, and $\xi \leftrightarrow -\zeta$) and parity P ($\hat{a} \leftrightarrow \hat{a}^\dagger$) turns out to be a symmetry operation. These three operations commute with each other. By the inclusion of PRX, the walker evolves by $([PRX]SB)^t$. At each step, the walker evolves according to

$$\begin{aligned} W_P &\equiv PR\begin{pmatrix} 0 & 1 \\ 1 & 0 \end{pmatrix}\left[\begin{pmatrix} 1 & 0 \\ 0 & 0 \end{pmatrix}\otimes \hat{a} + \begin{pmatrix} 0 & 0 \\ 0 & 1 \end{pmatrix}\otimes \hat{a}^\dagger\right]\begin{pmatrix} e^{i\xi}\cos(\theta) & e^{i\zeta}\sin(\theta) \\ e^{-i\zeta}\sin(\theta) & -e^{-i\xi}\cos(\theta) \end{pmatrix} \\ &= \left[\begin{pmatrix} 1 & 0 \\ 0 & 0 \end{pmatrix}\otimes \hat{a} + \begin{pmatrix} 0 & 0 \\ 0 & 1 \end{pmatrix}\otimes \hat{a}^\dagger\right]\begin{pmatrix} e^{i\xi}\cos(\theta) & -e^{i\zeta}\sin(\theta) \\ e^{-i\zeta}\sin(\theta) & e^{-i\xi}\cos(\theta) \end{pmatrix}. \end{aligned} \tag{3.14}$$

This is equivalent to replacing B by $B^{(2)}$ with $\phi = \pi$, which, according to Theorem 1, should leave the walk distribution invariant. Thus the operation PRX applied at each step, is a symmetry of the quantum walk. It will be convenient henceforth to choose $\xi = \zeta = 0$, so that R will simply correspond to the replacement $\theta \rightarrow \pi/2-\theta$.

Representing the inclusion of operations P, R or X at each step of the walk by $\mathbf{P}$, $\mathbf{R}$ or $\mathbf{X}$, respectively, we express this symmetry by the statements:

$$\widehat{W} \simeq \mathbf{PRX}\widehat{W}, \tag{3.15a}$$

$$\mathbf{X}\widehat{W} \simeq \mathbf{PR}\widehat{W}. \tag{3.15b}$$

The above expression (3.15a) was proved immediately above and (3.15b) follows from (3.15a), since the operations $\mathbf{P}$, $\mathbf{R}$ and $\mathbf{X}$ mutually commute, and $X^2 = \mathbb{I}$. It expresses the fact that applying the X operation at each step is equivalent to replacing a quantum walk by its angle-reflected, spatially inverted counterpart. The observation made at the beginning of this section pertains to the special case of $\theta = 45^\circ$. By a similar technique the following symmetries may be proved,

$$\mathbf{X}\widehat{W} \simeq \mathbf{XZ}\widehat{W} \simeq \mathbf{ZX}\widehat{W}. \tag{3.16}$$

The first equivalence easily follows from (3.13).

3.2.2 Environmental effects

A quantum walk implemented on a physical system is is inevitably affected by noise due to the environment. We consider three physically relevant models of noise: a phase flip channel (which is equivalent to a phase damping or purely dephasing channel), a bit flip channel and a generalized amplitude damping channel

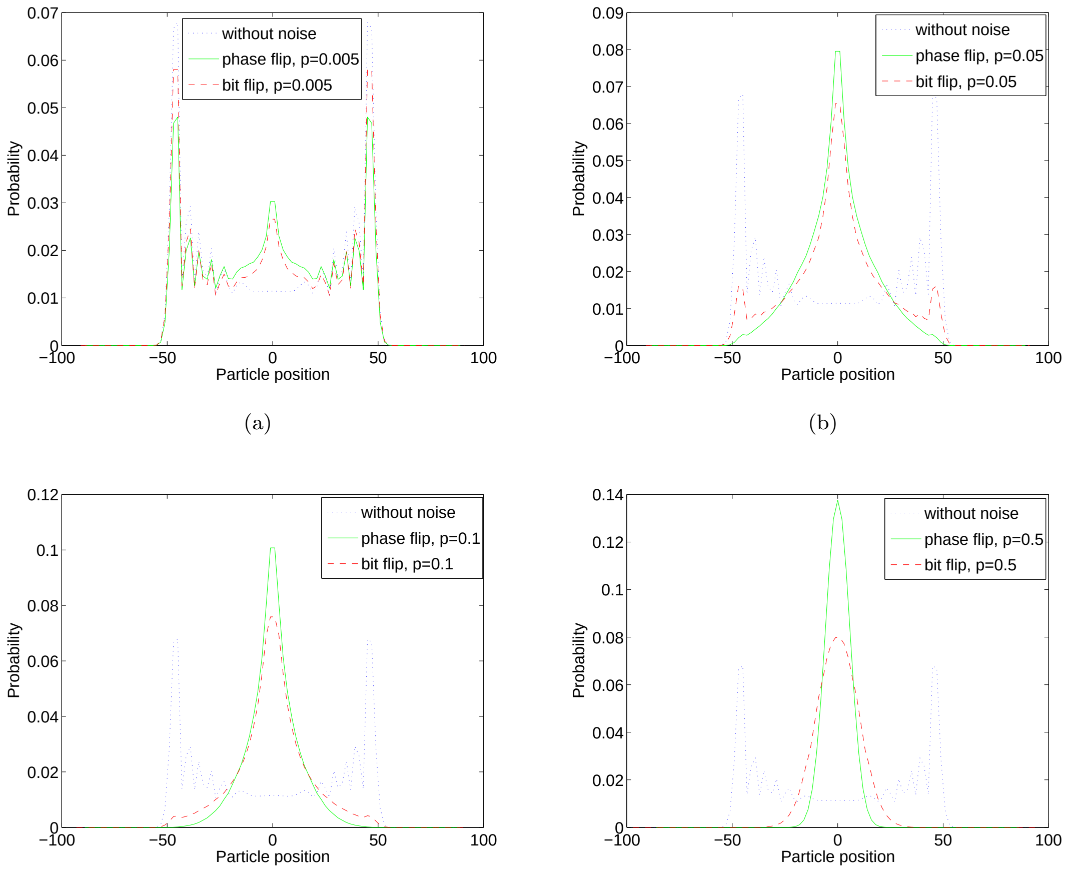

(a) (b)

(c) (d)

FIGURE 3.1: The effect of environmental decoherence on the position probability distribution of a quantum walk subjected to a noisy channel. Coin bias is of the form (2.37) with $\theta = 60°, \xi = \zeta = 0$. The noise is modeled as a phase flip (solid line) or bit flip (dashed line) channel, characterized by (3.24) and (3.30), respectively, at various noise levels p : (a) $p = 0.005$; (b) $p = 0.05$; (c) $p = 0.1$; (d) $p = 0.5$, which corresponds to a fully classical random walk. Comparing Figure (d) with Figure 3.2(d), we note that the distribution in the case of maximal bit flip noise is the same. The distribution is for 100 steps.

$(T \geq 0)$. In all cases, our numerical implementation of these channels evolves the density matrix employing the Kraus operator representation for them. However to explain symmetry effects, it is convenient to use the *quantum trajectories* approach, discussed below.

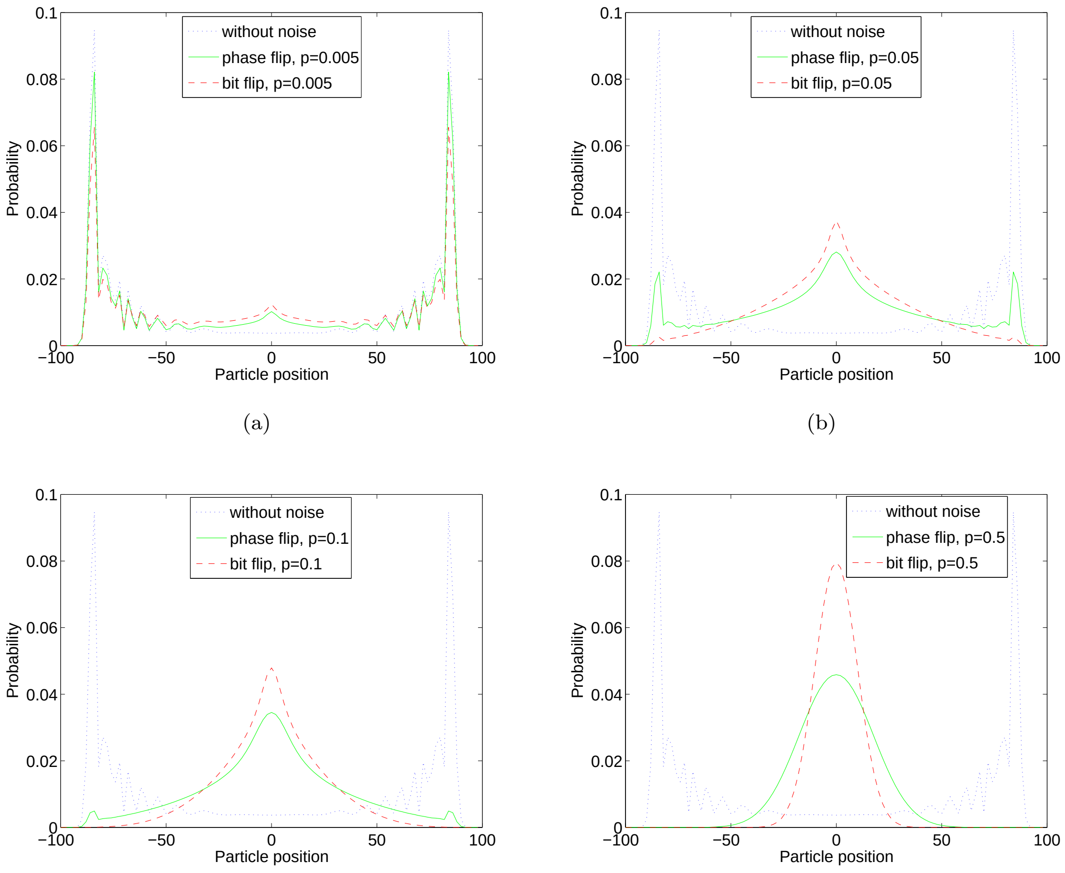

(a) (b)

(c) (d)

FIGURE 3.2: The effect of environmental decoherence on the position probability distribution of a quantum walk subjected to a noisy channel. Coin bias is of the form (2.37) with $\theta = 30°, \xi = \zeta = 0$. The noise is modeled as a phase flip (solid line) or bit flip (dashed line) channel, characterized by (3.24) and (3.30), respectively, at various noise levels p: (a) $p = 0.005$ (b) $p = 0.05$; (c) $p = 0.1$; (d) $p = 0.5$, which corresponds to a fully classical random walk. The distribution is for 100 steps.

3.2.2.1 Phase damping and bit flip channels

In studying the status of the walk symmetries in the presence of noise, it is advantageous to employ the quantum trajectories approach [104]. This simplifies the description of an open quantum system in terms of a stochastically evolving pure state, which allows us to adapt the symmetry results for the pure states, given in the preceding section, to mixed states.

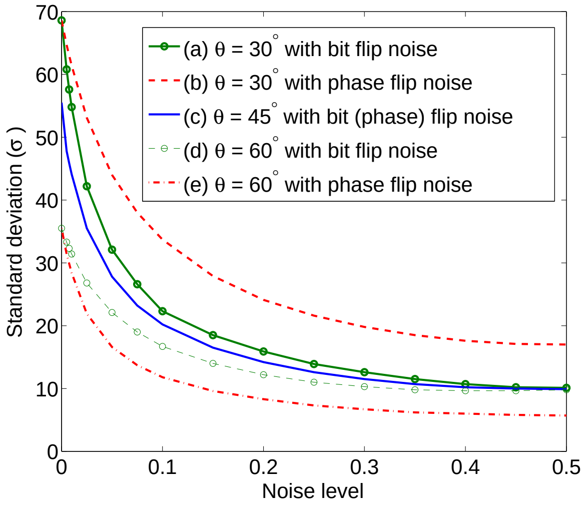

FIGURE 3.3: Variation of standard deviation with noise level, for both phase noise and bit flip noise. (a) and (b) is for $\theta = 30°$; (c) is for Hadamard walk ($\theta = 45°$); (d) and (e) is for $\theta = 60°$ in the quantum coin operation $B_{0,\theta,0}$. In the classical limit of $p = 0.5$, the standard deviation converges to a fixed value for bit flip noise, irrespective of θ, but different for phase flip noise. The convergence happens because, at maximum bit flip noise ($p = 0.5$), the measurement outcome in the computational basis is completely randomized. On the other hand, the non-convergence in the case of phase flip noise is due to the fact that the asymptotic mixed state obtained via a phase damping channel depends on the value of the θ. The standard deviation was calculated for 100 steps of quantum walk.

We call the sequence of walk step operations,

$$\widehat{X} \equiv (SB_t)(SB_{t-1}) \cdots (SB_x) \cdots (SB_1), \tag{3.17}$$

a 'quantum trajectory'. (More precisely, a trajectory refers to the sequence of states produced by these operations, for which the above serves as a convenient representation.) If all the B_x's with x taking values from 1 to t are the same, then $\widehat{X}$ is the usual 'homogeneous' quantum walk $\widehat{W}$. In general, the B_x's may be different $U(2)$ operators, $B^{(\mathrm{f})}$. More generally, each step of the walk may include generalized measurements whose outcomes are known (Section 3.2.2.2). If each walk step in $\widehat{X}$ is subjected to a fixed symmetry operation G, the result is a new quantum trajectory

$$\mathbf{G}\widehat{X} \equiv (SB_t^{\star})(SB_{t-1}^{\star}) \cdots (SB_1^{\star}). \tag{3.18}$$

We have the following generalization of Theorem 1 to inhomogeneous quantum walks on a line.

Theorem 2. Given any quantum walk trajectory $\widehat{X} = (SB_t)\cdots(SB_1)$, the symmetry $\mathcal{G}$ holds, i.e., $\widehat{X} \simeq \mathbf{G}\widehat{X}$. If the operation $\mathbf{\Phi}$ (3.11) is restricted to $\mathbf{Z}$, that is operation Z at each step of the walk, then the symmetries hold even when some of the S's are replaced by $S^\dagger$'s.

Proof. In the proof of Theorem 1, we note that if, in each step of the walk, we alter the rotation B by the transformation G, the proof still goes through. That is, $|\Psi_1\rangle \equiv (SB_t)(SB_{t-1})\cdots(SB_1)|\alpha,\beta\rangle$ and $|\Psi_2\rangle \equiv (SB_t^\star)(SB_{t-1}^\star)\cdots(SB_1^\star)|\alpha,\beta\rangle$ produce the same position distribution.

Suppose that in some of the walk steps, S is replaced with $S^\dagger$. In place of (3.7), we have

$$\begin{aligned}|\Psi_1\rangle &= (SB_t)\cdots(S^\dagger B_x)\cdots(SB_1)|\alpha,\beta\rangle \\ &= \sum_{q_1,q_2,\cdots,q_t} b_{q_t,q_{t-1}}\cdots b_{q_2,q_1}b_{q_1,\alpha}|q_t,\beta+2(Q_1-Q_2)-(t_1-t_2)\rangle, \qquad (3.19a)\\ |\Psi_2\rangle &= (SB_t^{(1)})\cdots(S^\dagger B_x^{(1)})\cdots(SB_1^{(1)})|\alpha,\beta\rangle \\ &= \sum_{q_1,q_2,\cdots,q_t} b_{q_t,q_{t-1}}\cdots b_{q_2,q_1}b_{q_1,\alpha}(-1)^{q_{t-1}+\cdots+q_1+\alpha}|q_t,\beta+2(Q_1-Q_2)-(t_1-t_2)\rangle, \qquad (3.19b)\end{aligned}$$

where $Q_1 = \sum_k q_k$ for the t_1 steps k where operator S is used, and $Q_2 = \sum_l q_l$ for the t_2 steps l where operator $S^\dagger$ is used. Here $Q = Q_1 + Q_2$ and $t = t_1 + t_2$. Observe that the exponent of (-1) is effectively evaluated in modulo-2 arithmetic. We can thus replace Q by $Q_1 - Q_2$ in the exponent. Following the argument in Theorem 1, we find that

$$\langle a,b|\Psi_1\rangle = e^{i\Theta}\langle a,b|\Psi_2\rangle, \qquad (3.20)$$

where $\Theta = Q_1 - Q_2 - a + \alpha$. ■

As a corollary, the symmetries **Z** and **PRX** hold good because they reduce to special cases of **G**. A question of practical interest is whether **PRX** and **Z** are symmetries of a noisy quantum walk. Suppose we are given a noise process $\mathcal{N}$ in the Kraus representation :

$$\rho \longrightarrow \mathcal{N}(\rho) = \sum_{x=0}^{t-1} E_x \rho E_x^\dagger, \quad \sum_x E_x^\dagger E_x = \mathbb{I}. \tag{3.21}$$

With the inclusion of noise, each step of the quantum walk becomes augmented to $(\Pi S B_k)$, where Π is a random variable that takes Kraus operator values E_x. Thus, $\mathcal{N}$ corresponds to a mixture of upto t^t trajectories or 'unravellings'

$$\widehat{X}_l \equiv (\Pi(l_t) S B_t) \cdots (\Pi(l_1) S B_1) \,, \tag{3.22}$$

each occurring with some probability p_l, where $\sum_l p_l = 1$. If $\mathbf{Z}$ and $\mathbf{PRX}$ are symmetries of an unraveling $\widehat{X}_l$, then the operations $\widehat{X}_l$ and

$$\mathbf{D}\widehat{X}_l \equiv (\Pi(l_t) DUB_t) \cdots (\Pi(l_1) DUB_1) \,, \tag{3.23}$$

where $\mathbf{D}$ denotes $\mathbf{Z}$ or $\mathbf{PRX}$, must yield the same position probability distribution. In the case of bit-flip and phase-flip channels, there is a representation in which the E_x's are proportional to unitary operators.

Theorem 3. If trajectories $\widehat{X}_l$ are individually symmetric under operation $\mathbf{G}$, then so is any noisy quantum walk represented by a collection $\{\widehat{X}_l, p_l\}$.

Proof. The state of the system obtained via $\mathcal{N}$ is a linear combination (the average) of states obtained via the $\widehat{X}_x$'s. Thus, the invariance of the $\widehat{X}_x$'s under $\mathbf{G}$ implies the invariance of the former. ■

This result, together with those from the preceding Section, can now be easily shown to imply that the symmetry $\mathbf{D}$ is preserved in the case of phase-flip and bit-flip channels.

Decoherence via a purely dephasing channel, without any loss of energy, can be modeled as a phase flip channel [8]:

$$\mathcal{E}(\rho) = (1-p)\rho + pZ\rho Z. \tag{3.24}$$

An example of a physical process that realizes (3.24) is a two-level system interacting with its bath via a quantum non-demolition (QND) interaction given by the Hamiltonian

$$\begin{aligned} \mathbf{H} &= \mathbf{H}_S + \mathbf{H}_R + \mathbf{H}_{SR} \\ \mathbf{H} &= \mathbf{H}_S + \sum_k \hbar\omega_k \hat{b}_k^\dagger \hat{b}_k + \mathbf{H}_S \sum_k g_k(\hat{b}_k + \hat{b}_k^\dagger) + \mathbf{H}_S^2 \sum_k \frac{g_k^2}{\hbar\omega_k}. \end{aligned} \tag{3.25}$$

Here $\mathbf{H}_S$ stands for the Hamiltonian of the system (S), for our noise channels the system is only the particle (coin degree of freedom). $\mathbf{H}_R$ and $\mathbf{H}_{SR}$ are reservoir (R) and system-reservoir (SR) interaction, respectively. Operators $\hat{b}$ and $\hat{b}^\dagger$ are the annihilation and creation operators. The last term on the RHS of (3.25) is a renormalization inducing 'counter term'. Since $[\mathbf{H}_S, \mathbf{H}_{SR}] = 0$, (3.25) is of QND type.

Following [105] (apart from a change in notation which switches $|0\rangle \longleftrightarrow |1\rangle$), taking into account the effect of the environment modeled as a thermal bath, the reduced dynamics of the system can be obtained, which can be described using Bloch vectors as follows. Its action on an initial state

$$\rho_0 \equiv \begin{pmatrix} \frac{1}{2}\left(1 + \langle\sigma_z(0)\rangle\right) & \langle\sigma_-(0)\rangle \\ \langle\sigma_+(0)\rangle & \frac{1}{2}\left(1 - \langle\sigma_z(0)\rangle\right) \end{pmatrix}, \tag{3.26}$$

is given in the interaction picture by

$$\mathcal{E}(\rho_0) = \begin{pmatrix} \frac{1}{2}\left(1 + \langle\sigma_z(0)\rangle\right) & \langle\sigma_-(0)\rangle e^{-(\hbar\omega)^2\gamma(t)} \\ \langle\sigma_+(0)\rangle e^{-(\hbar\omega)^2\gamma(t)} & \frac{1}{2}\left(1 - \langle\sigma_z(0)\rangle\right) \end{pmatrix}. \tag{3.27}$$

Here σ_+ and σ_- are the standard raising and lowering operators given by

$$\sigma_+ = |1\rangle\langle 0| = \frac{1}{2}(\sigma_x + i\sigma_y) \quad ; \quad \sigma_- = |0\rangle\langle 1| = \frac{1}{2}(\sigma_x - i\sigma_y) \tag{3.28}$$

where σ_x, σ_y and σ_z are the Pauli spin operator in x, y and z directions, respectively. The initial state (3.26) may be mixed. (The derivation of the superoperator $\mathcal{E}$ in terms of environmental parameters for the pure state case, given explicitly in [105], is directly generalized to the case of an arbitrary mixture of pure states, since the environmental parameters are assumed to be independent of the system's state.)

Comparing (3.27) with (3.24) allows us to relate the noise level p in terms of physical parameters. In particular,

$$p = \frac{1}{2}\left(1 - \exp\left[-(\hbar\omega)^2\gamma(t)\right]\right). \tag{3.29}$$

When $\gamma(t) \approx 0$ (either because the coupling with the environment is very weak or the interaction time is short or the temperature is low), $p \approx 0$, tending towards the noiseless case. On the other hand, under strong coupling, $\gamma(t)$ is arbitrarily large, and $p \rightarrow 1/2$, the maximally noisy limit. The result of implementing channel (3.24) is to drive the position probability distribution towards a classical Gaussian pattern [103]. The effect of increasing phase noise in the presence on quantum walk is depicted in Figure 3.1, for the case of $\theta = 60^\circ$, and in Figure 3.2, for the case of $\theta = 30^\circ$. The onset of classicality is observed in the Gaussianization of the probability distribution. This is reflected also in the fall of standard deviation, as shown in Figure 3.3.

Decoherence can also be introduced by another noise model, the bit flip channel [8],

$$\mathcal{E}(\rho) = (1-p)\rho + pX\rho X. \tag{3.30}$$

As with the phase damping channel, the bit flip channel also drives the probability distribution towards a classical, Gaussian pattern, with increasing noise [103]. The effect of increasing bit flip noise in the presence of biased walk is depicted in Figures 3.1 and 3.2. Here again, the onset of classicality is observed in the Gaussianization of the probability distribution, as well as in the fall of standard deviation, as shown in Figure 3.3.

A difference in the classical limit of these two noise processes, as observed in Figure 3.3, is that whereas the standard deviation (in fact, the distribution) is unique in the case of the bit flip channel irrespective of θ, in the case of phase flip noise, the classical limit distribution is θ dependent. This is because phase flip noise leads, in the Bloch sphere picture, to a coplanar evolution of states towards the σ_z axis. Thus all initial pure states corresponding to a fixed θ evolve asymptotically to the

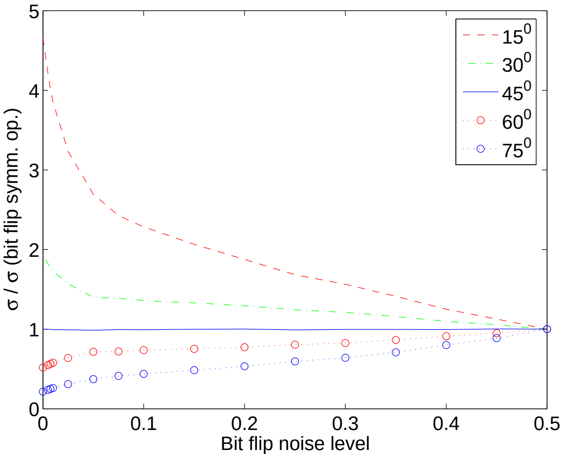

FIGURE 3.4: Variation of the ratio of standard deviation without any symmetry operation to the bit flip symmetry operation with increasing bit flip noise level. The standard deviation was calculated for 100 steps of walk.

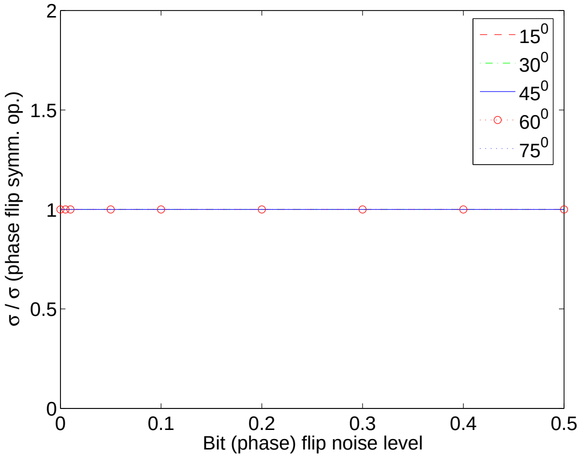

FIGURE 3.5: Variation of the ratio of standard deviation without any symmetry operation to the phase flip symmetry operation with increasing bit flip (phase flip) noise level. The standard deviation was calculated for 100 steps of walk.

same mixed state [8, 105]. This also explains the contrasting behavior of bit flip and phase flip noise with respect to θ, as seen by comparing Figures 3.1 and 3.2.

Representing the walk distribution by its standard deviation σ, we may describe

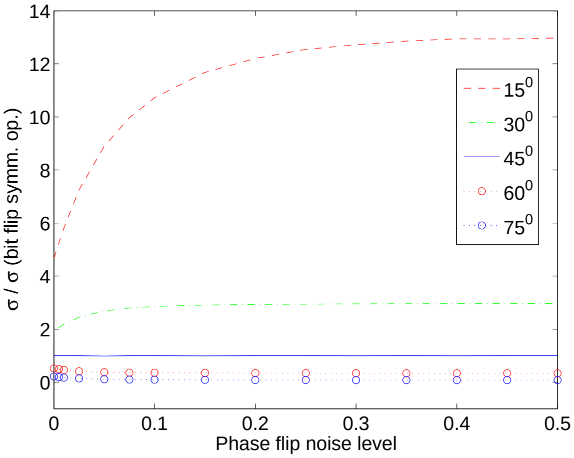

FIGURE 3.6: Variation of the ratio of standard deviation without any symmetry operation to the bit flip symmetry operation with increasing phase flip noise level. The standard deviation was calculated for 100 steps of walk.

symmetry by the ratio of σ without the symmetry operation to σ with the symmetry operation. Figure 3.4 depicts the symmetry operation **X** for various bit flip noise levels. The convergence of the curves representing various θ's is a consequence of the complete randomization of the measured bit outcome in the computational basis. This implies that although **X** is not a symmetry of non-Hadamard walk ($\theta \neq \pi/4$), it does become one in the fully classical limit. On the other hand, the symmetries **PRX** remain unaffected by noise. We note that, since the quantum walk here is evolved from the symmetric state $\frac{1}{\sqrt{2}}(|0\rangle + i|1\rangle)$, and the bit flip and phase flip noise are not partial to the state $|0\rangle$ or $|1\rangle$, this is equivalent to setting **P** to 1, which explains the fact that the distributions in Figures 3.1 and 3.2 are spatially symmetric. Thus, **RX** by itself becomes a symmetry operation, which is manifested in the fact that in Figure 3.4 the values of the curve for complementary angles are the inverse of each other. Figure 3.5 shows that for either of the two noises, **Z** is a walk symmetry.

Figure 3.6 depicts the symmetry of the **RX** operation at all phase flip noise levels, as evident from that fact that the values of the curve for complementary angles are the inverse of each other. From Figures 3.4, 3.5 and 3.6, we note that for the Hadamard walk, all three symmetry operations $\mathbf{Z}, \mathbf{X}$ and **R** are individually preserved. This is expected because here $\mathbf{P} = 1$ as stated earlier, $\mathbf{R} = 1$ by definition, so that the symmetry of $\mathbf{PRX}$ implies $\mathbf{X} = 1$.

With the non-Hadamard coin operation and an initial arbitrary state, the full symmetries $\mathbf{Z}$ and $\mathbf{PRX}$ would be required, as proved by the following theorem.

Theorem 4. The operations $\mathbf{PRX}$ and $\mathbf{Z}$ are symmetries for the phase-flip and bit-flip channels.

Proof. We may look upon the phase flip channel (3.24) as a probabilistic mixture (in the discretized walk model) of 2^t quantum trajectories with $\Pi \in \{\mathbb{I}, Z\}$. By virtue of Theorem 3, it suffices to show that any given unraveling is invariant under $\mathbf{Z}$ and $\mathbf{PRX}$. Consider an unraveling

$$\widehat{X}^1 \equiv \cdots (ISB)(ZSB)(ISB) \cdots = \cdots (SB)(ZSB)(SB) \cdots . \tag{3.31}$$

This is the same as: $\cdots (SB)(SB')(SB) \cdots$, where $B' = ZB$, noting that Z commutes with S. Now,

$$\mathbf{Z}\widehat{X}^1 = \cdots (IZSB)(ZZSB)(IZSB) \cdots = \cdots (ZSB)(ZSB')(ZSB) \cdots , \tag{3.32}$$

which, by Theorem 2, is equivalent to $\widehat{X}^1$. Also, by Theorem 2

$$\begin{aligned} \mathbf{PRX}\widehat{X}^1 &= \cdots (PRX\ SB)(Z\ PRX\ SB)(PRX\ SB) \cdots \\ &= \cdots (PRX\ SB)(PR\ ZX\ SB)(PRX\ SB) \cdots \\ &= \cdots (PRX\ SB)(PR\ ZXZ\ ZSB)(PRX\ SB) \cdots \\ &= \cdots (PRX\ SB)(PR\,(-X)\ SB')(PRX\ SB) \cdots , \end{aligned} \tag{3.33}$$

which, by Theorem 2, is equivalent to $\widehat{X}^1$, since an overall phase factor of ± 1 is irrelevant. Thus, the phase-flip channel is symmetric with respect to the operations $\mathbf{Z}$ and $\mathbf{PRX}$.

Regarding the bit-flip channel (3.30): as in the above case, consider an unraveling

$$\widehat{X}^2 \equiv \cdots (SB)(XSB)(SB) \cdots . \tag{3.34}$$

This is the same as: $\cdots(SB)(S^\dagger B'')(SB)\cdots$, where, as may be seen by direct calculation, $B'' = XB$. Now,

$$\begin{aligned}\mathbf{Z}\widehat{X}^2 &= \cdots(Z\ SB)(X\ Z\ SB)(Z\ SB)\cdots \\ &= \cdots(Z\ SB)(X\ ZX\ XSB)(Z\ SB)\cdots \\ &= \cdots(Z\ SB)((-Z)\ S^\dagger B'')(Z\ SB)\cdots\,, \qquad (3.35)\end{aligned}$$

which, by Theorem 2, is equivalent to $\widehat{X}^2$, since an overall phase factor of ±1 is irrelevant. Further,

$$\begin{aligned}\mathbf{PRX}\widehat{X}^2 &= \cdots(PRX\ SB)(X\ PRX\ SB)(PRX\ SB)\cdots \\ &= \cdots(PRX\ SB)(PRX\ X\ SB)(PRX\ SB)\cdots \\ &= \cdots(PRX\ SB)(PRX\ S^\dagger B'')(PRX\ SB)\cdots\,, \qquad (3.36)\end{aligned}$$

by Theorem 2, is also equivalent to $\widehat{X}^2$. ■

3.2.2.2 Generalized amplitude damping channel

Here we study the behavior of quantum walk subjected to a generalized amplitude damping (with temperature $T \geq 0$), which would reduce at $T = 0$ to the amplitude damping channel. As an example of a physical process that realizes the generalized amplitude damping channel, we consider a two-level system interacting with a reservoir of harmonic oscillators, with the system-reservoir interaction being dissipative and of the weak Born-Markov type [106, 107] leading to a standard Lindblad equation, which in the interaction picture has the following form [108]

$$\frac{d}{dt}\rho^s(t) = \sum_{k=1}^{2}\left(2\mathcal{R}_k\rho^s\mathcal{R}_k^\dagger - \mathcal{R}_k^\dagger\mathcal{R}_k\rho^s - \rho^s\mathcal{R}_k^\dagger\mathcal{R}_k\right), \qquad (3.37)$$

where

$$\mathcal{R}_1 = (\gamma_0(N_{\rm th}+1)/2)^{1/2}\mathcal{R} \quad ; \quad \mathcal{R}_2 = (\gamma_0 N_{\rm th}/2)^{1/2}\mathcal{R}^\dagger (3.38)$$

and

$$N_{\rm th} = (\exp(\hbar\omega/k_B T) - 1)^{-1}, \qquad (3.39)$$

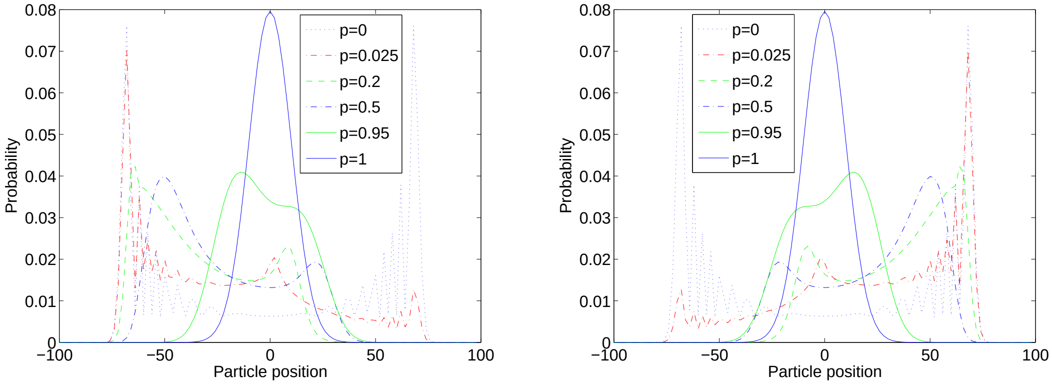

(a) (b)

FIGURE 3.7: Amplitude damping channel acting on a Hadamard walk at temperature $T = 0$. The distribution corresponding to intermediate values of p clearly show the breakdown of the **RX** symmetry. However, the extended symmetry, **PRX** (where **P** stands for parity operation (spatial inversion)) holds good. This is observed at all temperatures. (a) Probability distribution of finding the particle on which amplitude damping channel is acting. This shows that even at $T = 0$, for sufficiently high coupling, the distribution turns classical. (b) Amplitude damping channel with a bit flip symmetry.

is the Planck distribution giving the number of thermal photons at the frequency ω, and γ_0 is the system-environment coupling constant. Here

$$\mathcal{R} = \sigma_- \cosh(r) + e^{i\delta}\sigma_+ \sinh(r), \tag{3.40}$$

and the quantities r and δ are the environmental squeezing parameters and

$$\sigma_\pm = \frac{1}{2}\left(\sigma_x \pm i\sigma_y\right). \tag{3.41}$$

For the generalized amplitude damping channel, we set $r = \delta = 0$. If $T = 0$, so that $N_{\text{th}} = 0$, then $\mathcal{R}_2$ vanishes, and a single Lindblad operator suffices. The generalized amplitude damping channel is characterized by the following Kraus

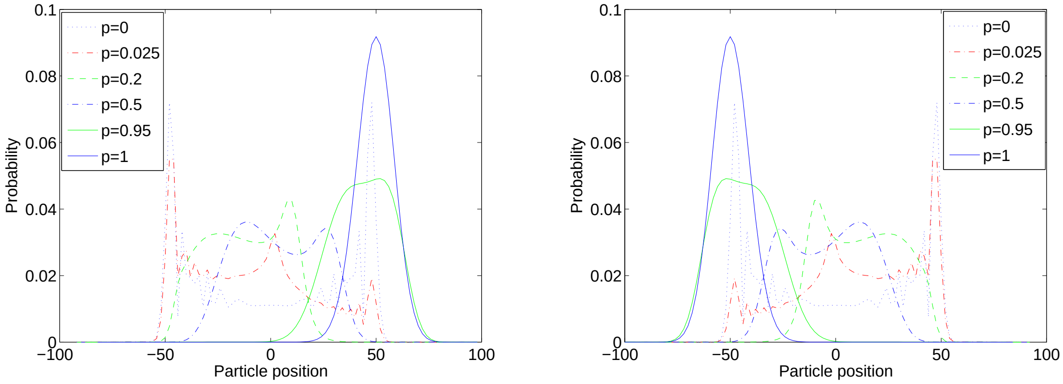

(a)

(b)

FIGURE 3.8: **PRX** symmetry seen to hold in quantum walk (with $\theta = 60°$ and $\theta = 30°$) subjected to amplitude damping ($T = 0$). The two cases are spatial inversions of each other. This holds for a generalized amplitude damping at any temperature. (a) walk with $\theta = 60°$; (b) $\theta = 30°$ and bit flip.

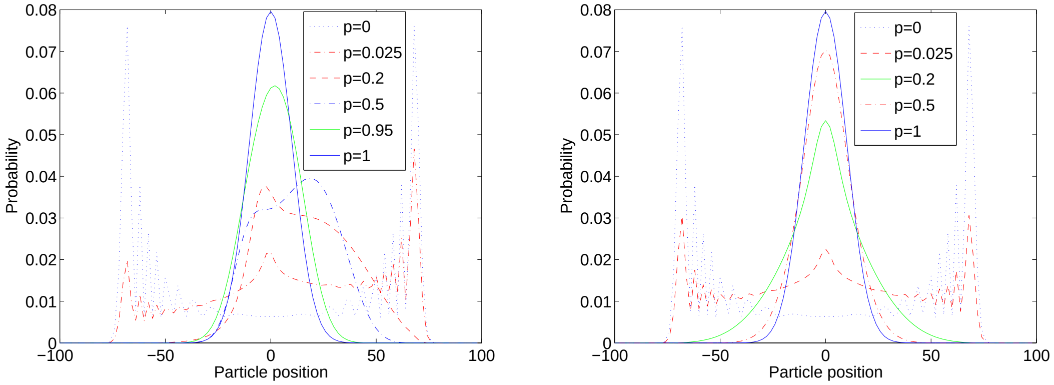

(a)

(b)

FIGURE 3.9: Onset of classicality is seen to be accentuated in a Hadamard walk subjected to generalized amplitude damping followed by bit flip with increasing temperatures (without bit flip the damping would have been to the right). Figure 3.7(a) depicts the $T = 0$ case ($\chi = 1$ in (3.43)). (a) Finite temperature corresponding to $\chi = 0.75$ (b) $T = \infty$, corresponding to $\chi = 0.5$. It may be noted that even at $T = \infty$, for sufficiently small coupling the distribution remains non-classical.

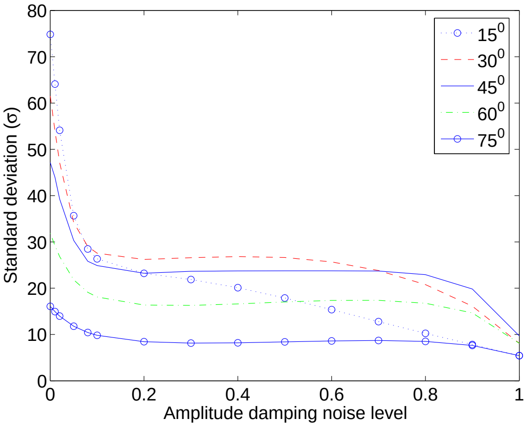

FIGURE 3.10: Variation of standard deviation with amplitude damping noise level for various value of θ, 15°, 30°, 45°, 60° and 75°. Note that the standard deviation for complementary angles converge to the same value.

operators,

$$E_0 \equiv \sqrt{\chi}\begin{bmatrix} 1 & 0 \\ 0 & \sqrt{1-p(t)} \end{bmatrix}; \qquad E_1 \equiv \sqrt{\chi}\begin{bmatrix} 0 & \sqrt{p(t)} \\ 0 & 0 \end{bmatrix},$$
$$E_2 \equiv \sqrt{1-\chi}\begin{bmatrix} \sqrt{1-p(t)} & 0 \\ 0 & 1 \end{bmatrix}; \qquad E_3 \equiv \sqrt{1-\chi}\begin{bmatrix} 0 & 0 \\ \sqrt{p(t)} & 0 \end{bmatrix}, \tag{3.42}$$

where

$$p(t) \equiv 1 - e^{-\gamma_0(2N_{\text{th}}+1)t}; \qquad \chi \equiv \frac{1}{2}\left[1 + \frac{1}{2N_{\text{th}}+1}\right]. \tag{3.43}$$

When $T = 0$, $\chi = 1$, and for $T \to \infty$, $\chi = 1/2$.

The density operator at a future time can be obtained as [108]

$$\rho^s(t) = \begin{pmatrix} \frac{1}{2}(1 + A_1) & A_2 \\ A_2^* & \frac{1}{2}(1 - A_1) \end{pmatrix}, \tag{3.44}$$

where

$$A_1 \equiv \langle\sigma_z(t)\rangle = e^{-\gamma_0(2N_{\text{th}}+1)t}\langle\sigma_z(0)\rangle - \frac{1}{(2N_{\text{th}}+1)}\left(1 - e^{-\gamma_0(2N_{\text{th}}+1)t}\right), \tag{3.45}$$

$$A_2 = e^{-\frac{\gamma_0}{2}(2N_{\text{th}}+1)t}\langle\sigma_-(0)\rangle\rangle. \tag{3.46}$$

Figures 3.7, 3.8 and 3.9 depict the onset of classicality with increasing coupling strength (related to p) and temperature (coming from χ). Figure 3.7, which shows the effect of an amplitude damping channel on a Hadamard walk at zero temperature, illustrates the breakdown of **RX** symmetry even though the initial state is $\frac{1}{\sqrt{2}}(|0\rangle + i|1\rangle)$. This is because, in contrast to the phase-flip and bit-flip channels, the generalized amplitude damping is not symmetric towards the states $|0\rangle$ and $|1\rangle$. However, the extended symmetry **PRX** is preserved both for Hadamard as well as quantum walks with $\theta \neq \pi/2$, as seen from Figures 3.7 and 3.8, respectively.

From Figures 3.7(a) and 3.9(a,b), the onset of classicality with increasing temperature is clearly seen. Figure 3.10 presents the standard deviation for quantum walks on a line with various biases, subjected to amplitude damping noise. The standard deviation for complementary angles ($\theta \leftrightarrow \pi/2 - \theta$) is seen to converge to the same value in the fully classical limit. This may be understood as follows. First, we note that since **PRX** is a symmetry of the quantum walk, and the effect of **P** does not show up in the standard deviation plots, **RX** by itself is an apparent symmetry. Further, in the classical limit the measurement outcome being a unique asymptotic state for the (generalized) amplitude damping channel, effectively $\mathbf{X} \simeq 1$, which makes **R** a symmetry operation.

The following theorem generalizes Theorem 2 to an open system subjected to a generalized amplitude damping channel.

Theorem 5. The operations **Z** and **PRX** are symmetries for the generalized amplitude damping channel.

Proof. By virtue of Theorem 3, it suffices to show that any given unraveling is invariant under **Z** and **PRX**. Consider an unraveling

$$\widehat{X}^3 \equiv \cdots (E_0 SB)(E_1 SB)(E_2 SB)(E_3 SB) \cdots \tag{3.47a}$$

$$\equiv \cdots (SB_{(0)})(S^\dagger B_{(1)})(SB_{(2)})(S^\dagger B_{(3)}) \cdots , \tag{3.47b}$$

where the non-unitary matrices are given by $B_{(x)} = E_x B$. Now,

$$\begin{aligned}
\mathbf{Z}\widehat{X}^3 &= \cdots(E_0ZSB)(E_1ZSB)(E_2ZSB)(E_3ZSB)\cdots \\
&= \cdots(ZE_0SB)((-Z)E_1SB)(ZE_2SB)((-Z)E_3SB)\cdots \\
&= \cdots(ZSB_{(0)})((-Z)S^\dagger B_{(1)})(ZSB_{(2)})((-Z)S^\dagger B_{(3)})\cdots \\
&= \cdots(SB^{(1)}_{(0)})(-S^\dagger B^{(1)}_{(1)})(SB^{(1)}_{(2)})(-S^\dagger B^{(1)}_{(3)})\cdots . \qquad (3.48)
\end{aligned}$$

Ignoring the overall ±1 factor in (3.48), and comparing it with (3.47a), and noting that that the derivation of the proof of Theorem 2 did not require the matrices B_j to be unitary, we find along similar lines that $\mathbf{Z}\widehat{X}^3$ is equivalent to $\widehat{X}^3$.

The following may be directly verified

$$\begin{aligned}
\mathbf{PRX}\widehat{X}^3 &= \cdots(E_0PRXSB)(E_1PRXSB)(E_2PRXSB)(E_3PRXSB)\cdots \qquad (3.49a) \\
&= \cdots(E_0SB^{(2)})(E_1SB^{(2)})(E_2SB^{(2)})(E_3SB^{(2)})\cdots \qquad (3.49b) \\
&= \cdots(SB^{(2)}_{(0)})(S^\dagger B^{(2)}_{(1)})(SB^{(2)}_{(2)})(S^\dagger B^{(2)}_{(3)})\cdots , \qquad (3.49c)
\end{aligned}$$

which, by Theorem 2, is equivalent to $\widehat{X}^3$. For proof of (3.49b), see the proof of Theorem 1. Equation (3.49c) is obtained analogously to (3.47b), except that the matrix $B^{(2)}$ is used instead of B. ■

This may be expressed by the statement

$$\begin{aligned}
\mathcal{N}\widehat{W} &\simeq \mathcal{N}\mathbf{Z}\widehat{W}, \qquad (3.50a) \\
\mathcal{N}\widehat{W} &\simeq \mathcal{N}\mathbf{PRX}\widehat{W}, \qquad (3.50b)
\end{aligned}$$

which generalizes (3.10). These results show that the symmetries persist for dephasing (phase flip), bit flip and (generalized) amplitude damping channels.

3.3 Symmetry and noise operations on an $n-$cycle

In previous section we considered symmetries for a quantum walk on a line, and the influence of noise on them. In this section we will extend the ideas to quantum walks on an $n-$cycle. We will show the breakdown of symmetry when the quantum walk is implemented on an $n-$cycle, the effect of noise and its influence on the restoration of symmetry.

3.3.1 Breakdown in symmetry

In contrast to the case of quantum walk on a line, none of the four discrete symmetries of Theorem 1 hold in general for unitary quantum walk on an $n-$cycle or closed path. Thus, if B (2.31) is replaced by any of $B^{(1)}$, $B^{(2)}$, $B^{(3)}$, or $B^{(4)}$, given by (3.5), the spatial probability distribution is not guaranteed to be the same.

Theorem 6. The operation $G : B \rightarrow B^{\star}$ is in general not a symmetry of the quantum walk on an $n-$cycle.

Proof. For the cyclic case, in place of (3.7), we now have

$$|\Psi_1\rangle = (SB)^t|\alpha,\beta\rangle = \sum_{q_1,q_2,\cdots,q_t} b_{q_t,q_{t-1}}\cdots b_{q_2,q_1}b_{q_1,\alpha}|q_t,\beta+2Q-t \text{ (mod } n)\rangle, \tag{3.51a}$$

$$\begin{aligned}|\Psi_2\rangle &= (SB^{(1)})^t|\alpha,\beta\rangle \\ &= \sum_{q_1,q_2,\cdots,q_t} b_{q_t,q_{t-1}}\cdots b_{q_2,q_1}b_{q_1,\alpha}(e^{i\phi})^{q_{t-1}+\cdots+q_1+\alpha}|q_t,\beta+2Q-t \text{ (mod } n)\rangle,\end{aligned} \tag{3.51b}$$

where n is the number of sites in an $n-$cycle. For an arbitrary state $|a,b\rangle$ in the computational-and-position basis, we have

$$\langle a,b|\Psi_1\rangle = \sum_{q_1,q_2,\cdots,q_{t-1}\in\mathcal{Q}} b_{a,q_{t-1}}\cdots b_{q_2,q_1}b_{q_1,\alpha} \tag{3.52a}$$

$$\begin{aligned}\langle a,b|\Psi_2\rangle &= \sum_{q_1,q_2,\cdots,q_{t-1}\in\mathcal{Q}} b_{a,q_{t-1}}\cdots b_{q_2,q_1}b_{q_1,\alpha}(e^{i\phi})^{q_{t-1}+\cdots+q_1+\alpha} \\ &\equiv \sum_{q_1,q_2,\cdots,q_{t-1}\in\mathcal{Q}} b_{a,q_{t-1}}\cdots b_{q_2,q_1}b_{q_1,\alpha}(e^{i\phi\epsilon}),\end{aligned} \tag{3.52b}$$

where $\mathcal{Q}$ is the set of binary $(t-1)$-tuples $q_1, q_2, \cdots, q_{t-1}$ such that

$$Q = q_1 + q_2 + \cdots + q_{t-1} + a \tag{3.53}$$

satisfies

$$b = \beta + 2Q - t \pmod{n}. \tag{3.54}$$

We find that

$$\epsilon = \alpha - a + Q \quad \text{and} \quad Q = (b + t - \beta)/2 + mR, \tag{3.55}$$

where $m = 0, 1, 2, \cdots, \lfloor t/n \rfloor$. Thus, the terms in the superposition (3.52a) are not in general identical with those in (3.52b), apart from a common factor, unless $\phi = 0, 2\pi, 4\pi, \cdots$. A similar argument can be used to show that the terms in $\langle \overline{a}, b|\Psi_1\rangle$ are not in general the same as those in $\langle \overline{a}, b|\Psi_2\rangle$. Given the independence of ϕ from the coefficients $b_{q_2,q_1} b_{q_1,\alpha}$, it is not necessary that

$$|\langle a, b|\Psi_1\rangle|^2 + |\langle \overline{a}, b|\Psi_1\rangle|^2 = |\langle a, b|\Psi_2\rangle|^2 + |\langle \overline{a}, b|\Psi_2\rangle|^2. \tag{3.56}$$

The equality holds in general (for arbitrary unitary matrix B and time t) if and only if $\phi = 0, 2\pi, 4\pi, \cdots$. Repeating the argument for $B^{(2)}$, $B^{(3)}$ and $B^{(4)}$, we find that all the four discrete symmetries of Theorem 1 break down in general. ■

We note that for phase flip symmetry, where $e^{i\phi} = -1$, the superposition terms in (3.52b) may differ from the corresponding terms in (3.52a) only with respect to sign. Given that all the terms like b_{q_2,q_1}, $b_{q_1,\alpha}$, etc. are built from a small set of trigonometric functions of the three parameters θ, ζ and ξ, certain values of t may render the right hand sides of (3.52a) and (3.52b) equal. However in general, this equality will not hold for arbitrary t.

An instance of breakdown of phase flip symmetry in the unitary quantum walk on a cycle is demonstrated in the example of Figure 3.11. The profile of the position probability distribution varies depending on the number of sites and the evolution time.

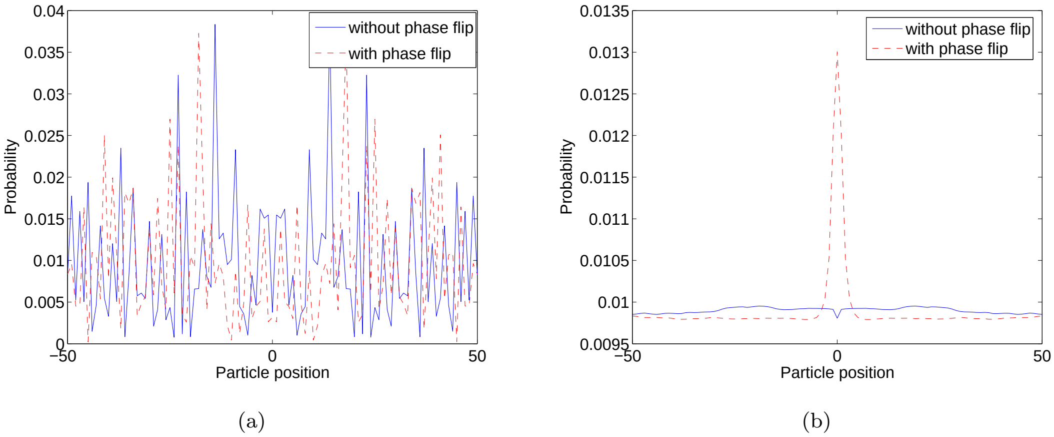

(a)

(b)

FIGURE 3.11: An instance of breakdown of phase flip symmetry in a unitary quantum walk on a cycle, where the two extreme points (located at positions ±50) on the plot are spatially adjacent. The number of sites is 101 and $t = 5000$ (in units of discrete time-steps), with coin parameter $\theta = 30°$. (a) The solid curve represents the positional probability distribution without any symmetry operation applied, while the dashed curve represents that with a phase flip operation applied at each walk step. (b) The same as the above, but with time-averaging applied over every 50 steps, in order to more clearly bring out the breakdown in symmetry.

3.3.2 Breakdown using a generalized phase gate

We will introduce a generalized phase gate, an element from the parameter group

$$G(\beta) = \begin{pmatrix} 1 & 0 \\ 0 & e^{i\beta} \end{pmatrix}, \tag{3.57}$$

to act on the $\mathcal{H}_c$. We find that the operation $W \longrightarrow GW$ leaves the probability distribution $p(j, t)$ of the particle on the line invariant; hence the walk is symmetric under the operation

$$G(\beta) : |q\rangle \mapsto e^{iq\beta}|q\rangle \tag{3.58}$$

for $|q\rangle$ in the computational basis (eigenstates of the Pauli operator σ_z) and $q = 0, 1$. The physical significance of G is that it helps identify a family of quantum walks that are equivalent from the viewpoint of physical implementation, which can sometimes allow a significant practical simplification [67]. For example, suppose the application of the conditional shift is accompanied by a phase gate. The walk symmetry implies that this gate need not be corrected for, thereby resulting in a saving of experimental resources. The inclusion of a phase gate on the coin operator is equivalent to a phase gate at each lattice site in the sense of quantum lattice gas automata (QLGA) [27, 28], with the physical meaning of a constant potential. The evolution rules for single-particle QLGA can be classified into gauge equivalent classes, there being a difference between the class of rules for periodic ($n-$cycle) and non-periodic 1-dimensional lattice and this feature can be used to distinguish between these two spatial topologies [109].

It turns out that in the case of quantum walk on an n-cycle, this symmetry breaks down. To see this, we note that the t-fold application of the operation GSB on a particle with initial state $|\Psi_{in}\rangle$ on the line and on an $n-$cycle produces, respectively, the states

$$(GSB)^t|\Psi_{in}\rangle = \sum_{q_1,q_2,\cdots,q_t} e^{iQ_t\beta} B_{q_t,q_{t-1}}\cdots B_{q_2,q_1}(B_{q_10}a + B_{q_11}b)|q_t\rangle|2Q_t - t\rangle, \tag{3.59a}$$

$$(GUB)^t|\Psi_{in}\rangle = \sum_{q_1,q_2,\cdots,q_t} e^{iQ_t\beta} B_{q_t,q_{t-1}}\cdots B_{q_2,q_1}(B_{q_10}a + B_{q_11}b)|q_t\rangle|2Q_t - t \mod n\rangle, \tag{3.59b}$$

where $Q_t = q_1 + q_2 + \cdots + q_t$. All terms in superposition (3.59a) contributing to the probability to detect the walker at a given position $j = 2Q_t - t$ have the *same* phase factor, $e^{iQ_t\beta}$, which is fixed by $Q_t = (j+t)/2$ (where, it may be noted, j and t are both even or both odd). Thus, this factor does not affect the probability to detect the walker at j, whence the symmetry. In the case of quantum walk on an n-cycle the breakdown of the symmetry, see Figure 3.12, can be attributed to the topology of the cycle, which introduces a periodicity in the walker position (determined by a congruence relation with modulus given by the number of sites), but not in the phase of the superposition terms. As a result, fixing j fixes $Q_t \mod n = (j+t)/2 \mod n$, but not Q_t itself, so that the phase terms in the superposition (3.59b) do not factor out globally. Thus if β is non-vanishing, then in general the symmetry G is absent in the cyclic case. We quantify the breakdown in symmetry by means

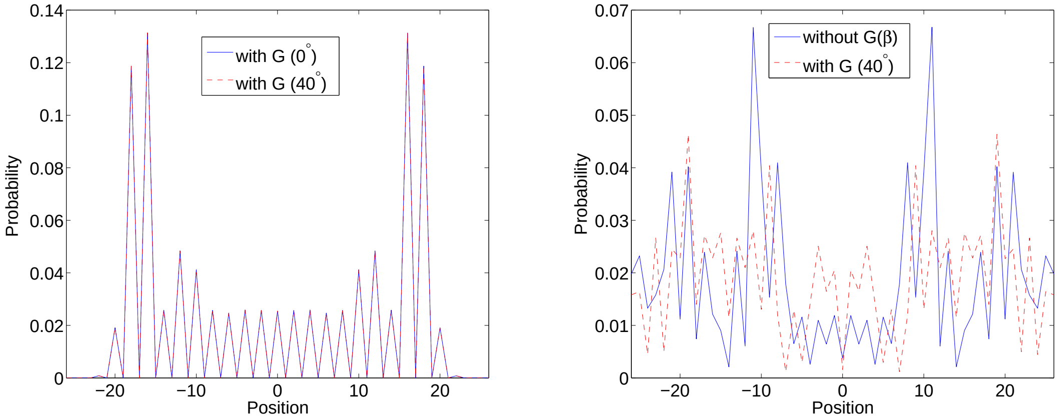

(a) (b)

FIGURE 3.12: Position probability distribution for a Hadamard walk, $B(0°, 45°, 0°)$ on (a) a line, and (b) an n-cycle, with $(n = 51)$ and initial state $(1/\sqrt{2})(|0\rangle + i|1\rangle)$, for the unitary case $(\gamma_0 = 0)$ and $\tau_u = 50$. Each figure presents the distribution with and without being subjected to the phase operation $G(40°)$. In (a), there is perfect symmetry, since both distributions coincide. In (b) the two plots do not overlap, indicating the breakdown of the symmetry.

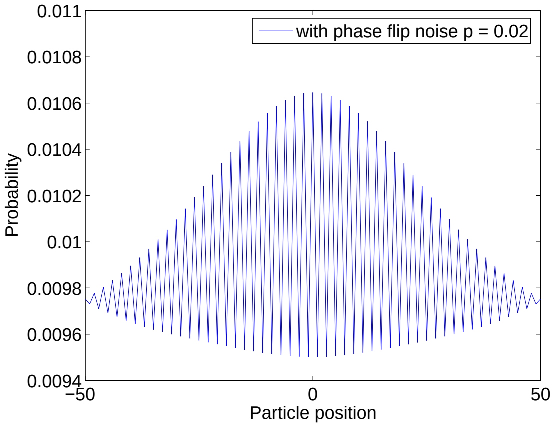

FIGURE 3.13: Restoration of phase flip symmetry in a noisy quantum walk on a cycle, where the two extreme points on the plot are spatially adjacent. The number of sites is 101 and $t = 5000$ (in units of discrete time-steps), with coin parameter $\theta = 30°$. The figure depicts the position probability distribution with or without phase flip symmetry operation applied at each step, with phase damping noise level $p = 0.02$ (3.24). After sufficiently long time, the quantum walk reaches the uniform distribution, typical of classical random walk.

of the Kolmogorov distance (or, trace distance [8]), given by

$$d(t) = (1/2) \sum_j |P(j,t) - P'(j,t)|, \tag{3.60}$$

between the particle position distributions obtained without and with the symmetry operation, given by $P(j,t)$ and $P'(j,t)$, respectively. The breakdown in symmetry for a noiseless cyclic quantum walk is depicted by the bold curve in Figure 3.14 as a function of the number of turns τ_u (where $t = \tau_u s$, with $n = 2s+1$).

3.3.3 Effect of noise and symmetry restoration

Remarkably, this symmetry is restored above a threshold value of noise. The pattern in Figure 3.13 corresponds to phase noise with $p = 0.02$ applied to a quantum walk, either with or without a phase flip symmetry operation. We note that the introduction of noise tends to classicalize the random walk, hence causing it to asymptotically reach a uniform distribution [79, 110]. The above-mentioned symmetry restoration happens well before the uniformity sets in. The initial lack of symmetry gradually transit to full symmetry as the noise level is increased. Thus, the role of symmetry operations and noise is quite different in the case of quantum walk on an $n-$cycle as compared with that on a line.

We now describe the n-cycle quantum walk on the particle, a two level system, when subjected to noise. The situation is modeled as an interaction with a thermal bath, characterized by phase damping or a generalized amplitude damping channel, the latter process being represented by the Kraus operators (3.42). The density operator ρ_c of the coin evolves according to

$$\rho_c \rightarrow \sum_x E_x \rho_c E_x^\dagger. \tag{3.61}$$

The full evolution of the walker, described by density operator $\rho(t)$, is given by

$$\rho(t)v = \sum_j E_x(W\rho(t-1)W^\dagger)E_x^\dagger, \tag{3.62}$$

where the E_x's are understood to act only in the coin space.

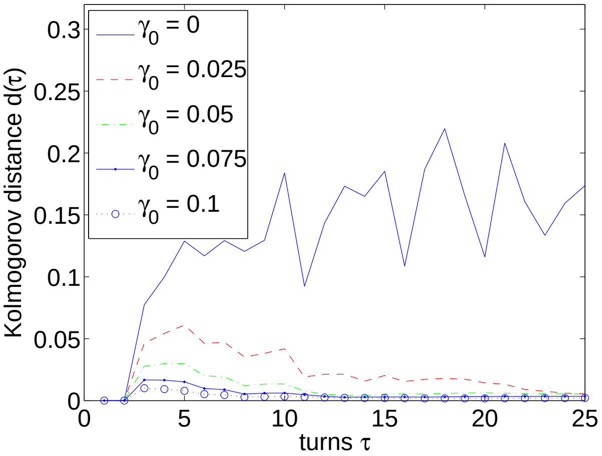

FIGURE 3.14: Kolmogorov distance $d(\tau_u)$ against the number of turns (τ_u) of the cyclic quantum walk in the noiseless and noisy case with $n = 51$. For the unitary case ($\lambda = 0$, γ_0 ; bold line) the walk becomes increasingly asymmetric as the number of turns is increased, until about 7–10 turns, after which it fluctuates around $d \approx 0.15$. The plots represent generalized amplitude damping noise at different noise levels at temperature $T = 3.5$ (in units where $\hbar \equiv k_B \equiv 1$). The walk is evolved with the initial state of the particle parameters $\delta = 30°$, $\eta = 40°$ in (2.11), with $B(20°, 10°, 30°)$ and $G(10°)$.

The curves in Figure 3.14 plot $d(\tau_u)$ as a function of turns in the case of unitary and noisy quantum walk (parametrized by γ_0), and demonstrate the gradual restoration of symmetry with time on account of the noise. Although the figure employs generalized amplitude damping noise, qualitatively the same behavior can be seen for a phase damping noise. Here, a general feature is that $d(\tau_u)$ is non-zero when $\tau_u < 2$, being equivalent to (noisy) quantum walk on a line. Thereafter, $d(\tau_u)$ at first increases with increasing turns, being dominated by unitary evolution, and eventually falls down, being dominated by noise. It is observed that for sufficiently low noise levels, the time at which this turnover in slope happens remains constant, for given θ. This is depicted in Figure 3.14 for the case of a generalized amplitude damping channel corresponding to a fixed temperature and varying γ_0. However, we note that for strong enough noise, the turnover happens earlier.

Typical noisy probability distributions are depicted in Figure 3.15(a),(b) at an instant where the symmetry has been almost fully restored while the walk is well

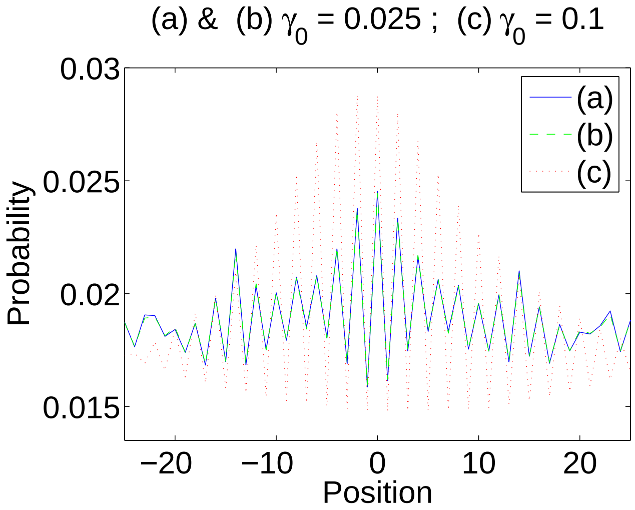

FIGURE 3.15: Position probability distribution for a Hadamard walk $B(0, 45^\circ, 0)$ on an n-cycle ($n = 51$) with initial state $(1/\sqrt{2})(|0\rangle + i|1\rangle)$ when subjected to generalized amplitude damping noise with $\Delta = 0.1$ and finite T ($= 6.0$) for $\tau_u = 11$. For (a) and (b) $\gamma_0 = 0.025$. (b) is the distribution for the quantum walk augmented by operation $G(20^\circ)$ and (a) is without any augmented operation; note the overlap of (b) on (a), walk remains quantum yet with symmetry completely restored ;
(c) classicalized pattern (indicated by the regular envelope) obtained with larger noise level corresponding to $\gamma_0 = 0.1$.

within the quantum regime. Figure 3.15(c) represents a classicalized distribution, indicated by the regular envelope (that will eventually turn into a uniform distribution).

We define coherence $\mathbf{C}$ as the sum of the off-diagonal terms of states in $\mathcal{H}_c \otimes \mathcal{H}_p$, where $\mathcal{H}_c$ and $\mathcal{H}_p$ are the coin and position Hilbert space of the quantum walker, respectively. If the state of the quantum walker is

$$\rho = \sum_{ab;jk} \alpha_{ab;jk} |a\rangle |j\rangle \langle b| \langle k|, \tag{3.63}$$

where $|a\rangle$, $|b\rangle \in \mathcal{H}_c$ and $|j\rangle$, $|k\rangle \in \mathcal{H}_p$, then

$$\mathbf{C} \equiv \left(\sum_{a\neq b, j=k} + \sum_{a,b,j\neq k} + \sum_{a\neq b, j\neq k} \right) |\alpha_{ab;jk}|, \tag{3.64}$$

the sum of the absolute values of all off-diagonal terms of ρ in the computational-position basis. The coherence function is defined as the quantity $C(m)$, where $m \in \{1, 2, \cdots, M\}$, obtained by partitioning $\mathbf{C}$ into M intervals of size s/M, such that for the mth interval

$$(m-1)(s/M) \leq |j-k| < m(s/M). \tag{3.65}$$

Physically, $C(m)$ is a measure of coherence between two points on a (in general, noisy) quantum walker, as a function of their mutual separation. Let $C_0(m)$ represent the coherence function of the corresponding noiseless walk. At any turn τ_u, we define the normalized coherence function by

$$c(m) \equiv C(m)/C_0(m), \tag{3.66}$$

and, analogously, normalized Kolmogorov distance by

$$D(\tau_u) \equiv d(\tau_u)/d_0(\tau_u). \tag{3.67}$$

Since noise tends to destroy superpositions, and the breakdown in symmetry is essentially a phenomenon of superposition of the forward and backward waves, noise tends to restore symmetry, as seen from Figure 3.15. This is brought out by Figure 3.16 for two possible values of G. In the figure, in spite of its considerable spikiness, the bold curve, representing $c(m = M)$, shows an overall fall. A similar trend as depicted in this figure, has been numerically checked for various other values of G. This raises the question whether symmetry restoration of the cyclic quantum walk can be considered as a good indicator of classicalization. Here we note that from Figure 3.15(a),(b) the probability distribution pattern is seen to be clearly quantum, even though symmetry has been almost fully restored. This is suggestive of the notion that that symmetry tends to be restored *even* in the regime where the walk still possesses some quantum features.

The reason $D(t)$ is not a faithful indicator of classicalization of the walk has to do with the effect of noise on the sensitivity of the symmetry operation $G(\beta)$ to the topology of the path. Since this operation senses the closure of the path through the superposition of the forward and backward waves, the suppression of

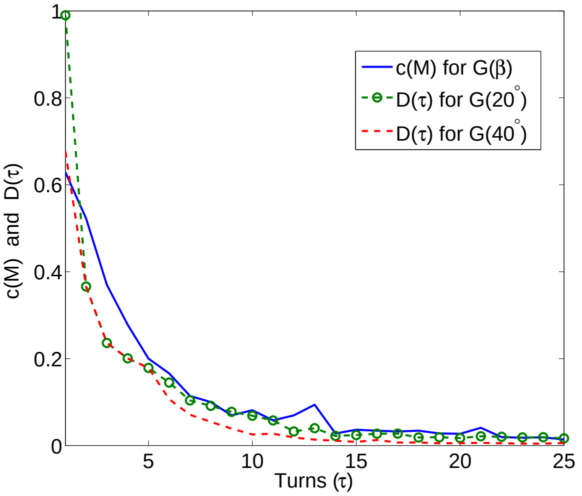

FIGURE 3.16: Normalized coherence function $c(M)$ (bold) and the normalized Kolmogorov distance $D(\tau_u)$ (dashed) for an $n-$ cyclic quantum walk as a function of turns τ_u. An overall reduction of both $c(M)$ and $D(\tau_u)$ with time is seen for the generalized amplitude damping noise characterized by temperature $T = 3.5$ and $\Delta = 0.1$. The Hadamard walk is evolved with the initial state parameters (in degrees) $\delta = 45°$, $\eta = 0°$ (2.11), and $G(\beta)$. The line-with-circle plot represents $D(\tau_u)$ with $G(20°)$ and dashed line represents for $G(40°)$. The $c(M)$ (solid line) remains roughly the same for both β. For a clear depiction of the notion of symmetry restoration in the walk even in the quantum regime, Figure (3.15).

superposition through noise will also have the effect of desensitizing the operation to the closure of the path, thereby moving the noisy cyclic quantum walk towards a noisy quantum walk on a line from the perspective of this operation, before further classicalization transforms it into a cyclic classical random walk. And as shown in Section 3.2, all the above symmetries are respected by a (noisy) quantum walk on a line, both in the case of phase damping noise and generalized amplitude damping [3]. This brings out the point that decoherence (T_2 process) is the principal mechanism responsible for the restoration of symmetries. It also highlights the interplay between topology and noise in a quantum walk on an $n-$cycle. A similar interplay may be expected also in the case of quantum walk with other nontrivial topologies.

---

[3] In NMR nomenclature, phase damping is called a T_2 process, and generalized amplitude damping, which is a T_1 ,T_2 process [111].

Further extensions would be quantum walks on a more general graph [79, 110] or in higher dimensions $d > 2$ [112]. In the former, the 1D walk is generalized to an n-cycles and to hypercubes, including the effect of phase noise in the coin space, and decoherence in position space. In the latter, the Hadamard transformation is generalized to a non-entangling tensor product of Hadamards, or to an entangling discrete Fourier transform or the Grover operator. They bring in many novel features absent in the quantum walk on a line.

The interplay between geometry and decoherence has been noted before in the case of delocalized bath modes [113], as against localized bath modes [113–115]. This is of relevance as the noise processes considered here [67, 108] are described by the interaction of the system with delocalized bath modes.

3.4 Experimental implications

Experimental realization of quantum walk using any of the proposed schemes is not free from noise due to environmental conditions and instrumental interference. In particular, noise can be a major issue in the scaling up of the number of steps in already realized quantum walk systems. Understanding the symmetries of the noisy and noiseless quantum walk could greatly help in the improvement of implementation technique (see for example Section 4.5.1) and in further exploration of other possible systems where quantum walk can be realized on a large scale.

The experimental study of the decoherence and decay of quantum states of a trapped atomic ion's harmonic motion subjected to engineered reservoirs, both of the phase damping and amplitude damping kind, have been reported in [101, 102]. The phase reservoir is simulated by random variation of the trap frequency ω without changing its energy (non-dissipative), while the amplitude reservoir is simulated by random electric field along the axis of the trap (dissipative). Coupling the reservoirs reported in [101, 102] to the scheme presenting the combination of pulses required to implement a quantum walk on a line and on a cycle in an ion trap [57] provides a convenient set up to demonstrate the symmetry-noise interplay.

3.4.1 NMR quantum-information processor

Continuous time [53] and discrete time [54] quantum walk have been successfully implemented in a nuclear magnetic resonance (NMR) quantum-information processor. In NMR spectroscopy of the given system (molecule) the extent of its isolation from the environment is determined in terms of its phase coherence time T_2 and its energy relaxation time T_1. If the pulse sequence is applied to the NMR quantum-information processor within the time $T < T_2, T_1$, the environmental effects on the system are less significant. The pulse sequence exceeding the time T_2 can be considered to be affected by the dephasing channel and the pulse sequence exceeding the time T_1 can be considered to be affected by the amplitude damping channel. In experiments of time scale greater than the time T_2 or T_1, a refocusing pulse sequence is applied to compensate for the environmental effects. In the implementation of discrete-time quantum walk, the pulse sequence was implemented within the time T_1 and T_2 and by introducing dephasing, the transition from quantum walk to the classical random walk was shown [54].

The environmental effect (noise) on quantum walk symmetries presented in this chapter can be verified in the NMR system by scaling up the number of steps of quantum walk realized. By applying a controlled amount of the refocusing pulse sequence, the effect of different levels of noise can be experimentally verified.

3.4.2 Ultracold atoms

There have been other proposals for physical realization of quantum walk using Bose-Einstein condensate (BEC) [60] where the unitary shift operator induces a bit flip. A *stimulated Raman kick* is used as a unitary shift operator to translate the Bose-Einstein condensate in the Schrödinger cat state to a superposition in position space. Two selected levels of the atoms in the Bose-Einstein condensate are coupled to the two modes of counter-propagating laser beams. The stimulated Raman kick, in imparting a translation in position space, also flips the internal state of the Bose-Einstein condensate. An rf pulse (π pulse) is suggested as a compensatory mechanism to flip the internal state of the condensate back to its initial value after every unitary shift operator. From the **PRX** symmetry pointed in this chapter, it follows that there is no need for the compensatory operation for an unbiased quantum walk for a particle initially in the state $\frac{1}{\sqrt{2}}(|0\rangle + i|1\rangle)$. The availability of walk symmetries could also be useful for exploring other possible physical implementations which induce such symmetry operations along with the translation.

In the most widely studied version of quantum walk, a quantum coin operation is used after every displacement operation. Continuous external operations on a particle confined in a trap reduces the confinement time of the particle. Reducing the number of external operations will benefit the scaling up of the number of steps of the quantum walk. One can configure a system where a separate quantum coin operation is eliminated by using a single coin-embedded conditional shift operator to shift the particle in superposition of position space retaining the superposition of the coin state (Section [66]). Further, systems of this kind are expected to be affected by amplitude damping as one of the basis states might be more stable than the other one in the trap. The present study of effect of noise could help to optimize and use quantum walk with in the system limitations.

3.4.3 Other condensed matter systems

Breaking of the symmetry due to the change in walk topology causes long-range correlations to develop, in analogous to the hydrodynamics of ordered systems such as spin waves in: ferromagnets, antiferromagnets (where it is the spin wave of staggered magnetization), second sound in He^3, nematic liquid crystals [116]. Here the correlations may be identified with symmetry-broken terms (whose measurement probability depends on β in the walk augmented by $G(\beta)$) in the superposition of the quantum walker. One finds that correlations are set up rapidly over large distances with increase in the winding of the walker, until symmetry is broken throughout the cycle. However, as noted above, the randomization produced by noise causes the reappearance of symmetries. The symmetry breaking and the symmetry restoring agents are thus different, the former given by the topological transition from a line to an n-cycle, the latter being the noise-induced randomization.

Coherence is also widely used to understand quantum phase transitions, the transition from superfluid to Mott insulator state in an optical lattice being one specific example [84, 85]. In Chapter 4 the quantum phase transition using quantum walk in a one dimensional optical lattice is discussed [52]. Using various lattice techniques, desired geometries to trap and manipulate atoms can be created. In most physical situations one deals with closed geometries. The characteristics of the $n-$cycle walk, in particular the re-appearance of the symmetry (implying a family of implementationally equivalent noisy cyclic quantum walks) while still in the quantum regime, presented here could be of direct relevance to such situations.

The ubiquity of the ideas developed in this chapter can be seen from the fact that the quantum dynamics of a particle on a ring (cycle) subject to decoherence along with dissipation finds its place in the physics of quantum dots. The effective action of a quantum dot accounting for the joint effect of charging and coupling to an environment [117, 118] mirrors the behavior of the quantum dynamics of a particle on a ring (cycle) subject to a dissipative damping mechanism describing the dissipation of the energy stored in dynamic voltage fluctuations into the microscopic degrees of freedom of the quasi-particle continuum. In the absence of dissipation, the action describes the ballistic motion of a quantum particle on a ring. The ring topology reflects the 2π-periodicity of the quantum phase, which is in turn related to the quantization of charge, thereby highlighting the point that the main source of charge quantization phenomena, in the approach developed in [117, 118], is the periodicity, of the relevant variable, due to the ring topology. With the increase in the effect of dissipation, the particle begins to forget its ring topology (full traversal of the ring become increasingly unlikely), leading to a suppression of charge quantization phenomena. This behavior is similar to that seen here for the case of quantum walk on a cycle, where with an increase in the effect of the environment, i.e., with increasing noise, the walker in unable to perceive the cyclic structure of the walk space. That the topology-noise interplay studied here has an impact on a concrete condensed matter system, viz. the crossover from strong to weak charge quantization in a dissipative quantum dot, highlights the generality and scope of these ideas.

3.5 Summary

- Our work considers variants of quantum walks on a line which are equivalent in the sense that the final positional probability distribution remains the same in each variant. In particular, we consider variants obtained by the experimentally relevant operations of Z or X applied at each quantum walk step, with the symmetry operations given by $\mathbf{Z}$ and $\mathbf{PRX}$. This could be experimentally advantageous since practical constraints may mean that one of the variants is preferred over the rest. What is especially interesting is that these symmetries are preserved even in the presence of noise, in particular, those characterized by the phase flip, bit flip and generalized amplitude damping channels. This is important because it means that the equivalence of these variants is not affected by the presence of noise, which would be inevitable in actual experiments. The symmetry of the phase operation under phase noise is intuitive, considering that this noise has a Kraus representation consisting of operations that are symmetries of the noiseless quantum walk. However, for the PRX symmetry under phase noise, and for any symmetry under other noisy channels (especially in the case of generalized amplitude damping channel), the connection was not obvious before the analysis was completed.

- An interesting fact that comes out while extending the studies to walk on an $n-$cycle is that the symmetry breaks down in general but is restored above a certain noise level. This symmetry-topology-noise interplay presented would be of relevance to quantum information processing systems, and have wider implications to the condensed matter systems.

- Our results in this chapter to study noise model are supported by several numerical examples obtained by evolving the density operator in the Kraus representation. However, analytical proofs of the effect of noise on symmetries are obtained using the quantum trajectories approach, which we find convenient for this situation.

Part III

Applications

Chapter 4

Quantum phase transition using quantum walks

4.1 Introduction

In Chapter 2 we saw that the dynamics of the quantum walk can be controlled by varying the quantum coin parameters. From Chapter 3 we concluded that the symmetries and addition of small amount of experimentally engineered noise or environmental effect can be used as an additional tool to control the dynamics and hence the probability distribution of the quantum walk.

These enhanced properties of the quantum walk purely due to quantum dynamics and small amount of engineered noise [67, 76, 77] can be used to enlarge the toolbox for controlling the dynamics in a physical system, to demonstrate coherent quantum control over, for example, atoms, photons or spin chain systems. Therefore, the use of the quantum walk to study the dynamics of particles in 1D magnetic systems [87], atoms in optical lattice [84], and photonic Mott insulators [119] or to observe complex quantum phase transitions [120] and quantum annealing [51] would be of both theoretical and experimental relevance. In this chapter we will consider the use of a quantum walk to control and study the dynamics of ultracold bosonic atoms in an optical lattice.

Traditionally, theoretical studies of the dynamics of atoms in an optical lattice are done using mean field approaches [80] and quantum Monte Carlo methods [81–83]. The quantum correlation induced between atoms and position space by the quantum walk can serve as an alternate method for theoretical studies. In particular, we will consider the quantum phase transition from the Mott insulator (MI) - a regime where no phase coherence is prevalent - to the superfluid (SF) - a regime with long-range phase coherence [84, 85] and vice versa by redistributing the density profile of atoms using quantum walk. The simulation of the quantum phase transition using the quantum walk occurs quadratically faster in one dimension (1D) compared to, varying the optical lattice depth and letting the atom-atom interaction follow the classical random walk behavior. Compared to ballistically moving the atoms, which just relocates the atoms to the new lattice site, quantum walk on atoms spread the wavepacket of each atom over the lattice sites (for example, SF regime). We will consider the discrete-time quantum walk with quantum coin operation $B_{0,\theta,0}$ and small amounts of three physically relevant models of noise that can be experimentally induced: a bit-flip channel, a phase-flip channel and an amplitude-damping channel discussed in Chapter 3 [67], to act as an enhanced toolbox to control the redistribution of atoms in an optical lattice. We will also discuss the scheme for the experimental implementation of quantum walk on ultracold atoms in an optical lattice.

This chapter is organized as follows. In Section 4.2 we review phase transition in optical lattice using Bose-Hubbard model. The implementation of the quantum walk on atoms in 1D MI and SF regimes is discussed in Section 4.3, where we analyze the dynamics and present the density profile obtained by using some of the properties of the quantum walk. In Section 4.4 we discuss the quantum walk with a noisy channel as a tool to control the redistribution of atoms. In Section 4.5 we propose a scheme for an experimental implementation of quantum walk on atoms (Bose-Einstein condensates) in optical lattice and conclude with summary in Section 4.6.

4.2 Quantum phase transition in optical lattice

Bosons do not obey the exclusion principle, as temperature $T \to 0$ they all begin to get into the lowest energy eigenstate available, with energy $\epsilon = 0$ and the effects of quantum degeneracy begin to emerge. That is, a large fraction of an atomic wave packets of bosonic atoms when cooled below a critical temperature T_c, begins to condense into the lowest quantum state called as Bose-Einstein condensate (BEC). A BEC at low enough temperature is a superfluid described by a wave function that exhibits long-range coherence [121]. When the BEC is transferred to the lattice potential, the atoms move from one lattice site to the next by tunnel coupling. Bose-Hubbard model is the standard model used to discuss the dynamics of the boson and quantum phase transition in optical lattice. The simple possible approximation for the wavefunction of the many body system is a product of single particle state, usually known as Gross-Pitaevskii or mean-field approximation. Below we will briefly discuss the Bose-Hubbard model [122].

4.2.1 Bose-Hubbard model

The elementary degree of freedom in this model are, as the name implies spinless bosons, this takes the place of the spin-1/2 fermionic electrons in the original Hubbard model introduced as a description of the motion of electrons in transition metals. The Hamiltonian of the Bose-Hubbard model is

$$\mathbf{H}_B = -J \sum_{\langle jk \rangle} (\hat{b}_j^\dagger \hat{b}_k + \hat{b}_k^\dagger \hat{b}_j) - \mu_j \sum_j \hat{n}_j + \frac{U}{2} \sum_j \hat{n}_j (\hat{n}_j - 1). \tag{4.1}$$

J is the hopping element which allows hopping of bosons between the nearest neighbor pair of sites represented by $\langle jk \rangle$. $\hat{b}_j$ and their Hermitian conjugate $\hat{b}_k^\dagger$ are the boson operators, which annihilates and creates bosons on the sites j and k of a regular lattice in D dimensions respectively. The two operators obey the commutation relation

$$[\hat{b}_j, \hat{b}_k^\dagger] = \delta_{jk} \tag{4.2}$$

while the two creation or annihilation operators always commute.

$$\hat{n}_j = \hat{b}_j^\dagger \hat{b}_j \tag{4.3}$$

is the boson number operator which counts the number of bosons on each site. μ_j is the chemical potential of the bosons, denotes the energy offset due to external harmonic confinement of the atoms in the jth lattice site, and U is the repulsive interaction between two atoms in a single lattice site. $U > 0$, represents the simplest possible on-site repulsive interaction between the bosons (on-site repulsion). $\mathbf{H}_B$ is invariant under global $U(1) \equiv O(2)$ phase transformation under which

$$b_j \rightarrow b_j e^{i\phi}. \tag{4.4}$$

We can also notice that the J term couples neighboring sites in a manner that prefers a state that breaks the global symmetry. However these terms compete with the U term in $\mathbf{H}_B$, which are local and prefer states that are invariant under symmetry transformation. Therefore we can expect a quantum phase transition in $\mathbf{H}_B$ as a function of J/U between a state in which the $U(1)$ symmetry (4.4) is unbroken to one in which it is broken. As the consequence of $U(1)$ symmetry we have the conservation on the total number of bosons

$$\hat{N}_b = \sum_j \hat{n}_j, \tag{4.5}$$

and this is easily verified by noting that the N_b commutes with $\hat{H}$. We can notice that the chemical potential μ in $\mathbf{H}_B$ is coupled to the conserved total number of bosons $\hat{N}_b$. In contrast, it can be noted that $\mathbf{H}_B$ remains invariant under (4.4) for any value of μ and μ term does not break any symmetries. This gives no choice but to examine $\mathbf{H}_B$ for all μ and can be done by using a mean-field theory approach.

Using the mean-field theory approach, the properties of $\mathbf{H}_B$ are modeled by the best possible sum, $\mathbf{H}_{MF}$, of single Hamiltonians

$$\mathbf{H}_{MF} = \sum_j \left(-\mu \sum_j \hat{n}_j + \frac{U}{2} \hat{n}_j(\hat{n}_j - 1) - \Psi_B^* \hat{b}_j - \Psi_B \hat{b}_j^\dagger \right) \tag{4.6}$$

where the complex number Ψ_B is a variational parameter and a field to represent the influence of the neighboring sites; this field has to be self consistently determined. This breaks the $U(1)$ symmetry and does not conserve the total number of particles. As the mean-field Hamiltonian is the same on every site, the ground state does not spontaneously break a translational symmetry of the lattice.

To determine the optimal value of the parameter Ψ_B, the ground state wavefunciton of $\mathbf{H}_{MF}$ for an arbitrary Ψ_B is determined. This wavefunction will simply be a product of single-site wavefunctions. Next the expectation value of $\mathbf{H}_B$ in the wavefunction is evaluated by adding and subtracting $\mathbf{H}_{MF}$ by $\mathbf{H}_B$. Then the mean-field value of the ground state energy is written in the form

$$\frac{E_0}{M} = \frac{E_{MF}(\Psi_B)}{M} - ZJ\langle\hat{b}^\dagger\rangle\langle\hat{b}\rangle + \langle\hat{b}\rangle\Psi_B^* + \langle\hat{b}^\dagger\rangle\Psi_B, \tag{4.7}$$

where M is the number of the lattice sites, $E_{MF}(\Psi_B)$ is the ground state energy of $\mathbf{H}_{MF}$, Z is the number of nearest neighbors around each lattice point (the coordination number), and the expectation values are evaluated in the ground state of $\mathbf{H}_{MF}$. Final step is to minimize (4.7) over variations in Ψ_B. By taking the derivative of (4.7) with respect to Ψ_B, it can be show that at the optimum the value of Ψ_B

$$\Psi_B = ZJ\langle\hat{b}\rangle; \tag{4.8}$$

this relation, however does not hold at a general point in parameter space.

When $J = 0$, the sites are decoupled, and the mean field theory is exact, $\Psi_B = 0$, and we simply have to minimize the on-site interaction energy. The on-site Hamiltonian involves only the operator $\hat{n}$, and the solution involves finding the boson occupation number (which are integer-valued eigenvalues of $\hat{n}$) that minimizes $\mathbf{H}_B$. We get the ground state wavefunction

$$|m = n_0\,(\mu/U)\rangle, \tag{4.9}$$

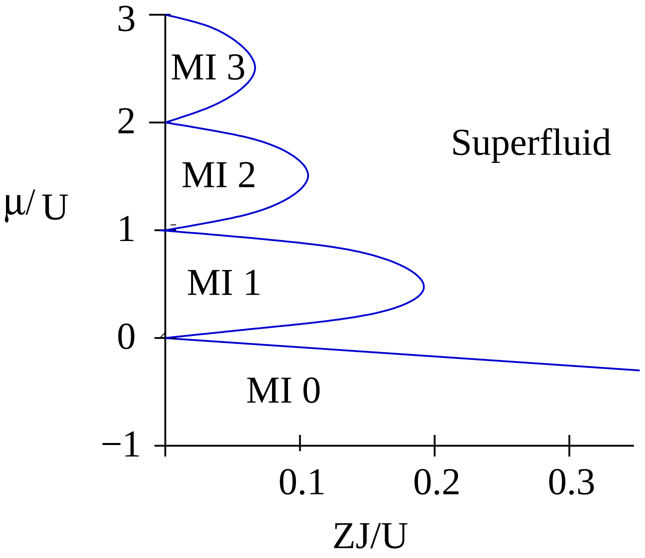

FIGURE 4.1: Mean-field phase diagram of the ground state of the boson Hubbard model $\mathbf{H}_B$. The notation MI n refers to a Mott insulator with $n_0(\mu/U) = n$.

where the integer-valued function $n_0(\frac{\mu}{U})$ is given by

$$n_0\left(\frac{\mu}{U}\right) = \begin{cases} 0, & \text{for} \quad \mu/U < 0, \\ 1, & \text{for} \quad 0 < \mu/U < 1, \\ 2, & \text{for} \quad 1 < \mu/U < 2, \\ . & \qquad\quad . \\ . & \qquad\quad . \\ n, & \text{for} \quad n-1 < \mu/U < n. \end{cases} \tag{4.10}$$

Each site has exactly the same number of bosons, which jumps discontinuously whenever μ/U goes through positive integer. When μ/U is exactly equal to a positive integer, there are two degenerate state on each site (with boson numbers differing by 1) and so the entire system has a degeneracy of 2^M. This large degeneracy implies a macroscopic entropy which can be lifted once we turn on a nonzero J. Figure 4.1 is the phase diagram of the ground state of the Bose-Hubbard model $\mathbf{H}_B$ (4.1). As shown in the Figure 4.1, the regions with $\Psi_B = 0$ survive in lobes around $J = 0$, (4.9) characterized by a given integer value of $n_0(\mu/U)$. Only at degenerate point with μ/U = integer does a nonzero J immediately lead to a state with $\Psi_B \neq 0$. First we will consider the additional property of the lobes with $\Psi_B = 0$. The expectation value of the number of each site is given by

$$\langle \hat{b}_j^\dagger \hat{b}_j \rangle = n_0(\mu/U). \tag{4.11}$$

Existence of an energy gap and the fact that $\hat{N}_b$ commutes with H_B are the important ingredients of the above expression. First recall that for $J = 0$, provided μ/U was not exactly equal to positive integer, there was a unique ground state, and there was a nonzero energy gap. As a result, when we turn on a small nonzero J , the ground state will move adiabatically without undergoing any level crossings with other state. Now the $J = 0$ state is exact eigenstate of $\hat{N}_b$ with eigenvalue $Mn_0(\mu/U)$, and the perturbation arising from a nonzero J commutes with $\hat{N}_b$. Consequently the ground state will remain an eigenstate of $\hat{N}_b$, with precisely the same eigenvalue, $Mn_0(\mu/U)$, even for small nonzero J. These regions with a quantized value of the density and an energy gap to all excitations are known as Mott insulators. The Mott insulators are also known as incompressible because their density does not change under changes of the chemical potential μ or other parameter in $\mathbf{H}_B$:

$$\frac{\partial \langle \hat{N}_b \rangle}{\partial \mu} = 0. \tag{4.12}$$

The boundary of the Mott insulating phase is a second order quantum phase transition, i.e., a nonzero Ψ_B turns on continuously.

When we turn to the phase with $\Psi_B \neq 0$. The mean-field parameter Ψ_B varies continuously as the parameters are varied. As a result all thermodynamic variables also change, and the density can be varied smoothly across any real positive value. So this is a compressible state in which

$$\frac{\partial \langle \hat{N}_b \rangle}{\partial \mu} \neq 0 \tag{4.13}$$

The presence of $\Psi_B \neq 0$ implies that the $U(1)$ symmetry is broken, and there is a nonzero stiffness to twists in the orientation of the order parameter. This state is a superfluid and that the stiffness is just a superfluid density.

From the above description we can conclude that when J dominates the Hamiltonian, the ground-state energy is minimized if the single-particle wave functions of all N atoms are spread out over the entire M-lattice site. If μ_j = const. (homogeneous system) then the many-body ground state is called the superfluid state and is given by

$$|\psi_{SF}\rangle_{U=0} \propto \left(\sum_{j=1}^{M} \hat{b}_j^\dagger \right)^N |V\rangle, \tag{4.14}$$

where $|V\rangle$ is a vacuum state. In this state the probability distribution for the local occupation n_j of atoms on a single lattice site is Poissonian. The state is well described by a macroscopic wave function with long-range phase coherence throughout the lattice. With increase in the ratio U/J, the system reaches a quantum critical point, the fluctuations in atom number of a Poisson distribution become energetically very costly, and the ground state of the system will instead undergo a quantum phase transition from the superfluid state to the Mott insulator state, a product of local Fock states of n atoms in each lattice site is given by [84, 85],

$$|\psi_{MI}\rangle_{J=0} \propto \prod_{j=1}^{M} (\hat{b}_j^\dagger)^n |V\rangle. \tag{4.15}$$

4.3 Quantum walk on atoms in 1D Mott insulator and superfluid regime

Lets first consider the localized atomic wave functions in the Mott insulator regime with one atom in each of the M lattice sites and implement the quantum walk on it. Atoms are first initialized into a symmetric superposition of any of the two internal trappable state, hyperfine levels, $|0\rangle$ and $|1\rangle$[1] at position j,

$$|\Psi_{MI}\rangle_{J=0} \propto \prod_{j=-\frac{M}{2}}^{\frac{M}{2}} \left(\frac{|0\rangle + i|1\rangle}{\sqrt{2}} \right)_j \otimes |j\rangle. \tag{4.16}$$

The $\mathcal{H}_c$ of each atom is spanned by the two hyperfine levels and $\mathcal{H}_p$ is spanned by the lattice site. The total system is then in the Hilbert space $\mathcal{H}_m = (\Pi_j \mathcal{H}_{c_j}) \otimes \mathcal{H}_p$. The unitary shift operation S (2.14) written in the form (3.1), on the above system will evolve each atom into superposition of the neighbor lattice site, establishing the quantum correlation between the states of the atom and the neighboring lattice site,

---

[1] A $\pi/2$ radio frequency pulse can evolve the atoms into an equal superposition of the two internal trappable states

$$S|\Psi_{MI}\rangle_{J=0} \propto \prod_{j=-\frac{M}{2}}^{\frac{M}{2}} \left(\frac{|0\rangle \otimes \hat{a}|j\rangle + i|1\rangle \otimes \hat{a}^{\dagger}|j\rangle}{\sqrt{2}} \right). \tag{4.17}$$

For a system initially in state given by (4.16), t steps of quantum walk is implemented by iterating the process of S followed by the quantum coin operation $B_{\xi,\theta,\zeta}$ (2.37), $W = (B_{\xi,\theta,\zeta} \otimes \mathbb{1})S$, upto t times. During the iteration, the atom and position correlations overlap resulting in,

$$\begin{aligned}(W)^t|\Psi_{MI}\rangle_{J=0} \propto \prod_{j=-\frac{M}{2}}^{\frac{M}{2}} (\beta_{j-t}|0\rangle \otimes |j-t\rangle + \\ \beta_{j-(t+1)}|0\rangle \otimes |j-(t+1)\rangle + ... + \beta_{j+t}|0\rangle \otimes |j+t\rangle \\ +\gamma_{j-t}|1\rangle \otimes |j-t\rangle + ... + \gamma_{j+t})|1\rangle \otimes |j+t\rangle).\end{aligned} \tag{4.18}$$

This can be written as

$$(W)^t|\Psi_{MI}\rangle_{J=0} \propto \prod_{j=-\frac{M}{2}}^{\frac{M}{2}} \left(\sum_{x=j-t}^{j+t} [\beta_x|0\rangle + \gamma_x|1\rangle] \otimes |x\rangle \right), \tag{4.19}$$

β_x and γ_x are the probability amplitudes of state $|0\rangle$ and $|1\rangle$ at lattice site x, which range from $(j-t)$ to $(j+t)$. For a quantum walk of t steps on a particle initially at position $j = 0$ using $B_{0,\theta,0}$ as the quantum coin, the probability distribution spread over the interval $(-t\cos(\theta), t\cos(\theta))$ in position space and ceases quickly outside this region [21, 64]. Therefore, after t steps the density profile of M atoms initially between $\pm\frac{M}{2}$ will correlate with the position space and spread over the lattice site $\pm(\frac{M}{2} + t\cos(\theta))$. Figure 4.2 is the redistribution of atomic density of 40 atoms initially in the Mott insulator state when subjected to a quantum walk of different number of steps with Hadamard operator $H = B_{0,45^\circ,0}$ as the quantum coin. In the lattice region range where all the 40 atoms are correlated can be seen as a superfluid region.

The redistributed atoms would be in either of their internal states and this can be retained to study the phase transition of the two-state bosonic atoms in an

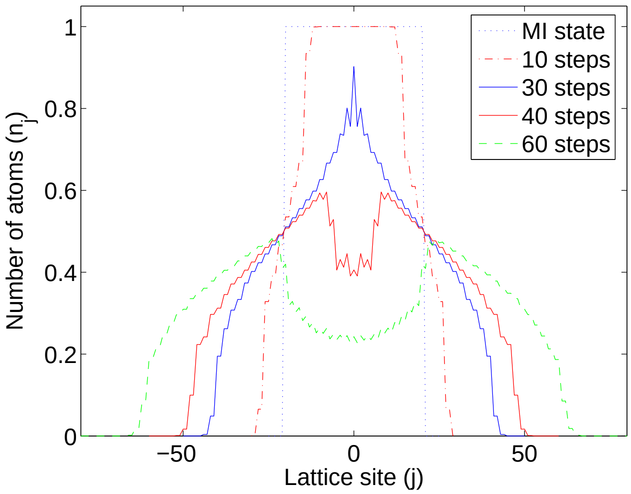

FIGURE 4.2: Density profile of the evolution of 40 atoms starting from Mott insulator state in correlation with the position space when subjected to a quantum walk of different numbers of steps with the Hadamard operator $B_{0,45^\circ,0}$ as the quantum coin. The distribution spreads with increase in the number of steps.

optical lattice [123] or all atoms can be transferred to one of the internal states. A technique based on adiabatic passage using crafted laser pulses can be used for a nearly complete transfer of population between two states [124], and a popular example of one such technique is stimulated Raman adiabatic passage (STIRAP) [125].

Along with the correlation between the atoms and the position space, (4.18) also reveals the overlap of the probability amplitude of different atoms in the position space. That is, during each step of the quantum walk, the amplitude of the states of each atom overlaps with the amplitude of the states of the atoms in the neighboring lattice site. After the iteration of the t steps $\geq \frac{M/2}{\cos(\theta)}$, the overlap of all atoms could be seen at the central region of the lattice.

When the number of steps of the quantum walk is equal to the number of lattice site ($t = M$), the overlap of the fraction of amplitude of all M atoms exists within the lattice sites $\pm\frac{M\cos(\theta)}{2}$ making the region identical to the superfluid state. Beyond $\pm\frac{M\cos(\theta)}{2}$ the number of atoms in correlation with that position space decreases and hence the number of overlapping atoms also decrease. To make all M atoms to spread between lattice site $\pm\frac{M}{2}$ with the usual method of lowering the optical potential depth following the classical random walk protocol takes M^2 steps. Therefore, we can conclude that using quantum walk a long range correlation can be induced quadratically faster than any other technique using the classical random walk protocol.

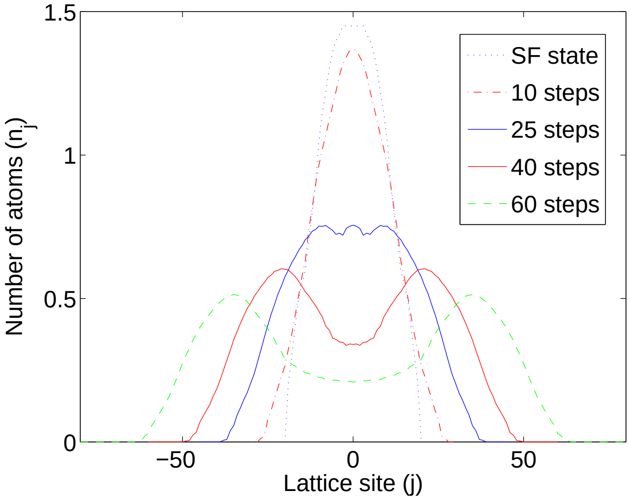

Figure 4.3: Density profile of the evolution of 40 atoms starting from superfluid state in correlation with the position space when subjected to a quantum walk of different numbers of steps with the Hadamard operator $B_{0,45^\circ,0}$ as the quantum coin. The distribution spread with increase in the number of steps and is almost uniform between the lattice site ± 20 when $t = 25$. At this stage the optical potential depth can be increased to cancel the correlation and obtain the Mott insulator state.

Similarly, Figure 4.3 is the redistribution of atomic density of 40 atoms initially in the superfluid states when subjected to the quantum walks of different number of steps using Hadamard operator $B_{0,45^\circ,0}$ as the quantum coin. To reach Mott insulator state the distribution should be uniform over the lattice site without correlation. A distribution that is approximately uniform within the region $\pm\frac{M}{2}$ can be obtained using the quantum walk. In Figure 4.3, when $t = 25$ the distribution is almost uniform between the lattice site ± 20 retaining the correlation with the position space. Once the distribution is uniform, the optical potential depth can be increased to cancel the correlation and obtain the Mott insulator state. The uniformity of the distribution can also be improved by introducing a noise channel, as we show later.

The variance and the probability distribution can be controlled using the parameters θ, ξ and ζ in $B_{\xi,\theta,\zeta}$. Figures 4.4 and 4.5 shows the density distribution obtained by implementing the quantum walk on atoms in Mott insulator and superfluid state ($t = M = 40$) respectively with different values of θ in the coin operator $B_{0,\theta,0}$. The spread is wider for $\theta = 30^\circ$ and decreases with increase in θ. In Figure 4.5 the distribution is almost uniform for $\theta = 60^\circ$ between the lattice site ±20. At this value the optical potential depth can be increased to cancel the correlation and obtain the Mott insulator state.

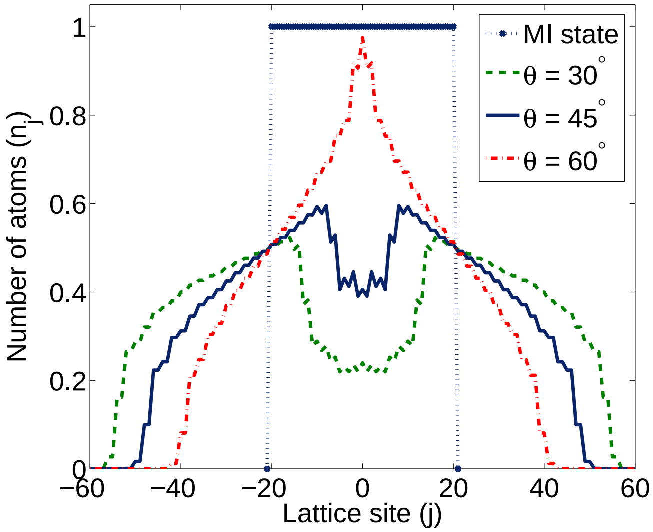

FIGURE 4.4: Distribution of atoms initially in Mott insulator state when subjected to quantum walk ($t = M = 40$) using different values for θ in the operator $B_{0,\theta,0}$. The spread is wider for $\theta = 30^\circ$ and decreases with increasing θ.

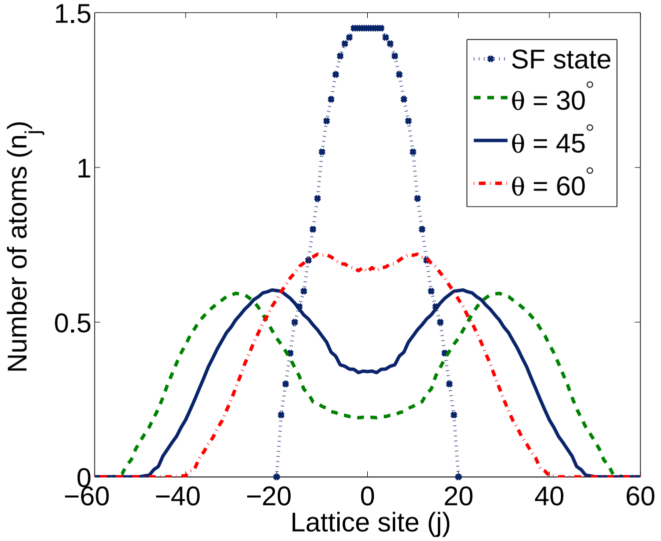

FIGURE 4.5: Distribution of atoms initially in superfluid state when subjected to a quantum walk ($t = M = 40$) using different values for θ in the coin operator $B_{0,\theta,0}$. The distribution is almost uniform for $\theta = 60°$ between the lattice site ±20. At this value the optical potential depth can be increased to cancel the correlation and obtain the Mott insulator state.

The Hamiltonian of the system in general can be described by the 1D Bose-Hubbard model for two-state atoms,

$$\begin{aligned}\mathbf{H}_{BH_2} = -J_{\uparrow}\sum_{\langle j,k\rangle}\hat{b}^{\dagger}_{j\uparrow}\hat{b}_{k\uparrow} - J_{\downarrow}\sum_{\langle j,k\rangle}\hat{b}^{\dagger}_{j\downarrow}\hat{b}_{k\downarrow} + \sum_{j,\alpha=\uparrow,\downarrow}\epsilon_{j,\alpha}\hat{n}_{j,\alpha} + \\ U\sum_{j}(\hat{n}_{j\uparrow}-\frac{1}{2})(\hat{n}_{j\downarrow}-\frac{1}{2}) + \frac{1}{2}\sum_{j,\alpha=\uparrow,\downarrow}V_{\alpha}\hat{n}_{j\alpha}(\hat{n}_{j\alpha}-1) \\ + \sum_{j}\left(d_L\hat{b}^{\dagger}_{(j-1)\uparrow}\hat{b}_{j\uparrow} + d_R\hat{b}^{\dagger}_{(j+1)\downarrow}\hat{b}_{j\downarrow}\right),\end{aligned} \tag{4.20}$$

here ↑ and ↓ represent the terms for atoms in state $|0\rangle$ and state $|1\rangle$ respectively. U is the interaction between atoms in state $|0\rangle$ and $|1\rangle$; $V_{\uparrow(\downarrow)}$ is the interaction between atoms in same state. d_L and d_R are the left and right displacement terms in the Hamiltonian operation. The Hamiltonian is evolved with coin toss operation in a regular interval of time τ, the time required to move the atom to the neighboring site. The optical lattice can be dynamically manipulated to evolve atoms in a superposition of lattice site without giving time for the atom-atom interaction, and the optical potential depth of the system can be configured just above the level where there is no direct tunneling. Then the dynamics of atoms in lattice will be dominated by the last term of the Hamiltonian in (4.20) ignoring the atom-atom interaction. Therefore scaling up the scheme of using the quantum walk on systems with large number of atoms in each lattice site or to infinitely large numbers of lattice site is also straight forward; whereas, the atom-atom interaction play a prominent role during the usual method of varying the potential depth.

4.4 Quantum walk with a noisy channel as a toolbox

We saw the effect of quantum walk with different number of steps and the coin parameters θ on atoms in optical lattice in the previous section. To demonstrate the effect of the quantum walk with a noisy channel on atoms in optical lattice we consider a bit-flip channel, a phase-flip channel and an amplitude-damping channel. The bit-flip channel flips the state of the particle from $|0\rangle$ ($|1\rangle$) to $|1\rangle$ ($|0\rangle$) (Pauli X operation) and a phase-flip channel flips the phase of $|1\rangle$ to $-|1\rangle$ (Pauli Z operation). We use the notation p for the noise level where, $0 \leq p \leq 1$. Therefore, the bit- (phase-)flip channel flips the state (phase) with probability p during each step of the quantum walk. An amplitude-damping channel leaves state $|0\rangle$ unchanged but looses the amplitude of state $|1\rangle$ with probability p resulting in an asymmetric distribution [8]. From Chapter 3 we know that the maximum decoherence effect using bit- and phase-flip channel is at $p = 0.5$ due to symmetries induced by these two channels during the quantum walk; whereas, the amplitude-damping channel does not obey any symmetry and hence the maximum effect is for $p = 1$ [67]. Our numerical implementation of these channels evolves the density matrix employing the Kraus operator representation.

Figure 4.6 is a comparison of the distribution obtained without noise channels to the distributions with phase-flip ($p = 0.02$ and $p = 0.1$) and amplitude-damping channel ($p = 0.2$) on atoms initially in the Mott insulator state. Similarly, the redistribution of atoms in superfluid state when subjected to quantum walk without and with noise channels is shown in Figure 4.7. In Figure 4.7, with the phase

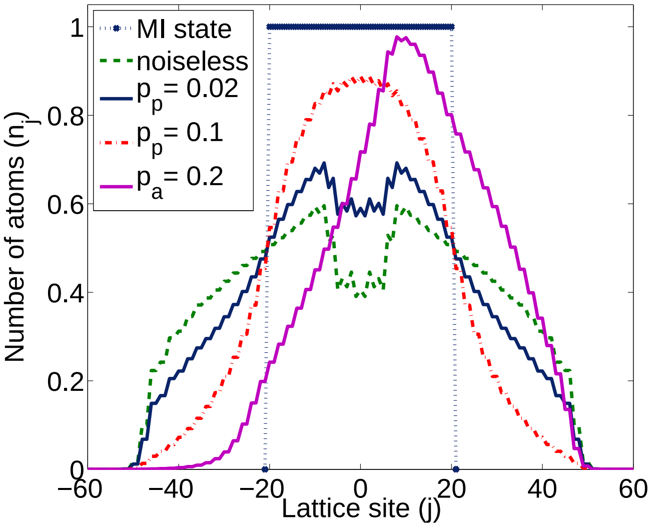

Figure 4.6: Atoms in Mott insulator state after implementing the quantum walk ($t = M = 40, \theta = 45°$) with noise channel. With increased phase damping from $p_p = 0.02$ to $p_p = 0.1$ the distribution (n_j) at the central region gets closure to Gaussian. Amplitude damping of state $|1\rangle$ followed by a bit flip at each step introduces asymmetry to the distribution, $p_a = 0.2$ (without a bit flip the shift would have been to the left).

flip noise of $p = 0.02$, a uniform distribution is obtained. Then the optical potential depth can be increased to cancel the correlation and obtain the Mott insulator state. Other plots shows the different redistribution of atoms that can be obtained using different noise channels.

The effect of bit-flip on the distribution is close to the one obtained using phase-flip channel and hence the redistribution in the Figures 4.6 and 4.7 are shown only for phase-flip and amplitude-damping channels. Increasing noise level affects the variance of the quantum walk [67], which proportionally affect the atom-position correlation and the atom-atom overlap region. Therefore, higher noise level classicalize the dynamics and hence, it is important to restrict the noise level to a very low value ($p \lessapprox 0.1$) to use noisy channel as a useful tool.

Some of the distribution presented in Sections 4.3 and 4.4 using quantum walks are visibly similar to some of the distribution presented using different technique; in [2] using time evolution density matrix renormalization group (t-DMRG) and in [1, 3] using quantum Monte Carlo simulation, Figure 4.8 and Figure 4.9. These

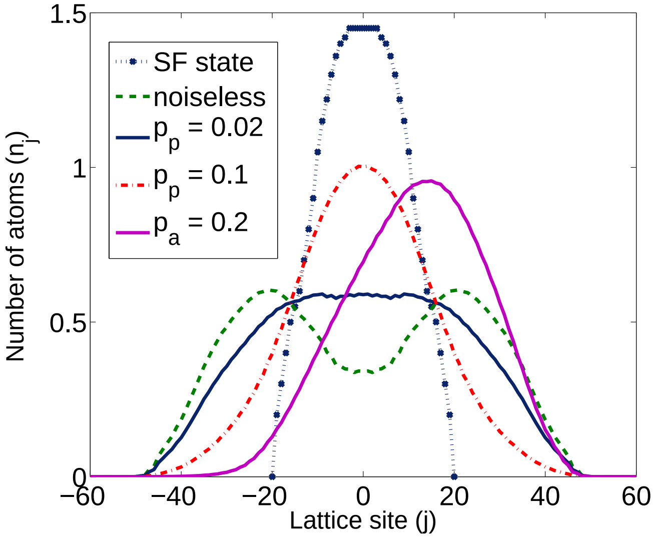

FIGURE 4.7: Atoms in superfluid state after implementing a quantum walk ($t = M = 40, \theta = 45°$). With noiseless quantum walk, the atoms spread, getting close to a uniform distribution. For phase damping $p_p = 0.02$ the distribution is uniform between ±20 and gets closer to Gaussian at $p_p = 0.1$. Amplitude damping of state $|1\rangle$ followed by a bit flip introduces asymmetry to the distribution, $p_a = 0.2$ (without a bit flip the shift would have been to the left).

technique present the change in density profile distribution with time, whereas in this chapter we have discussed the change with number of steps of the quantum walk.

In this section, we have shown the use of the quantum walk to study the dynamics of atoms in an optical lattice and expedite the process of quantum phase transition. We have also used the quantum walk with experimentally realizable noisy channels to show the additional control one can have over the evolution and atomic density redistribution. Theoretically, the evolution of the density profile with a quantum walk can be used in place of quantum Monte Carlo simulation to study the correlation and redistribution of atoms in optical lattices. We expect the quantum walk to play a wider role in simulating and expediting the dynamics in various physical systems.

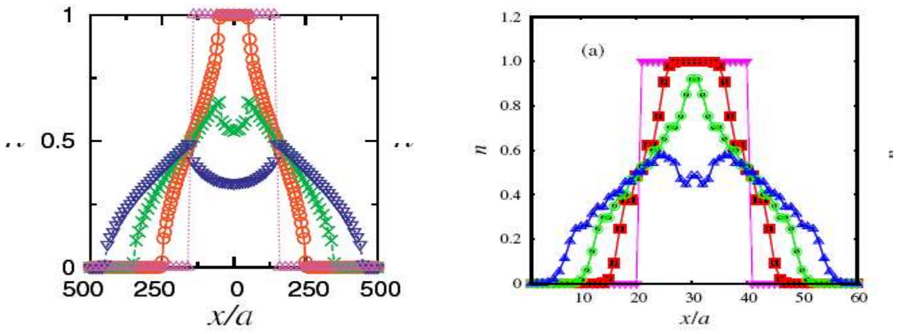

(a) (b)

Figure 4.8: Density profile of the evolution of atoms initially in MI state from other references. (a) Evolution of 100 atoms with time for atoms initially in MI state [1] . (b) Evolution of 20 atoms with time (the dynamics is driven by the potential depth and tunneling of atoms between the lattice) [2] . These profile have visibly similar distribution compared to Figure 4.2, Figure 4.4 and part of Figure 4.6 in this chapter.

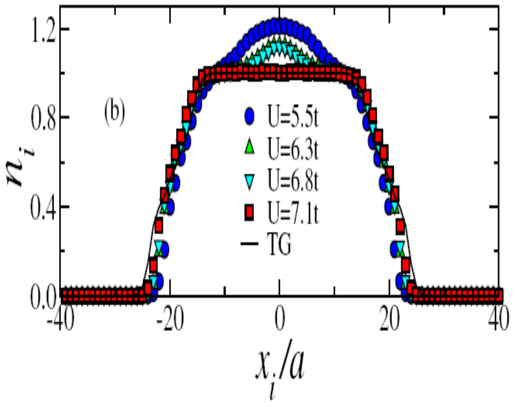

Figure 4.9: Density profile of the evolution of 40 atoms initially in SF state from [3]. The initial SF profile in our plots and in [3] are different and hence the similarity are not as close as we have for atoms in MI state). The profile in Figure 4.3 after 25 steps of quantum walk is similar to the Profile at TG limit (Tonks-Girardeau limit - leading to MI state) in the above figure.

4.5 Implementation

Experiments on ultra cold atoms has been one of the active areas of research in the last two decades. Optical lattices ranging from a simple periodic, square and cubic, to a more exotic ones, such as hexagonal and Kagome lattices using superlattice technique (see for example, [126–132]) have been created to trap and manipulate ultra cold atoms. Manipulation of cold atoms in time-varying optical lattice has also been reported [133, 134]. This has provided flexibility in designing and studying quantum phases and quantum phase transitions in coherent and strongly correlated ultracold atoms.

Various schemes have been proposed to implement quantum walk on neutral atoms in an optical lattice [58, 59]. In [135], the controlled coherent transport and splitting of atomic wave packets in spin dependent optical lattice has been experimentally demonstrated using rubidium atoms. A BEC of up to $N = 3 \times 10^5$ atoms is initially created in a harmonic magnetic trap. A three dimensional optical lattice is superimposed on the BEC and the intensity is raised in order to drive the system into a Mott insulating phase [85].

Two of the three orthogonal standing wave light fields is operated at one wavelength, $\lambda_{y,z} = 840$ nm and the third along the horizontal direction is tuned to the wavelength $\lambda_x = 785$ nm between the fine structure splitting of the rubidium $D1$ and $D2$ transitions. Along this axis a quarter wave plate and an electro-optical modulator (EOM) is placed to allow the dynamic rotation of the polarization vector of the retro-reflected laser beam through an angle θ by applying an appropriate voltage to the EOM. After reaching the Mott insulating phase, the harmonic magnetic field is completely turned off but a homogeneous magnetic field along the x direction is maintained to preserve the spin polarization of the atoms. The light field in the y and z direction is adiabatically turned off to reduce the interaction energy, which strongly depends on the confinement of the atoms at a single lattice site.

A standing wave configuration in the x direction is used to transport the atoms. By changing the linear polarization vector enclosing angle θ, the separation between the two potentials is controlled. By rotating the polarization angle θ by π, with the atom in a superposition of internal states, the spatial wave packets of the atom in the $|0\rangle$ and the $|1\rangle$ state are transported in opposite directions. The final state after such a movement is then given by $1/\sqrt{2}(|0, x-1\rangle + i\exp(i\beta_p)|1, x+1\rangle)$. The phase β_p between the separated wave-packets depends on the accumulated kinetic and potential energy phases in the transport process and in general will be nonzero. The coherence between the two wave-packets is revealed by absorption imaging of the momentum distribution. A $\pi/2$ microwave pulse is applied before absorption imaging to erase the which-way information encoded in the hyperfine states.

However, to increase the separation between the two wave-packets further, one could increase the polarization angle θ to integer multiples of 180°. To overcome the limitation of the maximum voltage that can be applied to the EOM, a π pulse after the polarization is applied, thereby swapping the roles of the two hyperfine states. The single particle phase β_p remains constant throughout the atomic cloud and is reproducible. After the absorption imaging a Gaussian envelope of the interference pattern is obtained.

One can build upon the above technique to implement a quantum walk. The above setup can be modified by dividing the separations (splitting) into small steps and introducing a rotation ($\pi/2$ pulse for Hadamard rotation) after each separation without intermediate imaging. The absorption imaging of the distribution of the atomic cloud after t steps would give the interference pattern similar to the probability distribution of the quantum walk.

This effect of the addition of phase during the quantum walk process can be easily understood from the phase damping channel and arbitrary phase rotation discussed in Chapter 2. The addition of π pulse to overcome the limit of EOM is a bit flip operation in the quantum walk.

In the following section we propose a scheme to implement a discrete time quantum walk on ultra cold atoms in BEC state. BEC being a macroscopic wave packet, the scheme we propose can implement a quantum walk retaining the macroscopic features of the wave packet [60] or the scheme can be accordingly modified to implement the walk at an individual atom level. For the transition from superfluid to the Mott insulator and vice versa using quantum walk, we need to consider the quantum walk on individual atom.

To implement a macroscopic quantum walk, atoms in BEC state is first evolved to macroscopic superposition state and a *stimulated Raman kick*, two selected levels of the atom are coupled to the two modes of counterpropagating laser beams to coherently impart a translation of atoms in the position space. After each translation, the wave packet again evolved into the macroscopic superposition state and the process is iterated to implement large number of steps of macroscopic quantum walk. With a certain modification to this scheme, that is, by evolving atoms to the superposition of the states at individual atom level and implementing the shift operation before the interatomic interaction takes over to form an macroscopic superposition, the quantum walk at individual atom level can be realized.

4.5.1 Quantum walk using Bose-Einstein condensate

As discussed in Section 2.3, two degrees of freedom, the coin Hilbert space $\mathcal{H}_c$ and the position Hilbert space $\mathcal{H}_p$ are required to implement the discrete-time quantum walk. The state of the BEC formed from the atoms in one of the hyperfine states $|0\rangle$ or $|1\rangle$ can be represented as $|0_{BEC}\rangle$ or $|1_{BEC}\rangle$ (macroscopic states of N condensed atoms). The BEC formed is then transferred to an optical dipole trap with long Rayleigh range z_R[2]. With the appropriate choice of power and beam waist, ω_0[3] of the trapping beam, the BEC can remain trapped at any point within the distance $\pm z$ from the focal point in the axial direction of the beam (See Appendix C for calculations).

The position of the BEC formed in one of the Hyperfine state $|0_{BEC}\rangle$ or $|1_{BEC}\rangle$ and trapped at the center of the optical trap is described by a wave packet $|\Psi_{j_0}\rangle$ localized around a position j_0, i.e., the function $\langle j|\Psi_{j_0}\rangle$ corresponds to a wave packet centered around j_0. The BEC formed in one of the Hyperfine state is evolved into the macroscopic superposition (Schrödinger cat) state

$$|\Psi_{in}\rangle = (a|0_{BEC}\rangle + b|1_{BEC}\rangle) \otimes |\Psi_{j_0}\rangle \tag{4.21}$$

---

[2] Distance at which the diameter of the laser beam size increases by a factor of $\sqrt{2}$.

[3] Minimum radius of the beam, at the focal point.

by applying the rotation (coin operation B), where $|a|^2 + |b|^2 = 1$. We will discuss this process in detail in Section 4.5.1.1. The coin Hilbert space $\mathcal{H}_c$ can then be defined to be spanned by the two internal trappable macroscopic states $|0_{BEC}\rangle$ and $|1_{BEC}\rangle$ of the BEC. The position Hilbert space $\mathcal{H}_p$ is spanned by the positions within the long Rayleigh range optical trap (trappable range). Once the BEC is in the superposition state, a unitary shift operator, *stimulated Raman kick*, Section 4.5.1.2, corresponding to one step length l in the form (3.2) is applied;

$$S' = (X \otimes \mathbb{I}) \exp(-i(|0_{BEC}\rangle\langle 0_{BEC}| - |1_{BEC}\rangle\langle 1_{BEC}|) \otimes Pl), \tag{4.22}$$

P being the momentum operator. Step length l is chosen to be less than the spatial width of the condensate wave packet $|\Psi_{j_0}\rangle$.

The application of the unitary shift operator (S') on the wave function of (4.21) entangles the position and the coin space and implements the quantum walk. Stimulated Raman kicks evolves the state to,

$$S'|\Psi_{in}\rangle = \left(a|1_{BEC}\rangle \otimes e^{-iPl} + b|0_{BEC}\rangle \otimes e^{iPl}\right)(\mathbb{I} \otimes |\Psi_{j_0}\rangle), \tag{4.23}$$

where the wave packet is centered around $j_0 \pm l$. Note that the values in the coin space have been flipped. This can be corrected by applying a compensating bit flip on the BEC, $S \equiv (X \otimes \mathbb{I})S'$. From the symmetries of quantum walk discussed in Chapter 3 we know that the distribution is invariant to bit flips at each step and therefore, augmenting S' with the X operation is unnecessary. To realize a large number of steps of the macroscopic quantum walk, the process of shift operation followed by the quantum coin operation $(B_{\xi,\theta,\zeta} \otimes \mathbb{I})S'$ is iterated without resorting to intermediate measurement in the long Rayleigh-range optical dipole trap.

However, the coin operation $B_{\xi,\theta,\zeta}$ can be performed such that, its action will evolve the individual atoms into the superposition of $|0\rangle$ and $|1\rangle$ and not the superposition of macroscopic state $|0_{BEC}\rangle$ and $|1_{BEC}\rangle$, Section 4.5.1.1. This can be used to drive the transition between the superfluid and the Mott insulator state. To realize transition from the superfluid to the Mott insulator phase, atoms are first redistributed by implementing the quantum walk using the rotation operation (coin operation) $B_{\xi,\theta,\zeta}$ on individual atoms in a long-Rayleigh-range optical trap and the optical lattice is switched on at the end to confine atoms and cancel the correlation. For transition from Mott insulator to the superfluid, the atoms initially in the optical lattice are transferred to long-Rayleigh-range dipole trap and quantum walk is implemented.

4.5.1.1 Macroscopic cat state of Bose-Einstein condensate

Various schemes have been proposed for producing macroscopic superposition or Schrödinger cat states in BECs [136–138]. The scheme described in [136], shows that the two species (two interacting Bose condensates) can be evolved to the macroscopic superposition of the internal atomic states. In this scheme, atom-atom interactions are mediated through atom-atom collisions and a Josephson-like laser coupling that interchanges internal atomic states in a coherent manner. In certain parameter regimes the ground state of the Hamiltonian is a superposition of two states involving a particle number imbalance between the two condensates. Such a state produced by the normal dynamic evolution of the system represents a superposition of two states which are macroscopically (or mesoscopically) distinguishable, and hence can be called a Schrödinger cat state. But, two interacting Bose condensates are needed for this scheme. In [137], it is shown that a macroscopic superposition state can be created by a mechanism involving the coherent scattering of far-detuned light fields and it neglects the collisional interactions between particles. The major drawback of the above schemes is that the time needed to evolve to a cat state can be rather long, and thus problems due to decoherence would be greatly increased. An other scheme proposed in [138] involves the creation if macroscopic superposition by an adiabatic transfer of the ground state of the Josephson-coupling Hamiltonian, that is, after the initial state preparation the Josephson coupling is turned on for some amount of time and turned off. The resulting modified quantum state is a Schrödinger cat state. But, the production of such a state involves considerable experimental difficulty.

The ideal scheme to demonstrate the quantum walk is to confine the BEC that has an attractive interaction between atoms in two hyperfine levels $|0\rangle$ and $|1\rangle$ in a single optical potential well. The rotation operation is applied on the BEC in the potential well to transfer (or rotate) the atoms part of way between states

$|0\rangle$ and $|1\rangle$ using a resonant rf pulse [4] of duration τ and detuning Δ from the rf resonance [139]. The resonance rf pulse couples the atomic hyperfine states $|0\rangle$ and $|1\rangle$ with a coupling matrix element $\hbar\omega_R/2$, where ω_R is the Rabi frequency and the duration of pulse is much shorter than the self-dynamics of the BEC. The amplitude of these states evolves according to the Schrödinger equation,

$$i\hbar\frac{d}{d\tau}\begin{pmatrix} a \\ b \end{pmatrix} = \hbar\begin{pmatrix} 0 & \omega_R/2 \\ \omega_R/2 & \Delta \end{pmatrix}\begin{pmatrix} a \\ b \end{pmatrix}. \tag{4.24}$$

At this stage, each atom evolves into the superposition state $a(\tau)|0\rangle + b(\tau)|1\rangle$, with $a(\tau) = \cos(\omega_R\tau/2)$ and $b(\tau) = \sin(\omega_R\tau/2)$ for detuning $\Delta = 0$. The N-particle wave function of the BEC is a product of the single-particle superpositions of $|0\rangle$ and $|1\rangle$, that is, it is still a microscopic superposition and is given by

$$[a(\tau)|0\rangle + b(\tau)|1\rangle]^N = \sum_{n=0}^{N}\sqrt{\frac{N!}{n!(N-n)!}}a(\tau)^{N-n}b(\tau)^n|N-n,n\rangle, \tag{4.25}$$

where $|N-n,n\rangle$ is the state with $N-n$ atoms in state $|0\rangle$ and n atoms in state $|1\rangle$. The individual atoms in the superposition state interact among themselves. Interatomic interactions, which provide nonlinear terms through binary collision as seen from the viewpoint of single-particle dynamics helps in generating highly entangled many body states [140, 141]. That is, the Hamiltonian that governs the BEC with its attractive inter-atomic interactions, after time τ_1, (4.25) evolves into the macroscopic superposition state in which all atoms are simultaneously in level $|0\rangle$ and level $|1\rangle$ [136, 142, 143],

$$[a(\tau_1)|0\rangle + b(\tau_1)|1\rangle]^N = a(\tau_1)^N|N,0\rangle + b(\tau_1)^N|0,N\rangle \tag{4.26}$$

where $|N,0\rangle = |0_{BEC}\rangle$ and $|0,N\rangle = |1_{BEC}\rangle$. Symmetric probability distribution $a(\tau_1) = b(\tau_1) = \frac{1}{\sqrt{2}}$ can be obtained by carefully choosing ω_R and τ.

---

[4] Microwave pulses are also used.

Microscopic superposition state of atoms :

Equation (4.25) gives the microscopic superposition state of N-atoms. Implementing the unitary shift operator before the individual atoms in the superposition states start interacting will prevent the evolution of atoms to macroscopic superposition state. Therefore we can choose between the macroscopic, Schrödinger cat state or the superposition of individual atoms, microscopic superposition state.

4.5.1.2 Unitary operator - Stimulated Raman kicks

A unitary shift (controlled-shift) operation S is applied on the BEC to spatially entangle the position and the coin space and implement the quantum walk. Various schemes have been worked out to give momentum kick to ultracold atoms in a trap [143, 144]. A technique was reported in [143] where coherent rf-induced transitions were used to change the internal state of the atoms in the magnetic trap from a trapped to an untrapped state and thus displacing the untrapped atoms from the trap. This method, however, did not allow the direction of the output-coupled atoms to be chosen. Later, controlling the direction of the fraction of the outgoing BEC using a stimulated Raman process between magnetic sublevels was experimentally demonstrated [144]. This technique was used to extract sodium atoms lasers from the trapped BEC.

A stimulated Raman process can also be used to drive the transition between two optically trappable states of the atom $|0\rangle$ and $|1\rangle$ using the virtual state $|e\rangle$ as an intermediary state, and impart a well-defined momentum to spatially translate the atoms in the coherent state (BEC). A unitary shift operation S' thus can be applied on the atom in the BEC using a stimulated Raman process. A pair of counterpropagating laser beams 1 and 2 (Figure 4.10) with frequency ω_1 and ω_2 and wave vectors k_1 and k_2 is applied on the BEC for a $2N$-photon transition time (N is the number of atoms in the BEC) to implement one unitary shift operation. These beams are configured to propagate along the axial direction of the optical dipole trap. A stimulated Raman transition occurs when an atom changes its state by coherently exchanging photons between the two laser fields, absorption of the photon from laser field 1 and stimulated emission into laser field 2 or by absorption from field 2 and stimulated emission into field 1. The BEC initially in

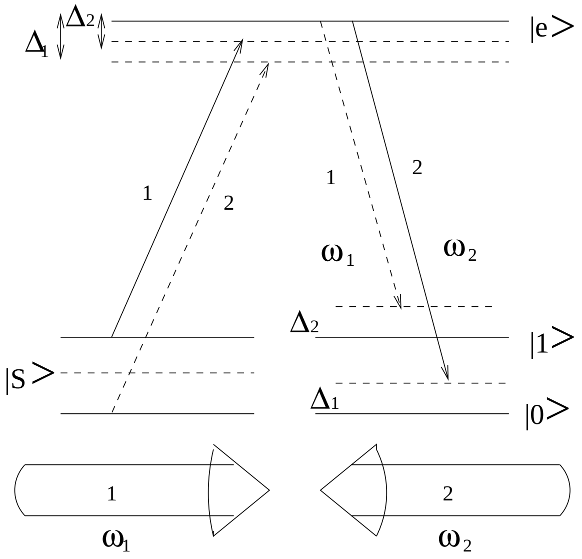

Figure 4.10: Light field configuration for a stimulated Raman transition process to give directional momentum kick. Δ is the detuning of the laser from its transition frequency. $|S\rangle$ signifies $(1/\sqrt{2})(|0\rangle \pm |1\rangle)$.

eigenstates of the atom $|0\rangle$ ($|1\rangle$) can absorb the photon from field 1 (2) and re-emit the photon into field 2 (1). This inelastic stimulated Raman scattering process imparts well-defined momentum on the coherent atoms,

$$\mathbf{P} = \hbar(k_1 - k_2) = \hbar\delta z \tag{4.27}$$

to the left during $|0\rangle \xrightarrow{\omega_1} |e\rangle \xrightarrow{\omega_2} |1\rangle$ and

$$\mathbf{P} = \hbar(k_2 - k_1) = -\hbar\delta z \tag{4.28}$$

to the right during $|1\rangle \xrightarrow{\omega_2} |e\rangle \xrightarrow{\omega_1} |0\rangle$, where

$$|k_1 - k_2| = |k_2 - k_1| = \delta,$$

Thus, conditioned to being in coin state $|0\rangle$ ($|1\rangle$), the atoms in the BEC receive a momentum kick (shift) $\hbar\delta z$ ($-\hbar\delta z$). This process of imparting momentum is called stimulated Raman kick and can be analyzed as a photon absorption and stimulated emission between three bare states $|0\rangle$, $|1\rangle$, and $|e\rangle$ driven by two monochromatic light fields. The matrix element for photon absorption and stimulated emission during each stimulated Raman kick can be written as

$$\langle n_{k_1}-1, n_{k_2}+1, 1|\hat{H}_{I_a}|n_{k_1}, n_{k_2}, 0\rangle \tag{4.29}$$

during $|0\rangle \xrightarrow{\omega_1} |e\rangle \xrightarrow{\omega_2} |1\rangle$ and

$$\langle n_{k_1}+1, n_{k_2}-1, 0|\hat{H}_{I_b}|n_{k_1}, n_{k_2}, 1\rangle \tag{4.30}$$

during $|1\rangle \xrightarrow{\omega_2} |e\rangle \xrightarrow{\omega_1} |0\rangle$. H_{I_a} and H_{I_b} are the interaction Hamiltonians (electric dipole Hamiltonians). The field causing the transitions between bare states $|0\rangle$ and $|e\rangle$ is detuned from resonance by Δ_1 and has a constant dipole matrix element V_1 and phase φ_1. The field causing transitions between bare states $|e\rangle$ and $|1\rangle$ is detuned from resonance by Δ_2 and has a constant dipole matrix element V_2 and phase φ_2. The time-independent Hamiltonian in the rotating-wave approximation for this system can be written in terms of projection operations as

$$\begin{aligned}\hat{H}_{I_a} &= \hbar\Delta_1|e\rangle\langle e| + \hbar(\Delta_1+\Delta_2)|1\rangle\langle 1| - \frac{\hbar V_1}{2}[|e\rangle\langle 0|\exp(-i\varphi_1) \\ &+ |0\rangle\langle e|\exp(i\varphi_1)] - \frac{\hbar V_2}{2}[|e\rangle\langle 1|\exp(i\varphi_2) + |1\rangle\langle e|\exp(-i\varphi_1)]\end{aligned} \tag{4.31}$$

In the above interaction picture, the energy of the bare state $|0\rangle$ is chosen to be zero.

$$\begin{aligned}\hat{H}_{I_b} &= \hbar\Delta_2|e\rangle\langle e| + \hbar(\Delta_1+\Delta_2)|0\rangle\langle 0| - \frac{\hbar V_2}{2}[|e\rangle\langle 1|\exp(-i\varphi_2) \\ &+ |1\rangle\langle e|\exp(i\varphi_2)] - \frac{\hbar V_1}{2}[|e\rangle\langle 0|\exp(i\varphi_1) + |0\rangle\langle e|\exp(i\varphi_1)].\end{aligned} \tag{4.32}$$

In the above interaction picture the energy of the bare state of the atom $|1\rangle$ is chosen to be zero. $V_i = \frac{\mu_i \cdot E_{0_i}}{\hbar}$, for $i = 1, 2$. μ_i is the dipole operator associated with the states $|0\rangle$,$|e\rangle$ and $|e\rangle$,$|1\rangle$ and E_0 is the electric field of the laser beam.

With the appropriate choice of V, Δ, and φ, the probability of being in bare state $|1\rangle$ (or $|0\rangle$ depending on the starting state) after time t can be maximized to be close to one, where t is the time required for one stimulated Raman kick. As discussed in Section 4.5.1.1, after every stimulated Raman kick on atoms due to the attractive interaction between atoms, they evolve into the BEC.

The coin state of the atoms in the BEC $|0\rangle$ ($|1\rangle$) after stimulated Raman kick flips the states to $|1\rangle$ ($|0\rangle$) and symmetries due to bit flip discussed in Chapter 3 will take care of these flip without affecting the distribution.

4.5.1.3 Physical setup for the implementation

Magnetic trap technique [145] played a major role in the first formation and early experiments on the BEC. But the magnetic trap has a limitation, it can trap and manipulate atoms only of certain sublevels. For example, If we consider ^{87}Rb atom as an example, the $|F = 2, m_f = 2\rangle$ state can be confined in the magnetic trap whereas $|F = 1, m_f = 1\rangle$ cannot be confined using the magnetic trap [146]. Under appropriate conditions, the dipole trapping mechanism works independent of the particular sub-level of the electronic ground state. Thus, internal ground state can thus be fully exploited using an optical dipole trap technique and be widely used for various experiments [147]. Today the BEC from bosonic atoms has been very consistently formed and manipulated using various configurations of magnetic and optical traps, an all optical dipole trap technique has also been developed [148].

A BEC first formed in one of their internal states (eigenstates) of atoms $|0\rangle$ or $|1\rangle$, using any of the techniques [145, 148] mentioned above, is transferred to a far detuned, long Rayleigh range (z_R) optical dipole trap. A sizable number of steps of the quantum walk can be implemented within the axial range $\pm z$ without decoherence in a long Rayleigh-range trap. Appendix C has calculated numerical values of potential depth, power required to trap ^{87}Rb atoms at distance $z = x_n$ from the focal point of the trapping beam (after compensating for gravity) using light fields of various frequency and beam waists ω_0. In the same way one can work out the required power and beam waists to trap ultracold atoms at a distance z from the focal point for different species of atoms using laser fields of different detuning from the resonance.

Once the BEC is transferred into the optical dipole trap, a resonant rf pulse (rotation) of duration τ and detuning Δ is applied to make it evolve into the Schrödinger cat state (or a microscopic superposition state depending on the requirement) after time τ_1. The Schrödinger cat state for the ^{87}Rb BEC trapped in one of the states $|0\rangle$=$|F = 1, m_f = 1\rangle$ or $|1\rangle$=$|F = 2, m_f = 2\rangle$, can be realized by applying a

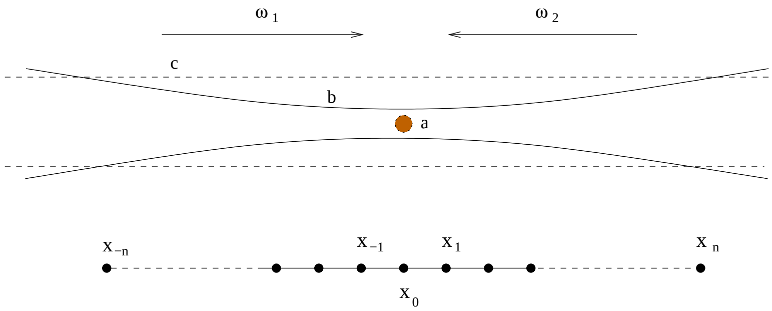

FIGURE 4.11: Physical setup to implement the quantum walk using the BEC. In the figure **a** is a BEC, **b** is a dipole trap with a long Rayleigh range, and **c** is the counterpropagating laser beam, ω_1 and ω_2 used to implement the stimulated Raman kick, unitary operator. A coin rotation and Raman pulse are applied throughout the trap region. The stimulated Raman pulse and the rf pulse are applied alternatively to realize the quantum walk.

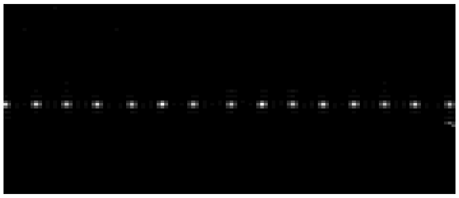

FIGURE 4.12: Multiple microtraps which can be used to confine the atom observe the distribution of atoms after implementing a considerable number of steps of the quantum walk on the BEC.

radio frequency (rf) pulse, fast laser pulse, a standard Raman pulse or microwave techniques.

The BEC in the superposition state is then subjected to a pair of counterpropagating beams to implement the stimulated Raman kick for duration t_d, $2N$ photon transition time (N being the number of photons). After implementing the stimulated Raman kick, the BEC is left to translate for a duration P/ml, the time taken by the BEC to move distance l during or after which the rf π pulse is applied. This process of applying a rf pulse (coin rotation) and a stimulated Raman kick (shift), followed by a compensatory rf pulse (bit flip) is iterated throughout the trapping range to realize a large number of steps (Figure 4.11).

Measuring the probability distribution :

After t steps of the quantum walk the superposition in position space is made to collapse by applying multiple microtraps to confine and redistribute atoms in the position space. The multiple microtraps with an equal spacing l between each potential well can be created using the known techniques [133, 149] (Figure 4.12). The microtraps are switched on, turning off the long Rayleigh range optical trap simultaneously after a time interval of T.

$$T = tt_d + (t-1)\tau_1 + tP/ml. \tag{4.33}$$

T is the time taken by the BEC to travel a t step quantum walk each of distance l in a line. The time t_d is the $2N$-photon transition time required to implement one unitary shift operation, τ is the time duration to bring the BEC to the superposition state, P/ml is the time taken by the BEC to move one step distance l with momentum P. Fluorescence measurement is performed on the atoms in the microtrap to identify the final position/distribution of atoms in the position space.

If the quantum walk was implemented on a BEC evolving the wave packet to the macroscopic superposition during each coin operation, the distribution of atoms will be similar to the distribution of single particle quantum walk. We should note that by retaining the macroscopic behavior during the walk we get the quantum walk distribution in a single measurement at the end. Where as the experiment would have to be repeated a large number of times if we intend to get a probability distribution of the quantum walk using a single particle.

If the quantum walk is implemented only by evolving the atoms to the superposition at individual atom level during each coin operation we get the distributions similar to the ones presented in the earlier sections of this chapter.

Decoherence and physical limitations :

The decoherence of the BEC also leads to the decoherence of the quantum walk. When the atoms in the trap are not coherent they no longer follow the coherent absorption and stimulated emission of light. Some atoms absorb light field 1 and emit light field 2 and bring atoms to state $|1\rangle$ and some absorb light field 2 and emit light field 1 and bring atoms to state $|0\rangle$, displacing atoms in both directions in space giving no signature of displacement in the superposition of position space. This will contribute to collision and heating, and finally, atoms escape out of the trap. The number of implementable steps of quantum walk without decoherence depends mainly on (a) the Rayleigh range, as the BEC moves away from the trap center the width of the wavepacket increases and contributes to the internal heating of the atoms. Beyond a certain distance x_n from the dipole trap, center atoms in the trap decohere resulting in the collapse of the quantum behavior. (b) The stimulated Raman kick and rf pulse used to implement the quantum walk also contribute to the internal heating and decoherence of the atoms after a few iterations. With the careful selection of beam waist and laser power one can have a trap with a long Rayleigh range z_R (Appendix C) so that the one-dimensional quantum walk can be implemented in a line of close to one centimeter length.

4.6 Summary

- We proposed the use of the quantum walk to redistribute atoms, and studied its dynamics in an optical lattice and to expedite the process of quantum phase transition. We have demonstrated the coherent control over the atoms using the coin degree of freedom during the evolution of the walk. We have also used an experimentally realizable noisy channels to show the additional control over the evolution and atomic density redistribution. Theoretically, the evolution of the density profile with a quantum walk can be used in place of quantum Monte Carlo simulation or the time evolution density matrix renormalization group (t-DMRG) to study the correlation and redistribution of atoms in optical lattices. We expect the quantum walk to play a wider role in simulating and expediting the dynamics in various physical systems.

- We proposed a scheme to implement a discrete-time quantum walk on Bose-Einstein condensate (BEC). BEC being a macroscopic wave packet, the scheme we propose can implement a quantum walk retaining the macroscopic features of the wave packet or the scheme can be accordingly modified to implement the walk at an individual atom level. To realize the quantum phase transition from superfluid to the Mott insulator state and vice versa, implementation of walk on individual atom level will be effective.

Chapter 5

Spatial entanglement using quantum walk on many body system

5.1 Introduction

Entanglement in many body systems has been more than just a computational resource, it has been used as a signature of quantum phase transition [86–88]. Therefore, in the last few years, the study on entanglement in many body system has been one of important area of research interfacing between condensed matter system and quantum information sciences [150].

Measure of entanglement in a pure bipartite system is a function of the eigenvalues of the reduced density matrix. However, as the number of particles in the system increases, the complexity of finding the appropriate entanglement measures also increases making scalability of entanglement measure an enormous task. To address the scalability problems, a *scalable* entanglement measures which do not diverge with the system size were proposed and global entanglement measure, a polynomial measure of multipartite entanglement is one such measure [89]. Using this global entanglement measure, namely the Meyer-Wallach measure, we investigate the evolution of *spatial entanglement*– particle-number entanglement between regions of space in a many distinguishable particle system subjected to quantum walk process. Spatial entanglement has also been explored using different methods, for example, in an ideal bosonic gas it has been studied from off-diagonal long-range order [151]. For our investigations of spatial entanglement using multi particle quantum walk, we consider distinguishable particles whose dynamics can be controlled using the quantum coin parameters, initial state of the particles, number of particles in the system and the number of steps of quantum walk. In particular we consider distinguishable particles in one dimensional open and closed chains. The spatial entanglement thus created can be used, for example to create entanglement between distant atoms in optical lattice [152] or as a channel for state transfer in spin chain systems [153–155]. At this stage, we find calculating spatial entanglement for indistinguishable particle case computationally enormous time consuming.

This chapter is organized as follows. In Section 5.2 the entanglement between the particle and the position space has been discussed. In the same section we also introduce spatial entanglement and discuss spatial entanglement using single and many particle quantum walk. In Section 5.3, we present the measure of the spatial entanglement on the system using Meyer-Wallach global entanglement measure scheme for particles in one dimensional lattice and in a closed chain ($n-$cycle). We also demonstrate the control over the entanglement using the dynamical properties of quantum walk. We conclude with a summary in Section 5.4.

5.2 Entanglement

5.2.1 Position-particle entanglement

Quantum walk entangles the particle Hilbert space $\mathcal{H}_c$ and the position Hilbert space $\mathcal{H}_p$. As discussed in Chapter 2, H_c is spanned by the basis state (internal state) of the particle $|0\rangle$ and $|1\rangle$ and $\mathcal{H}_p$ is spanned by the basis state of the position $|\psi_j\rangle$, where $j \in \mathbb{Z}$. Lets consider a discrete-time quantum walk on a particle initially in state given by symmetric superposition state (2.28) at position

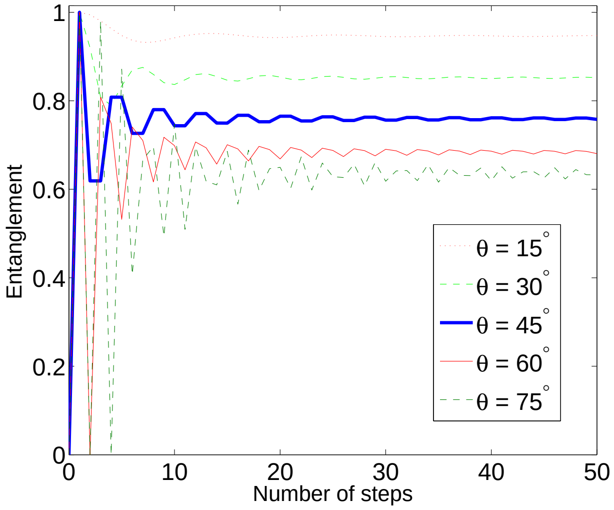

FIGURE 5.1: Entanglement of single particle with position space when subjected to quantum walk. The initial state of the particle is $\frac{1}{\sqrt{2}}(|0\rangle + i|1\rangle)$ and is evolved in position space using different values for θ in the quantum coin operation $B_{0,\theta,0}$. The entanglement initially oscillates and approaches asymptotic value with increase in number of steps. For smaller values of θ the entanglement is higher and decreases with increase in θ. Initial oscillation is also larger for higher θ.

j with coin operation

$$B_{0,\theta,0} \equiv \begin{pmatrix} \cos(\theta) & \sin(\theta) \\ \sin(\theta) & -\cos(\theta) \end{pmatrix}. \tag{5.1}$$

After the first step, $W_\theta = S(B_{0,\theta,0} \otimes \mathbb{1})$, the state takes the form

$$\begin{aligned} |\Psi_1\rangle &= W_\theta |\Psi_j\rangle \\ &= \gamma\left(|0\rangle \otimes |\psi_{j-1}\rangle\right) + \delta\left(|1\rangle \otimes |\psi_{j+1}\rangle\right) \end{aligned} \tag{5.2}$$

where $\gamma = \left(\frac{\cos(\theta)+i\sin(\theta)}{\sqrt{2}}\right)$ and $\delta = \left(\frac{\sin(\theta)-i\cos(\theta)}{\sqrt{2}}\right)$. Schmidt rank of $|\Psi_1\rangle$ is 2 which implies entanglement in the system. The value of entanglement can be further quantified with increase in number of steps by computing the Von Neumann entropy of the reduced density matrix of the position subspace. Position-particle entanglement in quantum walk on regular graph has been studied in detail in [156].

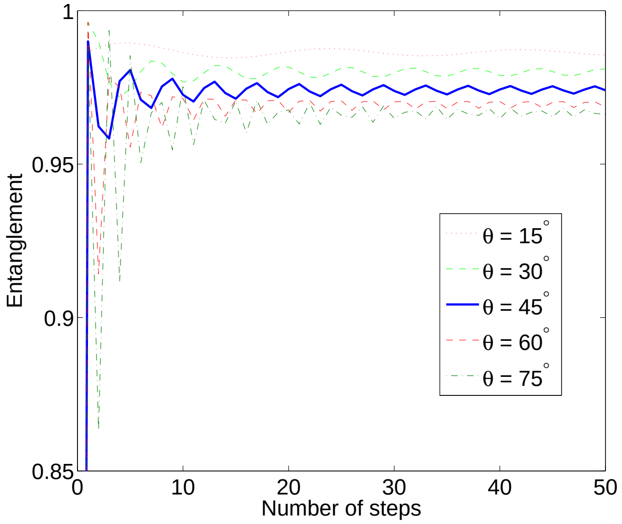

FIGURE 5.2: Entanglement of single particle with position space when subjected to quantum walk. The initial state of the particle is given by form (2.11) with $\delta = 40°$ and $\eta = 30°$ and is evolved in position space using different values for θ in the quantum coin operation $B_{0,\theta,0}$. The entanglement initially oscillates and approaches asymptotic value with increase in number of steps. For smaller values of θ the entanglement is higher and decreases with increase in θ. Initial oscillation is also larger for higher θ.

Figure 5.1 is the plot of the entanglement against the number of steps of the quantum walk on particle initially in symmetric superposition state using different values for θ in the operation W_θ. Von Neumann entropy of the reduced density matrix of the coin is used to quantify the entanglement between the coin and the particle position,

$$E_c(t) = -\sum_j \lambda_j \log_2(\lambda_\mathrm{j}) \tag{5.3}$$

where λ_j are the eigenvalues of the reduced density matrix of the coin after t steps (time). The entanglement initially oscillates and reaches an asymptotic value with increasing number of steps. In the asymptotic limit, entanglement value decreases with increase in θ and this dependence can be attributed to spread of the amplitude distribution in position space. That is, with increase in θ, constructive interference of quantum amplitudes towards the origin gets prominent narrowing the distribution in the position space. In Figure 5.2, the process is repeated for a particle initially in a non symmetric superposition state $|\Psi_{in}\rangle = [\cos(40°)|0\rangle +$

$e^{i30^{\circ}}\sin(40^{\circ})|1\rangle]\otimes|\psi_0\rangle$.

5.2.2 Spatial Entanglement

Spatial entanglement is the entanglement between the lattice points. This entanglement takes the form of non-local particle number correlations between spatial modes. To observe spatial entanglement we need to first associate the lattice with state of the particle.

5.2.2.1 Using single particle quantum walk

In a single particle quantum walk, each lattice point is associated with a Hilbert space spanned by two subspaces. The first is the zero-particle subspace which does not involve any coin (particle) states. The other is the one-particle subspace spanned by the two possible states of the coin, $|0\rangle$ and $|1\rangle$. To get the spatial entanglement we will write the state of the particle in the form of the state of the lattice. Following from (5.2) the state of the particles after first two steps of quantum walk takes the form :

$$\begin{aligned} |\Psi_2\rangle &= W_\theta|\Psi_1\rangle \\ &= \gamma\left[\cos(\theta)|0\rangle|\psi_{j-2}\rangle+\sin(\theta)|1\rangle|\psi_j\rangle\right] \\ &\quad +\delta\left[\sin(\theta)|0\rangle|\psi_j\rangle-\cos(\theta)|1\rangle|\psi_{j+2}\rangle\right]. \end{aligned} \tag{5.4}$$

In order to get the state of the lattice we can redefine the position state in the following way: the occupied position state $|\psi_j\rangle$ as $|1_j\rangle$, which means that the j-th position is occupied and rest of the lattice is empty. Therefore, we can rewrite (5.4) as,

$$\begin{aligned} |\Psi_2\rangle &= \gamma\left[\cos(\theta)|0\rangle|1_{j-2}\rangle+\sin(\theta)|1\rangle|1_j\rangle\right] \\ &\quad +\delta\left[\sin(\theta)|0\rangle|1_j\rangle-\cos(\theta)|1\rangle|1_{j+2}\rangle\right]. \end{aligned} \tag{5.5}$$

When $j-$th position is unoccupied (empty) the lattice state is written as $|0_j\rangle$. Since we are interested in the spatial entanglement we project this state into one of the coin state so that we can ignore the entanglement between the coin and the position state and consider only the lattice states. Here we will choose the coin state to be $|0\rangle$ and take the projection to obtain the state of the lattice in the form :

$$|\Psi_{lat}\rangle = |0\rangle \left(\gamma \cos(\theta)|1_{j-2}\rangle + \delta \sin(\theta)|1_j\rangle\right). \tag{5.6}$$

Each lattice site j can be considered as a Hilbert space with the basis state $|1_j\rangle$ (occupied state) and $|0_j\rangle$ (unoccupied state). Then, the above expression (5.6) in the extended Hilbert space of each lattice can be rewritten in terms of occupied and unoccupied lattice states as

$$|\Psi'_{lat}\rangle = \gamma \cos(\theta)|1_{j-2}\, 0_j\rangle + \delta \sin(\theta)|0_{j-2}\, 1_j\rangle. \tag{5.7}$$

We can see that after first two steps of quantum walk the lattice states $|1_j\rangle$ and $|1_{j-2}\rangle$ are entangled. One can check that the lattice states $|1_j\rangle$ and $|1_{j+2}\rangle$ are entangled if we choose the coin state to be $|1\rangle$. With increase in number of steps the state of the particle spread in position space and the projection over one of the coin state reduces the state considered to measure spatial entanglement. Therefore, with increase in number of steps the spatial entanglement from single particle quantum walk decreases.

5.2.2.2 Using many particle quantum walk

We will extend the study of the evolution of spatial entanglement as the quantum walk progresses on a many particle system.

To define a many particle quantum walk we will consider a one dimensional lattice with one particle at each position as initial state, Figure 5.3. M independent identical particles in M lattice with each particle having its own coin and position Hilbert space will have a total Hilbert space $\mathcal{H} = (\mathcal{H}_c \otimes \mathcal{H}_p)^{\otimes M}$. We consider the particles to be distinguishable for the time being.

The evolution of each particle is independent as they are not interacting, and hence the evolution operator is simply $W_\theta^{\otimes M}$. The initial state that we will consider for

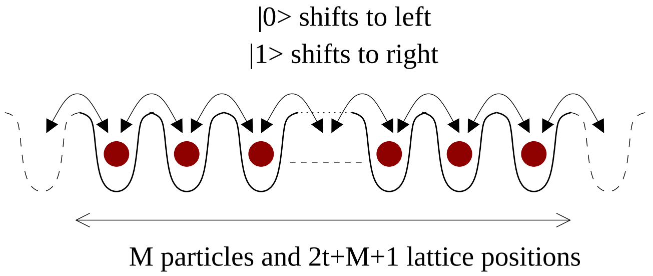

FIGURE 5.3: Many particle state with one non-interacting particle at each position space.

many particle system in one dimension will be

$$|\Psi_0^M\rangle = \bigotimes_{j=-\frac{M-1}{2}}^{j=\frac{M-1}{2}} \left(\frac{|0\rangle + i|1\rangle}{\sqrt{2}}\right) \otimes |\psi_j\rangle. \tag{5.8}$$

For an M particle system after t steps of quantum walk, the Hilbert space consists of the tensor products of single lattice position Hilbert space which are $(2t+M+1)$ in number. That is, after t steps of quantum walk, each of M particles spread between $(j-t)$ to $(j+t)$. In principle, each lattice point can be empty without any particle or can have a particle in state $|0\rangle$ or $|1\rangle$. That is, at each lattice point, each of M distinguishable particles are spanned by the state $|0\rangle$, $|1\rangle$ and no particle state. Therefore, after redefining the particle-position Hilbert space in the form of state of the lattice, the dimension of each lattice point will be 3^M and the dimension of total Hilbert space is $(3^M)^{\otimes M}$.

Let us first consider the analysis of the first two steps of Hadamard walk ($\theta = \pi/4$ in (5.1)) on a three particle system with initial state

$$|\Psi_0^{3p}\rangle = \bigotimes_{j=-1}^{+1} \left(\frac{|0\rangle + i|1\rangle}{\sqrt{2}}\right) \otimes |\psi_j\rangle. \tag{5.9}$$

We will label the three particles at positions -1, 0 and 1 as A, B and C. Since the evolution of these particles are independent, we write down the state after the first step as a tensor product of each of the three particle,

$$\begin{aligned}|\Psi_1^{3p}\rangle = W_\theta^{\otimes 3}|\Psi_0^{3p}\rangle &= [\gamma|0\rangle|-2\rangle + \delta|1\rangle|0\rangle]_{\mathrm{A}} \\ &= [\gamma|0\rangle|-1\rangle + \delta|1\rangle|+1\rangle]_{\mathrm{B}} \\ &= [\gamma|0\rangle|0\rangle + \delta|1\rangle|+2\rangle]_{\mathrm{C}} \end{aligned} \tag{5.10}$$

where $\gamma = (1+i)/2$ and $\delta = (1-i)/2$. After two step the tensor product of each of the three particle is given by

$$\begin{aligned}|\Psi_2^{3p}\rangle = &\left[\gamma\left(\frac{|0\rangle|-3\rangle + |1\rangle|-1\rangle}{\sqrt{2}}\right) + \delta\left(\frac{|0\rangle|-1\rangle - |1\rangle|+1\rangle}{\sqrt{2}}\right)\right]_{\mathrm{A}} \\ \otimes &\left[\gamma\left(\frac{|0\rangle|-2\rangle + |1\rangle|0\rangle}{\sqrt{2}}\right) + \delta\left(\frac{|0\rangle|0\rangle - |1\rangle|+2\rangle}{\sqrt{2}}\right)\right]_{\mathrm{B}} \\ \otimes &\left[\gamma\left(\frac{|0\rangle|-1\rangle + |1\rangle|+1\rangle}{\sqrt{2}}\right) + \delta\left(\frac{|0\rangle|+1\rangle - |1\rangle|+3\rangle}{\sqrt{2}}\right)\right]_{\mathrm{C}}\end{aligned} \tag{5.11}$$

By projecting this state onto a 1-D coin state we can get the state of the lattice to calculate spatial entanglement. We choose this state to be $|0\rangle \otimes |0\rangle \otimes \ldots |0\rangle$. Then the state of the lattice after projection and normalization is

$$\begin{aligned}|\Psi_{lat}\rangle =&\gamma^3\,|\mathrm{A}\rangle_{-3}|\mathrm{B}\rangle_{-2}|\mathrm{C}\rangle_{-1} \\ &+ \gamma^2\delta\,(\,|\mathrm{A}\rangle_{-3}|\mathrm{B}\rangle_{-2}|\mathrm{C}\rangle_{1} + |\mathrm{A}\rangle_{-3}|\mathrm{B}\rangle_{0}|\mathrm{C}\rangle_{-1} + |\mathrm{AC}\rangle_{-1}|\mathrm{B}\rangle_{-2}) \\ &+ \gamma\delta^2\,(\,|\mathrm{A}\rangle_{-3}|\mathrm{B}\rangle_{0}|\mathrm{C}\rangle_{1} + |\mathrm{AC}\rangle_{-1}|\mathrm{B}\rangle_{0} + |\mathrm{A}\rangle_{-1}|\mathrm{B}\rangle_{-2}|\mathrm{C}\rangle_{1}) \\ &+ \delta^3\,|\mathrm{A}\rangle_{-1}|\mathrm{B}\rangle_{0}|\mathrm{C}\rangle_{1}.\end{aligned} \tag{5.12}$$

From the above expression the spatial entanglement due to quantum walk on a three particle system can be calculated. But with increase in the number of particles and number of steps of quantum walk, the measure of entanglement gets complicated. For which a scalable entanglement measure scheme we discuss in next section would be useful.

5.3 Calculating spatial entanglement in a multipartite system

In a system with two particles, the state is separable if we can write it as a tensor product of the individual particle states, and entangled if not. However, it is somewhat more involved to define entanglement for a system with more than two particles. In general a state is said to be *partially* entangled if it can be written as

$$|\psi\rangle = |\phi_1\rangle \otimes |\phi_2\rangle \otimes \cdots |\phi_k\rangle \tag{5.13}$$

where $k < M$. In case $k = M$ the state is said to be fully separable and $|\phi_i\rangle$ will then denote the state of the $i-$th particle. If on the other hand $k = 1$ then the state will be fully entangled.

There are quite a few good entanglement measures for the multipartite state [89, 157–162]. We will be using the Meyer-Wallach (M-W) entanglement measure in the lattice as it does not diverge with increasing system size and it is easy to calculate [89]. The M-W measure is the entanglement of a single particle to the rest of the system, averaged over the whole of the system. For pure states, linear entropy can serve as a good measure for the entanglement of a single particle with the rest of the system. It is given by

$$E = \frac{d}{d-1}\left[1 - \mathrm{Tr}\rho^2\right] \tag{5.14}$$

for a d-dimensional particle Hilbert space. The M-W measure follows :

$$E = \frac{d}{d-1}\left[1 - \frac{1}{L}\sum_{i=1}^{L}\mathrm{Tr}\rho_i^2\right] \tag{5.15}$$

where L is the system size. In a multipartite quantum walk the dimension of each lattice point, after projection over and one of the coin (particle) state, is 2^M where M is the number of particles. So the expression for entanglement will be

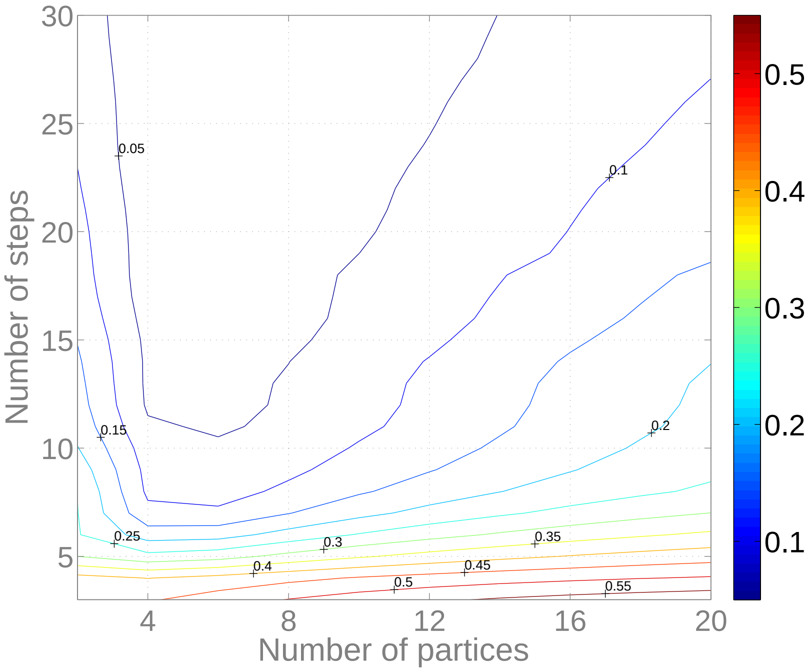

FIGURE 5.4: Evolution of spatial entanglement with increase in the number of steps of the quantum walk for different number of particles in an open one dimensional lattice chain. The entanglement first increases and with the further increase in the the number of steps, the number of lattice positions exceeds the number of particles in the system resulting in the decrease of the spatial entanglement. The distribution is obtained by implementing quantum walk on particles in the initial state $\frac{1}{\sqrt{2}}(|0\rangle + i|1\rangle)$ and Hadamard operation $B_{0,\pi/4,0}$ as quantum coin operation.

$$E(|\Psi_{lat}\rangle) = \frac{2^M}{2^M - 1}\left(1 - \frac{1}{2t + M + 1}\sum_{j=-(t+\frac{M}{2})}^{t+\frac{M}{2}} \mathrm{tr}\rho_j^2\right) \tag{5.16}$$

where t is the number of steps and ρ_j is the reduced density matrix of j^{th} lattice point. ρ_j can be written as

$$\rho_j = \sum p_k^j |k\rangle\langle k| \tag{5.17}$$

where $|k\rangle$ is one of the 2^M possible states available for a lattice point and p_k^j can be calculated once we have the probability distribution of individual particle on

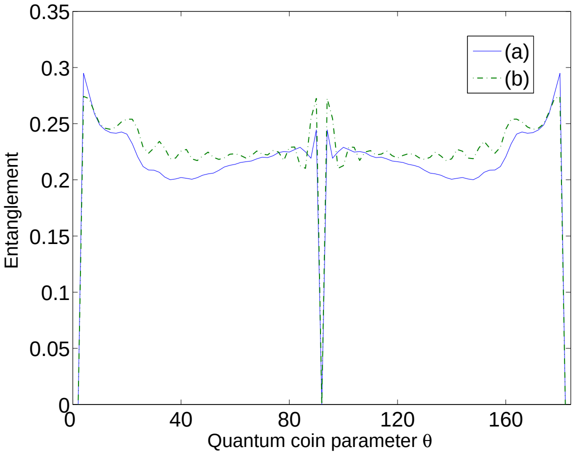

FIGURE 5.5: Value of spatial entanglement for 20 particles on a one dimensional lattice after 20 steps of quantum walk using different values of θ in the quantum coin operation $B_{0,\theta,0}$. (a) and (b) are the distributions for particles initially in state $\frac{1}{\sqrt{2}}(|0\rangle + i|1\rangle)$ and state $|0\rangle$ ($|1\rangle$) respectively. In (a), with increase in θ from 0 to $\pi/2$ the spread of the distribution in lattice position decreases first up to $\theta = \pi/4$ and again increase. Due to asymmetric distributions for particles in case of (b) the above effect is not very prominent. For both (a) and (b) when $\theta = \pi/2$, for every even number of steps of quantum walk, the system returns to the initial state where entanglement is 0. Entanglement is 0 for $\theta = 0$.

that lattice.

Since we have M distinguishable particles, we have 2^M configuration depending upon whether a given particle is present in the lattice point or not after freezing the state of the particle. That forms the basis for a single lattice point Hilbert space. Now we can calculate p_k^j, the probability of one of the possible $|k\rangle$ state of particle in the $j-$th lattice point as: let us say $a_j^{(l_i)}$ is the probability of $i-$th particle to be or not to be in the in the $j-$th lattice point depending on l_i. If l_i is 1 then it gives us the probability of the particle to be in the lattice point. If l_i is -1 then $a_j^{(l_i)}$ is the probability of the particle not to be in the lattice point so $a_j^{(-1)} = 1 - a_j^{(1)}$. And hence we can write

$$p_k^j = \prod_k a_j^{l_k}. \tag{5.18}$$

Thus the spatial entanglement can be conveniently calculated once we have the probability distribution of individual particle on that lattice. Since quantum walk is a controlled evolution, one can obtain a probability distribution of each particle over the entire lattice positions. In fact one can easily control the probability distribution by varying the quantum coin parameters during the quantum walk process and hence the entanglement.

Figure 5.4 is the phase diagram of the spatial entanglement using the many particle quantum walk. This figure gives us the information about the entanglement in the space for different number of particles with increasing number of steps of the quantum walk.

Here we have chosen Hadamard operation $B_{0,\pi/4,0}$ and $\frac{1}{\sqrt{2}}(|0\rangle + i|1\rangle)$ as quantum coin operation and initial state of the particles respectively for the walk evolution. To see the variation of entanglement for a fixed number of particles with increase in steps, we can pick a line parallel to y axis i.e, for fixed number of particles and see the entanglement varying with number of steps.

We see that the entanglement for an instance, after first iteration goes to maximum from zero and with the further increase in the number of steps, the number of lattice positions exceeds the number of particles in the system resulting in the decrease of the spatial entanglement. The decrease in entanglement before the number of steps is equal to number of particles should be noted. This is because, for Hadamard walk the spread of the probability distribution after t steps is between $\frac{-t}{\sqrt{2}}$ and $\frac{t}{\sqrt{2}}$ and not between $-t$ and t [64]. To see the variation of entanglement with parameter θ more clearly, in Figure 5.5 the spatial entanglement for 20 particles after 20 steps of quantum walk using different values of θ in the quantum coin operation $B_{0,\theta,0}$ is presented. Variation of entanglement with θ for two case, all particles in equal superposition state $\frac{1}{\sqrt{2}}(|0\rangle + i|1\rangle)$ (unbiased quantum walk) and in one of the basis state $|0\rangle$ or $|1\rangle$ (biased quantum walk) as initial state is presented. The effect of biasing the quantum walk by different magnitude can also be reproduced using the other two parameters ξ, ζ in the coin operation $B_{\xi,\theta,\zeta}$.

In Figure 2.3 we can seen that for a single particle quantum walk, with increase in θ from 0 to $\pi/4$ in the coin operation, along with decrease in the spread, the maximum point (two peaks) in the probability distribution in the position space also decrease. Whereas, with increase in θ from $\pi/4$ to $\pi/2$, the maximum point

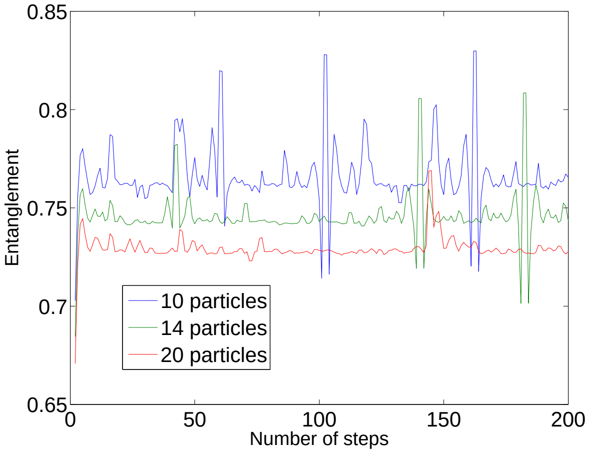

Figure 5.6: Evolution of spatial entanglement for a system with different number of particles in a closed chain. With increase in the number of steps, the entanglement value remains close to asymptotic value with some peaks in between. The peaks can be accounted for the cross over of the left and right propagating amplitudes of the internal state of the particle during quantum walk. The peaks are more for chain with smaller number of particles. Increase in the number of particles in the system results in the decrease in the entanglement value. The distribution is obtained by using $\frac{1}{\sqrt{2}}(|0\rangle + i|1\rangle)$ as the initial states of all the particles and Hadamard operation $B_{0,45^\circ,0}$ as quantum coin operation.

in the probability distribution in position space increases along with decrease in the spread. That is, we can see that the minima of the maximum point in the probability distribution is for $\theta = \pi/4$. Therefore, this attributes for the minimal in the spatial entanglement at $\theta = \pi/4$ in Figure 5.5. Note that we have ignored the extreme values of $\theta = 0$ and $\pi/2$ which evolves without any quantum interference effect.

For fixed number of steps of quantum walk, the spatial entanglement first decreases and then it starts reviving as we increase the number of particles.

Closed chain :

Since most of the physical system that will be considered for implementation will be of definite dimension we extend our calculations to one of the simple example of closed geometry, $n-$ cycle.

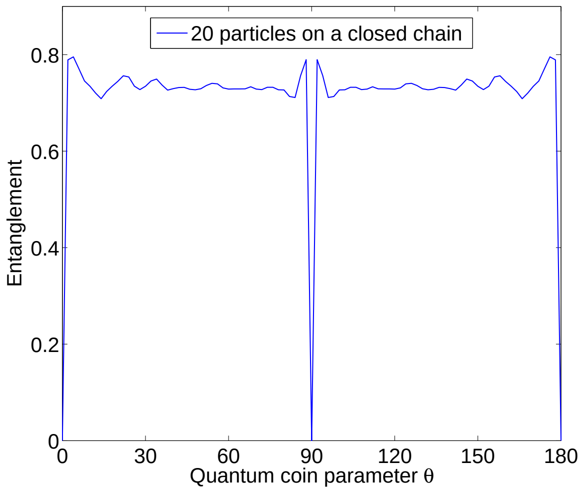

FIGURE 5.7: Value of spatial entanglement for 20 particles on a closed chain after 20 steps of quantum walk using different values of θ in the quantum coin operation $B_{0,\theta,0}$. (a) and (b) are the distributions for particles initially in state $\frac{1}{\sqrt{2}}(|0\rangle + i|1\rangle)$ and state $|0\rangle$ ($|1\rangle$) respectively. Since the system is in the closed chain, the quantum walk does not expand the position Hilbert space therefore for all values of θ from 0° to $\pi/2$ the entanglement value remains close to the asymptotic value except for a small peak at smaller values of θ. For $\theta = 0°$ when number of steps equal to number of particles, the amplitudes goes round the chain and returns to its initial state making the entanglement 0 and for $\theta = \pi/2$, for every even number of steps of quantum walk, the system returns to the initial state where entanglement is again 0.

When we consider a many particle system in a closed chain, with number of lattice position equal to number of particles M, the quantum walk process does not expand the position Hilbert space like it does on an open chain. Therefore the spatial entanglement does not decrease, remains close to the asymptotic value with increase in the number of steps of quantum walk. Figure 5.6 shows the evolution of entanglement for a system with different number of particles in a closed chain. The peaks seen in the plot can be accounted for the cross over of the left and right propagating amplitudes of the internal state of the particle during the quantum walk process. Therefore the frequency of the peaks are more for smaller number of particles (smaller closed chain). In general, one can also notice that the increase in the number of particles and number of lattice point in the closed cycle results in the decrease in the spatial entanglement of the system.

In Figure 5.7, the value of spatial entanglement for 20 particles on a closed chain after 20 steps of quantum walk using different values of θ in the quantum coin operation $B_{0,\theta,0}$ is presented. For all values of θ from 0 to $\pi/2$ the entanglement value remains close to the asymptotic value except for the extreme values of θ. For $\theta = 0$ when number of steps equal to number of particles the amplitudes goes round the ring and returns to its initial state making the spatial entanglement value = 0. For $\theta = \pi/2$, for every even number of steps of quantum walk, the system returns to the initial state where the spatial entanglement is again 0.

Therefore, spatial entanglement on a large lattice space can be created, controlled and optimized for maximum entanglement value by varying the quantum coin parameters and number of particles in the multi particle quantum walk. In [152] a scheme to implement a scalable quantum information processing using ultra cold molecules is proposed. Two different species of atoms held in independent optical lattices are entangled by translating the separate lattices to overlap. Implementing quantum walk on one of the species and creating spatial entanglement can possibly make the above scheme more robust.

5.4 Summary

- We have presented the evolution of spatial entanglement in many particle system subjected to the quantum walk process. By considering many particles in the one dimensional open and closed chain we have shown that the spatial entanglement of the system can be controlled by controlling the dynamics of the quantum walk, the quantum coin parameter, initial state and number of steps. Developing on this approach, many particle entanglement can be generated and controlled in a many body system using quantum walk as a tool.

Part IV

Conclusion

Chapter 6

Conclusion and future perspective

6.1 Conclusion

In this thesis we briefly reviewed the continuous- and discrete-time quantum walk which are structurally identical to Schrödinger and Dirac equations, respectively. By simple decoupling analysis of the evolution, structural similarity of the discrete-time quantum walk and the Dirac equation was shown. To optimize the discrete-time quantum walk, the use of three parameter quantum coin operation $B_{\xi,\theta,\zeta}$ from SU(2) group. Numerical data with supporting mathematical analysis, it was shown that parameter θ can be used to control the variance and parameters ξ and ζ to bias and control the biasing in the walk. The use of quantum coin $B_{\xi,\theta,\zeta}$ for walk on an $n-$cycle and its effect on optimizing mixing time was shown.

Recurrence is an important phenomenon in the study of dynamics. Recurrence we considered was the return of unit probability amplitude at the origin during the dynamics. Based on the numerical data and analysis we have shown that the quantum walk evolution dominated by the interference of quantum amplitudes fails to satisfy complete recurrence theorem. However, fractional recurrence characterized by the quantum Pólya number can be seen.

Symmetries and effect of noise on quantum walk on a line and $n-$cycle was studied. We considered the noise on the coin space in our study. Variants of quantum walks on a line was considered and showed that they are equivalent in the sense that the final positional probability distribution remains the same in each variant (symmetry in the probability distribution). In particular, we considered variants obtained by the experimentally relevant operations of Z or X applied at each quantum walk step, with the symmetry operations given by **Z** and **PRX**. Interestingly we observed that these symmetries were preserved even in the presence of noise, in particular, those characterized by the phase flip, bit flip and generalized amplitude damping channels. This is important because it means that the equivalence of these variants is not affected by the presence of noise, which would be inevitable in actual experiments. However, the symmetry of the phase operation under phase noise was intuitive, considering that this noise has a Kraus representation consisting of operations that are symmetries of the noiseless quantum walk. But, for the PRX symmetry under phase noise, and for any symmetry under other noisy channels (especially in the case of generalized amplitude damping channel), the connection was not obvious before the analysis was completed. When the studies were extended to the walk on an $n-$cycle, an interesting fact that we observed was the breakdown of the symmetries found in the walk on a line. Further, when the noise was introduced, above a certain noise level these symmetries were restored. Results to study noise model were supported by several numerical examples obtained by evolving the density operator in the Kraus representation and analytical proofs of the effect of noise on symmetries were obtained using the quantum trajectories approach, which we found convenient for this situation.

In this thesis two of the applications of quantum walk was considered. Use of quantum walk to redistribute atoms in optical lattice and evolution of spatial entanglement in many body system. We proposed the use of the quantum walk to redistribute atoms, and studied its dynamics in an optical lattice and to expedite the process of quantum phase transition. The coherent control over the atoms using the coin degree of freedom during the evolution of the walk was demonstrated. Experimentally realizable noisy channels studied in the dynamics part of this thesis was used to show the additional control over the evolution and atomic density redistribution. Making use of the stimulated Raman transition, we have proposed stimulated Raman kicks to act as shift operator along with rf-pulse as coin operation to implement discrete-time quantum walk on Bose-Einstein condensate (BEC). Our scheme can retain the macroscopic features of the wave packet or can be accordingly modified to implement the walk at an individual atom level which will be effective for transition from superfluid to the Mott insulator state and vice versa.

Entanglement is many body system is one of the important topic of interest. As a step towards using quantum walk to generate and control entanglement in many body system, both distinguishable and indistinguishable, we have presented the evolution of spatial entanglement in many distinguishable particle system. We considered Meyer-Wallach measure for our study. By considering many particles in one dimensional open and closed chain we have shown that the spatial entanglement of the system can be controlled by controlling the dynamics of the quantum walk, the quantum coin parameter, initial state and number of steps.

6.2 Future perspective

In this thesis we considered quantum walk on a line and on an $n-$cycle. Extension of these studies presented to general graph and higher dimension could reveal other interesting features of the quantum walk dynamics. For example, structural similarity of discrete-time quantum walk with Dirac equation was presented. Discrete-time quantum walk in higher dimension and its analysis following the decoupling approach used to walk on a line could reveal interesting structural similarity.

Derivation of dependency of variance on the parameter θ for a walk on a line $(1 - \sin(\theta))t^2$ from first principles (Fourier analysis) which has not be done in this thesis would be a step in a direction of deriving the dependency of variance in two- and higher dimensions.

The results from symmetries and effects of noise on quantum walk can be extended and generalized to walk on most of the symmetric closed graphs. This symmetry-topology-noise interplay presented would be of relevance to quantum information processing systems, and have wider implications to the condensed matter systems.

Theoretically, the evolution of the density profile with a quantum walk can be used in place of quantum Monte Carlo simulation [1, 3] or the time evolution density matrix renormalization group (t-DMRG) to study the correlation and redistribution of atoms in optical lattices [2]. We expect the quantum walk to play a wider role in simulating and expediting the dynamics in various physical systems. Similarly, entanglement in many body system using quantum walk could be an interesting topic to explore quantum phase transition and quantum annealing problems in various physical systems. Presently, the spatial entanglement studied in this thesis seems to have very little practical interest. Developing on this, further studies can be considered to extend the evolution of spatial entanglement using indistinguishable particle quantum walk. However, many particle-position entanglement using quantum walk will be an interesting and bigger problem to explore and use it to study phase transitions in quantum systems.

In general quantum walk seems to serve as a tool to understand dynamics in various quantum systems which can further motivate to be used for various applications in quantum systems.

Appendix A

Quantum walk and Dirac equation : derivation

Getting Equation (2.22) from Equation (2.21) From first equation in (2.21), solving for Ψ_L we get

$$\Psi_L(j-1,\tau) = \frac{i}{\sin(\theta)}\left[\Psi_R(j,\tau+1) - \cos(\theta)\Psi_R(j-1,\tau)\right].$$

Therefore

$$\Psi_L(j+1,\tau) = \frac{i}{\sin(\theta)}\left[\Psi_R(j+2,\tau+1) - \cos(\theta)\Psi_R(j+1,\tau)\right].$$

By substituting the above for $\Psi_L(j+1,\tau)$ in the second equation in (2.21), we get (2.22).

Getting Equation (2.23) from Equation (2.22)

The difference ∇_τ operator that corresponds to the differential operator $\partial/\partial\tau$ is

$$\nabla_\tau = \frac{\Psi(j,\tau+0.5) - \Psi(j,\tau-0.5)}{\tau}.$$

Therefore, the operator $\partial^2/\partial\tau^2$ will correspond to applying the difference operator in each of the above two terms, which yields

$$\nabla_\tau^2 = \frac{1}{\tau}\times\frac{[\Psi(j,\tau+1)-\Psi(j,\tau)]-[\Psi(j,\tau)-\Psi(j,\tau-1)]}{\tau} = \frac{(\Psi(j,\tau+1)-2\psi(j,\tau)+\Psi(j,\tau-1)}{\tau^2}$$

where time step τ can be treated as constant. The difference operators ∇_j and ∇_j^2 are also defined analogously for j keeping τ constant.

Appendix B

Variation of the variance as a function of θ

For a quantum walk using $B_{0,\theta,0}$ as quantum coin, after t steps the probability distribution is spread over the interval $(-t\cos(\theta), t\cos(\theta))$ and shrink quickly outside this region. The height of the distribution with θ is proportional to $\sin(\theta)$. Therefore the integral of the probability distribution with in the interval can be approximated to,

$$\int_{-t\cos(\theta)}^{t\cos(\theta)} P(j)dj \approx 1 \tag{B.1}$$

By approximating the probability distribution to fit the envelop of the quantum walk distribution,

$$\int_{-t\cos(\theta)}^{t\cos(\theta)} \frac{[1+\cos^2(2\theta)]}{\sqrt{t}} \exp\left[K(\theta)\left(\frac{j^2}{t^2\cos^2(\theta)} - 1\right)\right] dj \approx 1, \tag{B.2}$$

where $K(\theta) = \frac{\sqrt{t}}{2}\cos(\theta)[1+\cos^2(2\theta)][1+\sin(\theta)]$.

The position j in the interval $(-t\cos(\theta), t\cos(\theta))$ in position space can be represented as a function of ϕ,

$$j \approx f(\phi) = t\cos(\theta)\sin(\phi) \tag{B.3}$$

where ϕ range from $-\frac{\pi}{2}$ to $\frac{\pi}{2}$. For a walk with coin $B_{0,\theta,0}$, the mean of the distribution is zero and hence the variance can be analytically obtained by extrapolating,

$$\sigma^2 = \int P(j)j^2 dj \approx \int_{-t\cos(\theta)}^{t\cos(\theta)} P(j)j^2 dj = \int_{-\frac{\pi}{2}}^{\frac{\pi}{2}} P(f(\phi))(f(\phi))^2 f'(\phi) d\phi. \qquad \text{(B.4)}$$

$$\sigma^2 \approx \int_{-\frac{\pi}{2}}^{\frac{\pi}{2}} \frac{[1+\cos^2(2\theta)]}{\sqrt{t}} e^{K(\theta)\left(\frac{t^2\cos^2(\theta)\sin^2(\phi)}{t^2\cos^2(\theta)}-1\right)} \left(t\cos(\theta)\sin(\phi)\right)^2 \times \left(t\cos(\theta)\cos(\phi)\right) d\phi \qquad \text{(B.5)}$$

$$\sigma^2 \approx t^{\frac{5}{2}}[1+\cos^2(2\theta)]\cos^3(\theta) \int_{-\frac{\pi}{2}}^{\frac{\pi}{2}} e^{K(\theta)(\sin^2(\phi)-1)} \ \sin^2(\phi)\cos(\phi) \ d\phi. \qquad \text{(B.6)}$$

$$\begin{aligned} \sigma^2 &\approx t^{\frac{5}{2}}[1+\cos^2(2\theta)]\cos^3(\theta) \int_{-1}^{1} e^{K(\theta)(r^2-1)} \ r^2 \ dr \\ &= t^{\frac{5}{2}}\sin(\theta)\cos^3(\theta) \int_{-1}^{1} r \ e^{K(\theta)(r^2-1)} \ r \ dr \\ &= t^{\frac{5}{2}}[1+\cos^2(2\theta)]\cos^3(\theta)\frac{1}{e^{K(\theta)}} \left[\frac{re^{K(\theta)\ r^2}}{2K(\theta)}\Bigg|_{-1}^{1} - \int_{-1}^{1} \frac{e^{K(\theta)r^2}}{2K(\theta)} \ dr \right] \\ &= t^{\frac{5}{2}}[1+\cos^2(2\theta)]\cos^3(\theta)\frac{1}{e^{K(\theta)}2K(\theta)} \left[2e^{K(\theta)} - \int_{-1}^{1} e^{K(\theta)r^2} \ dr \right]. \qquad \text{(B.7)} \end{aligned}$$

The integration of $\int_{-1}^{1} e^{K(\theta)r^2} dr$ can be done using Taylor expansion,

$$\begin{aligned} I &= \int_{-1}^{1} e^{K(\theta)r^2} dr \\ &= \int_{-1}^{1} \left[1 + K(\theta)r^2 + \frac{K(\theta)^2 r^4}{2!} + \frac{K(\theta)^3 r^6}{3!} + \frac{K(\theta)^4 r^8}{4!} + ... + \frac{K(\theta)^n r^{2n}}{n!} \right] dr \\ &= 2\left[1 + \frac{K(\theta)}{3} + \frac{K(\theta)^2}{5*2!} + \frac{K(\theta)^3}{7*3!} + \frac{K(\theta)^4}{9*4!} + ... + \frac{K(\theta)^n}{(2n+1)*n!} \right] \qquad \text{(B.8)} \end{aligned}$$

$$I = 2\left[\sum_{0}^{n} \frac{K(\theta)^n}{(2n+1)*n!}\right] = \sum_{0}^{n}\left[\frac{2K(\theta)^n}{n!} - \frac{4\ n\ K(\theta)^n}{(2n+1)n!}\right]. \tag{B.9}$$

For large n, $\frac{4n}{2n+1} \approx 2$ in the above expression. When n is small $I \approx e^{K(\theta)}$. Substituting in (B.7), the variance is simplified to,

$$\begin{aligned}\sigma^2 \approx \frac{t^{\frac{5}{2}}[1+\cos^2(2\theta)]\cos^3(\theta)}{2K(\theta)} &= \frac{t^{\frac{5}{2}}[1+\cos^2(2\theta)]\cos^3(\theta)}{\sqrt{t}\cos(\theta)[1+\cos^2(2\theta)][1+\sin(\theta)]} \\ &= \frac{t^2(1-\sin(\theta))(1+\sin(\theta))}{1+\sin(\theta)} = (1-\sin(\theta))t^2. \end{aligned} \tag{B.10}$$

From the solution obtained empirically through numerical integration we find that the variation of B_θ with θ also fits $(1-\sin(\theta))$. That is,

$$\sigma^2 = C_\theta t^2 \approx (1-\sin(\theta))t^2. \tag{B.11}$$

Appendix C

Dipole trap for ^{87}Rb atoms using light of different wavelengths

Effective laser detuning Δ for alkalis can be calculated using,

$$\frac{1}{\Delta} = \left(\frac{1}{\Delta_1} + \frac{2}{\Delta_2}\right) \tag{C.1}$$

where Δ_i is detuning from D_i line.
Maximum potential depth is calculated using

$$U_0 = \frac{\hbar\Gamma}{2}\frac{P\Gamma}{\pi_0^2 I_0 \Delta}, \tag{C.2}$$

where Γ is natural linewidth, P is laser power, and I_0 is the saturation intensity given by,

$$I_0 = \frac{\pi^2 hc\Gamma}{3\lambda^3} = \frac{\pi}{3}\frac{hc}{\lambda^3\tau}, \tag{C.3}$$

where $\Gamma = 1/\tau$. The numerical value of saturation intensity I_0 for rubidium atoms is calculated to be 1.67 mW/cm^2=16.7 W/m^2.

C.1 Frequency-detuning and potential depth for different wavelength

Below is the table with numerical values of detuning and potential depth for dipole traps using laser lights of different wavelengths.

wavelength (nm)	Detuning Δ	Potential Depth U_0 W/m^2
1064	$-25 \times 10^5\Gamma$	$1.53 \times 10^{-35}\frac{P}{W_0^2}$
850	$-6.93 \times 10^5\Gamma$	$5.5 \times 10^{-35}\frac{P}{W_0^2}$
820	$-3.46 \times 10^5\Gamma$	$11.04 \times 10^{-35}\frac{P}{W_0^2}$
800	$-0.6 \times 10^5\Gamma$	$63.66 \times 10^{-35}\frac{P}{W_0^2}$

The ac stark shift creates a potential, U proportional to the light intensity

$$U(r,z) = U_0\left[\frac{e^{\frac{-2r^2}{W(z)^2}}}{1+(\frac{z}{z_R})^2}\right] \tag{C.4}$$

r and z being the radial and axial co-ordinates, $z_R = \frac{\pi W_0^2}{\lambda}$ is the Rayleigh range[1] at wavelength λ and beam waist W_0. $W(z)$ is the beam radius as a function of axial position z and is given by,

$$W(z) = W_0\sqrt{1+\left(\frac{z}{z_R}\right)^2}. \tag{C.5}$$

The overall potential due to effect of gravity is given by,

$$U_g(r,z) = -mgr - U_0\left[\frac{e^{\frac{-2r^2}{W(z)^2}}}{\left(1+\frac{z}{z_R}\right)^2}\right]. \tag{C.6}$$

---

[1] Distance at which the diameter of the spot size increases by a factor of $\sqrt{2}$.

To calculate the minimum power required to trap ^{87}Rb atoms at distance z from the focal point of the beam in the axial direction of the beam, the above equation is differentiated,

$$\frac{d^2U}{dr^2} = -mg + \frac{4U_0 r}{W(z)^2}\left[\frac{e^{\frac{-2r^2}{W(z)^2}}}{1+(\frac{z}{z_R})^2}\right] = 0 \tag{C.7}$$

$$\Longrightarrow r = \frac{mg}{4U_0}\frac{W(z)^2}{e^{\frac{-2r^2}{W(z)^2}}}\left[1+\left(\frac{z}{z_R}\right)^2\right]. \tag{C.8}$$

By substituting the appropriate values for the above equation one can calculate the minimum power required to trap atoms at distance z from the beam focus in the axial direction. Below is the table with the calculated power required to trap ^{87}Rb atoms using laser light with different wavelengths and beam waist.

For light with beam waist, $W_0 = 50\mu$m

$W_0 = 50\mu$m	1064 nm	850 nm	820 nm
z = 5 cm	3.33 W	450 mW	210 mW
z = 2 cm	30 mW	37 mW	26.5 mW
z =1 cm	16 mW	8.4 mW	4 mW
z = 0.5 cm	11.6 mW	3.8 mW	1.5 mW
z = 0 cm	9 mW	2.7 mW	1.4 mW

For $W_0 = 100\mu$m

$W_0 = 100\mu$m	1064 nm	850 nm	820 nm
z = 5cm	610 mW	110 mW	47 mW
z = 2cm	140 mW	31 mW	15 mW
z = 1cm	91 mW	23 mW	12 mW
z = 0.5cm	78 mW	22 mW	11 mW
z = 0cm	77 mW	22 mW	11 mW

For $W_0 = 200\mu$m

$W_0 = 200\mu$m	1064nm	850nm	820nm
$z = 5$cm	1.53 W	200 mW	1.1 W
$z = 2$cm	650 mW	180 mW	900 mW
$z = 1$cm	610 mW	180 mW	900 mW
$z = 0.5$cm	600 mW	180 mW	900 mW
$z = 0$cm	600 mW	180 mW	900 mW

The maximum photon scattering rate Γ_{sc} is given by

$$\Gamma_{sc} = \frac{\Gamma}{\Delta}\frac{U_0}{\hbar}. \tag{C.9}$$

For the laser light of 850nm the photon scattering rate at beam waist $3.8\mu m$ and power 0.12 mW will be,

$$\Gamma_{sc} = \frac{\Gamma}{6.93 \times 10^5 \Gamma}\frac{5.5 \times 10^{-35}}{1.054 \times 10^{-34}}\left(\frac{P}{W_0^2}\right) = 6.25 \times 10^6 \text{photons/sec.} \tag{C.10}$$

Bibliography

[1] Marcos Rigol and Alejandro Muramatsu. Quantum criticality in ultracold atoms on optical lattices. *Phys. Sat. Sol. (b)*, 9(242):1850–1856, 2005.

[2] K Rodriguez, S R Manmana, M Rigol, R M Noack, and A Muramatsu. Coherent matter waves emerging from Mott-insulators. *New J. Phys.*, 8: 169, 2006.

[3] P. Sengupta, M. Rigol, G. G. Batrouni, P. J. H. Denteneer, and R. T. Scalettar. Phase coherence, visibility, and the superfluid Mott-insulator transition on one-dimensional optical lattices. *Phys. Rev. Lett.*, 95:220402, 2005.

[4] R. P. Feynman. *Lectures on Physics III.* Addison Wesley Longman, 1970.

[5] R. Shankar. *Principles of Quantum Mechanics.* Springer, 2nd edition edition, 1994.

[6] Yuri Manin. *Computable and uncomputable.* Sovetskoye Radio (Moscow), 1980.

[7] Richard Feynman. Simulating physics with computers. *Int. J. Theor. Phys.*, 21:467, 1982.

[8] Michael Nielsen and Issac Chuang. *Quantum Computation and Quantum Information.* Cambridge University Press, 2000.

[9] Phillip Kaye, Raymond Laflamme, and Michele Mosca. *An Introduction to Quantum Computing.* Oxford University Press, USA, 2007.

[10] D. Deutsch. Quantum theory, the Church-Turing principle, and the universal quantum computer. *Proceeding of Royal Society of London, Series A*, 400: 97–117, 1985.

[11] D. Deutsch and R. Jozsa. Rapid solution of problems by quantum computation. *Proceeding of Royal Society of London, Mathematical and Physical Sciences*, 439(1907):553–558, 1992.

[12] D. Simon. On the power of quantum computation. *Proceedings of the 35th IEEE Symposium on the Foundations of Computer Science (FOCS)*, pages 116–123, 1994.

[13] D. Simon. On the power of quantum computation. *SIAM J. Computing*, 26: 1474–1483, 1997.

[14] P. Shor. Algorithms for quantum computation : discrete logarithms and factoring. *Proceedings of the 35th Annual Symposium on the Foundations of computer science, Edited by S. Goldwasser, (Los Alamitos, CA: IEEE Computer society Press)*, pages 124–134, 1994.

[15] P. Shor. Polynomial-time algorithms for prime factorization and discrete logarithms on a quantum computer. *SIAM J. Computing*, 26:1484 –1509, 1997.

[16] L. K. Grover. Quantum mechanics helps in searching for a needle in a haystack. *Phys. Rev. Lett.*, 79:325, 1997.

[17] Michele Mosca. Quantum algorithms. *Springer Encyclopedia of Complexity and Systems Science*, 2008.

[18] A. M. Childs and W. van Dam. Quantum algorithms for algebraic problems. *Rev. Mod. Phys. (To appear), arXiv : 0812.0380*, 2008.

[19] S. P. Meyn and R. L. Tweedie. *Markov Chains and Stochastic Stability*. Cambridge University Press, 1st edition edition, 2005.

[20] A. Ambainis, E. Bach, A. Nayak, A. Vishwanath, and J. Watrous. One-dimensional quantum walks. *Proceeding of the 33rd ACM Symposium on Theory of Computing*, (ACM Press, New York):60, 2001.

[21] A. Nayak and A. Vishwanath. Quantum walk on the line. *DIMACS Technical Report*, (No. 2000-43), 2001.

[22] M.N. Barber and B.W. Ninham. *Random and Restricted walks: Theory and Applications.* Gordon and Breach, New York, 1970.

[23] S. Chandrasekhar. Stochastic problems in physics and astronomy. *Phys. Mod. Phys.*, 15:1, 1943.

[24] Y. Aharonov, L. Davidovich, and N. Zagury. Quantum random walks. *Phys. Rev. A*, 48:1687, 1993.

[25] G. V. Riazanov. The Feynman path integral for the Dirac equation. *Sov. Phys. JETP*, 6:1107, 1958.

[26] R. P. Feynman and A.R. Hibbs. *Quantum Mechanics and Path Integrals.* McGraw-Hill, New York, 1965.

[27] David A. Meyer. From quantum cellular automata to quantum lattice gases. *J. Stat. Phys.*, 85:551, 1996.

[28] David A. Meyer. Quantum mechanics of lattice gas automata: one particle plane waves and potentials. *Phys. Rev. E*, 55:5261–5269, 1997.

[29] E. Farhi and S. Gutmann. Quantum computation and decision trees. *Phys. Rev. A*, 58:915, 1998.

[30] J. Watrous. Quantum simulations of classical random walks and undirected graph connectivity. *Journal of Computer and System Sciences*, 62:376–391, 2001.

[31] J. Kempe. Quantum random walk - an introductory overview. *Contemporary Physics*, 44:307, 2003.

[32] N. Shenvi, J. Kempe, and K. B. Whaley. Quantum random-walk search algorithm. *Phys. Rev. A*, 67:052307, 2003.

[33] A. M. Childs and J. Goldstone. Spatial search by quantum walk. *Phys. Rev. A*, 70:022314, 2004.

[34] A. M. Childs and J. Goldstone. Spatial search and the Dirac equation. *Phys. Rev. A*, 70:042312, 2004.

[35] A. Ambainis, J. Kempe, and A. Rivosh. Coins make quantum walks faster. *Proceedings of ACM-SIAM Symposium on Discrete Algorithms (SODA)*, (AMC Press, New York):1099–1108, 2005.

[36] S. Aaronson and A. Ambainis. Quantum search of spatial regions. *Theory of Computing (Also FOCS'03)*, 1:47–79, 2005.

[37] F. Magniez, A. Nayak, J. Roland, and M. Santha. Search via quantum walk. *Proceedings of the 39th ACM Symposium on Theory of Computing*, pages 575–584, 2007.

[38] A.M. Childs, R. Cleve, E. Deotto, E. Farhi, S. Gutmann, and D.A. Spielman. Exponential algorithmic speedup by quantum walk. *Proceeding of the 35th ACM Symposium on Theory of Computing*, (ACM Press, New York):59–68, 2003.

[39] Andris Ambainis. Quantum walks and their algorithmic applications. *International Journal of Quantum Information*, 1:507–518, 2003.

[40] A. Ambainis. Quantum walk algorithm for element distinctness. *SIAM Journal on Computing*, 37(1):210–239, 2007.

[41] F. Magniez, M. Santha, and M. Szegedy. Quantum walk algorithm for element distinctness. *Proceedings of the 16th ACM-SIAM Symposium on Discrete Algorithms*, pages 1109–1117, 2005.

[42] H. Buhrman and R. Špalek. Quantum verification of matrix products. *Proceedings of the 17th ACM-SIAM Symposium on Discrete Algorithms*, pages 880–889, 2006.

[43] F. Magniez and A. Nayak. Quantum complexity of testing group commutativity. *Algorithmica*, 48(3):221–232, 2007.

[44] E. Farhi, J. Goldstone, and S. Gutmann. A quantum algorithm for the Hamiltonian NAND tree. *quant-ph/0702144*, 2007.

[45] A. Ambainis, A. M. Childs, B. W. Reichardt, R. Špalek, and S. Zhang. Any AND-OR formula of size N can be evaluated in time $N^{1/2+o(1)}$ on a quantum computer. *Proceedings of the 48th IEEE Symposium on Foundations of Computer Science*, pages 363–372, 2007.

[46] B. W. Reichardt and R. Špalek. Span-program-based quantum algorithm for evaluating formulas. *Proceedings of the 40th ACM Symposium on Theory of Computing*, pages 103–112, 2008.

[47] B. Reichardt. Span programs and quantum query complexity: The general adversary bound is nearly tight for every boolean function. *arXiv : 0904.2759*, 2009.

[48] Takashi Oka, Norio Konno, Ryotaro Arita, and Hideo Aoki. Breakdown of an electric-field driven system: a mapping to a quantum walk. *Phys. Rev. Lett.*, 94:100602, 2005.

[49] Gregory S. Engel, Tessa R. Calhoun1, Elizabeth L. Read, Tae-Kyu Ahn1, Toms caron Manc caronal, Yuan-Chung Cheng, Robert E. Blankenship, and Graham R. Fleming. Evidence for wavelike energy transfer through quantum coherence in photosynthetic systems. *Nature (London)*, 446:782–786, 2007.

[50] Masoud Mohseni, Patrick Rebentrost, Seth Lloyd, and Aln Aspuru-Guzik. Environment-assisted quantum walks in photosynthetic energy transfer. *J. Chem. Phys.*, 129:174106, 2008.

[51] R. D. Somma, S. Boixo, H. Barnum, and E. Knill. Quantum stimulations of classical annealing processes. *Phys. Rev. lett.*, 101:130504, 2008.

[52] C. M. Chandrashekar and Raymond Laflamme. Quantum phase transition using quantum walks in an optical lattice. *Phys. Rev. A*, 78:022314, 2008.

[53] J. Du, H. Li, X. Xu, M. Shi, J. Wu, X. Zhou, and R. Han. Experimental implementation of the quantum random-walk algorithm. *Phys. Rev. A*, 67: 042316, 2003.

[54] C. A. Ryan, M. Laforest, J. C. Boileau, and R. Laflamme. Experimental implementation of discrete time quantum random walk on an NMR quantum information processor. *Phys. Rev. A*, 72:062317, 2005.

[55] Joshua M. Grossman, Donatella Ciampini, Michael D'Arcy, Kristian Helmerson, Paul D. Lett, William D. Phillips, Alipasha Vaziri, and Steven L.

Rolston. Implementation of a quantum random walk with a sodium Bose-Einstein condensate. *The 35th Meeting of the Division of Atomic, Molecular and Optical Physics, Tuscon, AZ*, (DAMOP04), 2004.

[56] Hagai B. Perets, Yoav Lahini, Francesca Pozzi, Marc Sorel, Roberto Morandotti, and Yaron Silberberg. Realization of quantum walks with negligible decoherence in waveguide lattices. *Phys. Rev. Lett.*, 100:170506, 2008.

[57] B. C. Travaglione and G. J. Milburn. Implementing the quantum random walk. *Phys. Rev. A*, 65:032310, 2002.

[58] W. Dür, R. Raussendorf, V. M. Kendon, and H. J. Briegel. Quantum walks in optical lattice. *Phys. Rev. A*, 66:052319, 2002.

[59] K. Eckert, J. Mompart, G. Birkl, and M. Lewenstein. One- and two-dimensional walks in arrays of optical traps. *Phys. Rev. A*, 72:012327, 2005.

[60] C. M. Chandrashekar. Implementing the one-dimensional quantum (Hadamard) walk using Bose-Einstein condensate. *Phys. Rev. A*, 74:032307, 2006.

[61] Z.-Y. Ma, K. Burnett, M. A. d'Arcy, and S. A. Gardiner. Quantum random walk using quantum accelerator modes. *Phys. Rev. A*, 73:013401, 2006.

[62] K. Manouchehri and J. B. Wang. Quantum walks in an array of quantum dots. *J. Phys. A: Math. Theor.*, 41:065304, 2008.

[63] Barry C. Sanders, Stephen D. Bartlett, Ben Tragenna, and peter L. Knight. Quantum quincunx in cavity quantum electrodynamics. *Phys. Rev. A*, 67: 042305, 2003.

[64] C. M. Chandrashekar, R. Srikanth, and Raymond Laflamme. Optimizing the discrete time quantum walk using SU(2) coin. *Phys. Rev. A*, 77:032326, 2008.

[65] C. M. Chandrashekar. Quantum recurrence theorem for quantum walks. *arXiv : 0810.5592*, 2008.

[66] C. M. Chandrashekar. Generic quantum walk using a coin-embedded shift operator. *Phys. Rev. A*, 78:052309, 2008.

[67] C. M. Chandrashekar, R. Srikanth, and S. Banerjee. Symmetries and noise in quantum walk. *Phys. Rev. A*, 76:022316, 2007.

[68] S. Banerjee, R. Srikanth, C. M. Chandrashekar, and P. Rungta. Symmetry-noise interplay in quantum walk on an n-cycle. *Phys. Rev. A*, 78:052316, 2008.

[69] Sandeep Goyal and C. M. Chandrashekar. Spatial entanglement in many body system using quantum walk. *arXiv : 0901.0671*, 2009.

[70] Ben Tregenna, Will Flanagan, Rik Maile, and Viv Kendon. Controlling discrete quantum walks: coins and initial states. *New J. Phys.*, 5:83, 2003.

[71] Luis Barreira. *Poincaré recurrence: old and new - pages : 415-422.* IVth International Congress on Mathematical Physics, World Scientific, 2006.

[72] U. Krengel. *Ergodic Theorems.* Walter de Gruyter, Berlin, New York, 1985.

[73] P. Bocchieri and A. Loinger. Quantum recurrence theorem. *Phys. Rev.*, 107: 337, 1957.

[74] L.S. Schulman. Note on the quantum recurrence theorem. *Phys. Rev. A*, 18: 2379, 1978.

[75] R.W. Robinett. Quantum wave packet revivals. *Phys. Rep.*, 392:1, 2004.

[76] T. A. Brun, H. A. Carteret, and A. Ambainis. Quantum to classical transition for random walks. *Phys. Rev. Lett.*, 91:130602, 2003.

[77] V. M. Kendon and B. Tregenna. Decoherence can be useful in quantum walks. *Phys. Rev. A*, 67:042315, 2003.

[78] A. Romanelli, R. Siri, G. Abal, A. Auyuanet, and R. Donangelo. Decoherence in the quantum walk on the line. *Phys. A*, 347C:137–152, 2005.

[79] V. Kendon. Decoherence in quantum walks - a review. *Math. Struct. in Comp. Sci*, 17(6):1169–1220, 2006.

[80] D. van Oosten, P. van der Straten, and H. T. C. Stoof. Quantum phases in an optical lattice. *Phys. Rev. A*, 63:053601, 2001.

[81] G. Bartrouni, V. Rousseau, R.T. Scalettar, M. Rigol, A. Muramatsu, P.J.H. Denteneer, and M. Troyer. Mott domains of bosons confined on optical lattices. *Phys. Rev. Lett.*, 89:117203, 2002.

[82] V. A. Kashurnikov, N. V. Prokofev, and B. V. Svistunov. Revealing the superfluid-Mott-insulator transition in an optical lattice. *Phys. Rev. A*, 66: 031601(R), 2002.

[83] Stefan Wessel, Fabien Alet, Matthias Troyer, and G. George Batrouni. Quantum Monte Carlo simulations of confined bosonic atoms in optical lattices. *Phys. Rev. A*, 70:053615, 2004.

[84] D. Jaksch, C. Bruder, J. I. Cirac, C. W. Gardiner, and P. Zoller. Cold bosonic atoms in optical lattices. *Phys. Rev. Lett.*, 81:3108, 1998.

[85] M. Greiner, O. Mandel, T. Esslinger, T. W. Hänsch, and I. Bloch. Quantum phase transition from a superfluid to a Mott insulator in a gas of ultracold atoms. *Nature (London)*, 415:39, 2002.

[86] T.J. Osborne and M.A. Nielsen. Entanglement in a simple quantum phase transition. *Phys. Rev. A*, 66:032110, 2002.

[87] A. Osterloh, L. Amico, G. Falci, and R. Fazio. Scaling of entanglement close to a quantum phase transition. *Nature (London)*, 416:608, 2002.

[88] Thiago R. de Oliveira, Gustavo Rigolin, Marcos C. de Oliveira, and Eduardo Miranda. Multipartite entanglement signature of quantum phase transitions. *Phys. Rev. Lett.*, 97:170401, 2006.

[89] D. A. Meyer and N. R. Wallach. Global entanglement in multiparticle systems. *J. Math. Phys.*, 43:4273, 2002.

[90] E. Bach, S. Coppersmith, M. P. Goldschen, R. Joynt, and J. Watrous. One-dimensional quantum walks with absorbing boundaries. *J. Comput. Syst. Sci.*, 69:562, 2004.

[91] Frederick Strauch. Relativistic effects and rigorous limits for discrete- and continuous-time quantum walks. *Journal of Mat. Phys.*, 48:082102, 2007.

[92] Norio Konno, Takao Namiki, and Takahiro Soshi. Symmetry of distribution for the one-dimensional Hadamard walk. *Interdisciplinary Information Sciences*, 10:11–22, 2004.

[93] P. L. Knight, E. Roldan, and J. E. Sipe. Quantum walk on the line as an interference phenomenon. *Phys. Rev. A*, 68:020301(R), 2003.

[94] D. Aharonov, A. Ambainis, J. Kempe, and U. Vazirani. Quantum walks on graphs. *Proceeding of the 33rd ACM Symposium on Theory of Computing*, (ACM Press, New York):50–59, 2001.

[95] P. Révész. *Random walk in Random and non-random Environments*. World Scientific, Singapore, 1990.

[96] G. Pólya. Uber eine Aufgabe betreffend die Irrfahrt im Strassennetz. *Math. Ann.*, 84:149–160, 1921.

[97] M. Štefaňàk, I. Jex, and T. Kiss. Recurrence and Pòlya number of quantum walks. *Phys. Rev. Lett.*, 100:020501, 2008.

[98] M. Štefaňàk, I. Jex, and T. Kiss. Recurrence properties of unbiased coined quantum walks on infinite d-dimensional lattices. *Phys. Rev. A*, 78:032306, 2008.

[99] N. Inui, Y. Konishi, and N. Konno. Localization of two-dimensional quantum walks. *Phys. Rev. A*, 69:052323, 2004.

[100] Norio Inui, Norio Konno, and Etsuo Segawa. One-dimensional three-state quantum walk. *Phys. Rev. E*, 72:056112, 2005.

[101] C. J. Myatt, B. E. King, Q. A. Turchette, C. A. Sackett, D. Kielpinski, W. M. Itano, C. Monroe, and D. J. Wineland. Decoherence of quantum superpositions through coupling to engineered reservoirs. *Nature (London)*, 403:269–273, 2000.

[102] Q. A. Turchette, C. J. Myatt, B. E. King, C. A. Sackett, D. Kielpinski, W. M. Itano, C. Monroe, , and D. J. Wineland. Decoherence and decay of motional quantum states of a trapped atom coupled to engineered reservoirs. *Phys. Rev. A*, 62:053807, 2000.

[103] V. M. Kendon and B. C. Sanders. Complementarity and quantum walks. *Phys. Rev. A*, 71:022307, 2005.

[104] T. A. Brun. A simple model of quantum trajectories. *Am. J. of Phys.*, 70: 719, 2002.

[105] S. Banerjee and R. Srikanth. Geometric phase of a qubit interacting with squeezed-thermal bath. *Eur. Phys. J. D*, 46:335, 2008.

[106] H.-P. Breuer and F. Petruccione. *The Theory of Open Quantum Systems.* Oxford University Press, 2002.

[107] S. Banerjee and R. Srikanth. An environment-mediated quantum deleter. *Phys. Lett. A*, 367:295, 2007.

[108] R. Srikanth and Subhashish Banerjee. Squeezed generalized amplitude damping channel. *Phys. Rev. A*, 77:012318, 2008.

[109] D. A. Meyer. From gauge transformations to topology computation in quantum lattice gas automata. *J. Phys. A: Math. Gen.*, 34:6981–6986, 2001.

[110] O. Maloyer and V. Kendon. Decoherence vs entanglement in coined quantum walks. *New J. Phys.*, 9:87, 2007.

[111] A. Abragam. *The Principles of Nuclear Magnetism.* Oxford University Press, 1961.

[112] T. D. Mackay, S. D. Bartlett, L. T. Stephenson, and B. C. Sanders. Quantum walks in higher dimensions. *J. Phys. A: Math. Gen*, 35:2745, 2002.

[113] U. Weiss. *Quantum Dissipative Systems.* World Scientific, 2nd edition edition, 1998.

[114] J. Allinger and U. Weiss. Non-universality of dephasing in quantum transport. *Z. Phys. B*, 98:289, 1995.

[115] D. Cohen. Unified model for the study of diffusion localization and dissipation. *Phys. Rev. E*, 55:1422, 1997.

[116] D. Forster. *Hydrodynamic Fluctuations, Broken Symmetries, Correlation Functions : Chapter 7.* Advanced Book Classics, Westview Press, 1995.

[117] V. Ambegaokar, U. Eckern, and G. Schon. Quantum dynamics of tunneling between superconductors. *Phys. Rev. Lett.*, 48:1745, 1982.

[118] U. Eckern, G. Schon, and V. Ambegaokar. Quantum dynamics of a superconducting tunnel junction. *Phys. Rev. B*, 30:6419, 1984.

[119] M.J. Hartmann and M. B. Plenio. Strong photon nonlinearities and photonic Mott insulators. *Phys. Rev. Lett.*, 99:103601, 2007.

[120] E. Demler and F. Zhou. Spinor bosonic atoms in optical lattices: symmetry breaking and fractionalization. *Phys. Rev. Lett.*, 88:163001, 2002.

[121] S. Stringari. Bose-Einstein condensation and superfluidity in trapped atomic gases. *C. R. Acad. Sci.*, 4:381–397, 2001.

[122] Subir Sachdev. *Quantum Phase Transitions*. Cambridge University Press, 1st edition edition, 2000.

[123] E. Altman, W. Hofstetter, E. Demler, and M. D. Lukin. Phase diagram of two-component bosons on an optical lattice. *New J. Phys.*, 5:113, 2003.

[124] N. V. Vitanov, M. Fleischhauer, B. W. Shore, and K. Bergmann. Coherent manipulation of atoms and molecules by sequential pulses. *Adv. Atomic Mol. Opt. Phys.*, 46:55, 2001.

[125] K. Bergmann, H. Theuer, and B. W. Shore. Coherent population transfer among quantum states of atoms and molecules. *Rev. Mod. Phys.*, 70:1003, 1998.

[126] G. Grynberg, B. Lounis, P. Verkerk, J.-Y. Courtois, and C. Salomon. Quantized motion of cold cesium atoms in two- and three-dimensional optical potentials. *Phys. Rev. Lett.*, 70:2249, 1993.

[127] K. I. Petsas, A. B. Coates, and G. Grynberg. Crystallography of optical lattices. *Phys. Rev. A*, 50:5173, 1994.

[128] L. M. Duan, E. Demler, and M.D. Lukin. Controlling spin exchange interactions of ultracold atoms in optical lattices. *Phys. Rev. Lett.*, 91:090402, 2003.

[129] P. Rabl, A. J. Daley, P. O. Fedichev, J. I. Cirac, and P. Zoller. Defect-suppressed ctomic crystals in an optical lattice. *Phys. Rev. Lett.*, 91:110403, 2003.

[130] L. Santos, M.A. Baranov, J.I. Cirac, H. U. Everts, H. Fehrmann, and M. Lewenstein. Atomic quantum gases in kagome lattices. *Phys. Rev. Lett.*, 93:030601, 2004.

[131] B. Damski, H. Fehrmann, H.-U. Everts, M. Baranov, L. Santos, and M. Lewenstein. Quantum gases in trimerized kagome lattices. *Phys. Rev. A*, 72:053612, 2005.

[132] S. V. Isakov amd S. Wessel, R. G. Melko, K. Sengupta, and Y. B. Kim. Hard-core bosons on the kagome lattice: valence-bond solids and their quantum melting. *Phys. Rev. Lett.*, 97:147202, 2006.

[133] V. Boyer, C. M. Chandrashekar, C. J. Foot, and Z. J. Laczik. Dynamic optical trap generation using FLC SLMs for the manipulation of cold atoms. *J. Mod. Opt.*, 51:2235, 2004.

[134] V. Boyer, R. M. Godun, G. Smirne, D. Cassettari, C. M. Chandrashekar, A. B. Deb, Z. J. Laczik, and C. J. Foot. Dynamic manipulation of Bose-Einstein condensates with a spatial light. *Phys. Rev. A*, 73:031402 (R), 2006.

[135] O. Mandel, M. Greiner, A. Widera, T. Rom, T.W. Hänsch, and I. Bloch. Coherent transport of neutral atoms in spin-dependent optical lattice. *Phys. Rev. Lett.*, 91:010407, 2003.

[136] J. I. Cirac, M. Lewenstein, M. Molmer, and P. Zoller. Quantum superposition states of Bose-Einstein condensates. *Phys. Rev. A*, 57:1208, 1998.

[137] J . Ruostekoski, M.J. Collett, R. Graham, and Dan. F. Walls. Macroscopic superpositions of Bose-Einstein condensates. *Phys. Rev. A*, 57:511, 1998.

[138] D. Gordon and C.M. Savage. Creating macroscopic quantum superpositions with Bose-Einstein condensates. *Phys. Rev. A*, 59:4623, 1999.

[139] Y. B. Band, P. S. Julienne, and M. Trippenbach. Radio-frequency output coupling of the Bose-Einstein condensate for atom lasers. *Phys. Rev. A*, 59: 3823, 1999.

[140] O. Mandel, M. Greiner, A. Widera, T. Rom, T.W. Hnsch, and I. Bloch. Controlled collisions for multi-particle entanglement of optically trapped atoms. *Nature (London)*, 425:937, 2003.

[141] F. Dalfovo, S. Giorgini, Lev P. Pitaevskii, and S. Stringari. Theory of Bose-Einstein condensation in trapped gases. *Rev. Mod. Phys.*, 71:463–512, 1999.

[142] D. A. R. Dalvit and J. Dziarmaga. Schrdinger cats in atom-trap BECs. *Los Alamos Sciences*, 27:166, 2002.

[143] M.-O. Mewes, M.R. Andrews, D.M. Kurn, D.S. Durfee, C.G. Townsend, and W. Ketterle. Output coupler for Bose-Einstein condensed atoms. *Phys. Rev. Lett.*, 78:582, 1997.

[144] E. W. Hagley, L. Deng, M. Kozuma, J. Wen, K. Helmerson, S. L. Rolston, and W. D. Phillips. A well-collimated quasi-continuous atom laser. *Science*, 283(5408):1706–1709, 1999.

[145] W. Ketterle, D.S. Durfee, and D.M. Stamper-Kurn. Making, probing and understanding Bose-Einstein condensates. *In Bose-Einstein condensation in atomic gases, Proceedings of the International School of Physics "Enrico Fermi", Course CXL, edited by M. Inguscio, S. Stringari and C.E. Wieman (IOS Press, Amsterdam)*, pages 67–176, 1999.

[146] A. Marte, T. Volz, J. Schuster, S. Dürr, G. Rempe, E.G.M. van Kempen, and B.J. Verhaar. Feshbach resonances in rubidium 87: precision measurement and analysis. *Phys. Rev. Lett.*, 89:283202, 2002.

[147] R.Grimm, M. Weidermüller, and Y.B. Ovchinnikov. Optical dipole traps for neutral atoms. *Advances in Atomic Molecular and Optical Physics*, 42: 95–170, 2000.

[148] M.D. Barrett, J.A. Sauer, and M.S. Chapman. All-optical formation of an atomic Bose-Einstein condensate. *Phys. Rev. Lett.*, 87:010404, 2001.

[149] R. Dumke, M. Volk, T. Müther, F.B.J. Buchkremer, G. Birkl, and W. Ertmer. Micro-optical realization of arrays of selectively addressable dipole traps: A scalable configuration for quantum computation with atomic qubits. *Phys. Rev. Lett.*, 89:097903, 2002.

[150] L. Amico, R. Fazio, A. Osterloh, and V. Vedral. Entanglement in many-body systems. *Rev. Mod. Phys.*, 80:517, 2008.

[151] Libby Heaney, Janet Anders, Dagomir Kaszlikowski, and Vlatko Vedral. Spatial entanglement from off-diagonal long-range order in a bose-einstein condensate. *Phys. Rev. A*, 76:053605, 2007.

[152] Kathy-Anne Brickman Soderberg, Nathan Gemelke, and Cheng Chin. Ultracold molecules: vehicles to scalable quantum information processing. *New Journal of Physics*, 11:055022, 2009.

[153] Sougato Bose. Quantum communication through an unmodulated spin chain. *Phys. Rev. Lett.*, 91:207901, 2003.

[154] Matthias Christandl, Nilanjana Datta, Artur Ekert, and Andrew J. Landahl. Perfect state transfer in quantum spin networks. *Phys. Rev. Lett.*, 92:187902, 2004.

[155] Matthias Christandl, Nilanjana Datta, Tony C. Dorlas, Artur Ekert, Alastair Kay, and Andrew J. Landahl. Perfect transfer of arbitrary states in quantum spin networks. *Phys. Rev. A*, 71:032312, 2005.

[156] Ivens Carneiro, Meng Loo, Xibai Xu, Mathieu Girerd, Viv Kendon, and Peter L. Knight. Entanglement in coined quantum walks on regular graphs. *New J. Phys.*, 7:156, 2005.

[157] Valerie Coffman, Joydip Kundu, and William K. Wootters. Distributed entanglement. *Phys. Rev. A*, 61:052306, 2000.

[158] H. Barnum and N. Linden. Monotones and invariants for multi-particle quantum states. *J. Phys. A : Math. Gen.*, 34:6787, 2001.

[159] Jens Eisert and Hans J. Briegel. Schmidt measure as a tool for quantifying multiparticle entanglement. *Phys. Rev. A*, 64:022306, 2001.

[160] Frank Verstraete, Jeroen Dehaene, and Bart De Moor. Normal forms and entanglement measures for multipartite quantum states. *Phys. Rev. A*, 68: 012103, 2003.

[161] Akimasa Miyake. Classification of multipartite entangled states by multidimensional determinants. *Phys. Rev. A*, 67:012108, 2003.

[162] Ali Saif M. Hassan and Pramod S. Joag. Experimentally accessible geometric measure for entanglement in n-qubit pure states. *Phys. Rev. A*, 77:062334, 2008.